

NATIONAL AERONAUTICS AND SPACE ADMINISTRATION  
CONTRACT NO. NAS 7-100

*Space Programs Summary No. 37-21, Volume VI*  
for the period March 1, 1963 to May 31, 1963

*Space Exploration Programs and Space Sciences*

JET PROPULSION LABORATORY  
CALIFORNIA INSTITUTE OF TECHNOLOGY  
PASADENA, CALIFORNIA

June 30, 1963

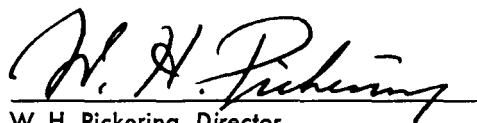
## Preface

The *Space Programs Summary* is a six-volume, bimonthly publication designed to report on JPL space exploration programs and on related supporting research and advanced development projects. These activities are conducted under the sponsorship of the National Aeronautics and Space Administration.

All information formerly documented in the *JPL Research Summary*, together with reports on advanced development projects, is reported in Volumes IV and V. The subtitles of all volumes of the *Space Programs Summary* are:

- Vol. I. The Lunar Program (Confidential)
- Vol. II. The Planetary-Interplanetary Program (Confidential)
- Vol. III. The Deep Space Instrumentation Facility (Unclassified)
- Vol. IV. Supporting Research and Advanced Development (Unclassified)
- Vol. V. Supporting Research and Advanced Development (Confidential)
- Vol. VI. Space Exploration Programs and Space Sciences (Unclassified)

The *Space Programs Summary*, Volume VI, is an unclassified digest of appropriate material from Volumes I through V, plus space science instrumentation studies. This instrumentation work is conducted by the JPL Space Sciences Division and also by individuals of various colleges, universities and other organizations. All such projects are supported by the Laboratory and are concerned with the development of instruments for use in the NASA space flight programs.

  
W. H. Pickering, Director  
Jet Propulsion Laboratory

### Space Programs Summary No. 37-21, Volume VI

Copyright © 1963, Jet Propulsion Laboratory, California Institute of Technology

Prepared under Contract No. NAS 7-100, National Aeronautics & Space Administration



## Contents

### THE LUNAR PROGRAM

<b>I. <i>Ranger</i> Project</b>	1
A. Introduction	1
B. <i>Ranger</i> Design Modifications	1
C. Subsystem and Component Testing	4
D. Functional Analyses	6
E. Block IV Design Status	6
F. Lunar Facsimile Capsule	10
G. TV Subsystem	12
H. Trajectory Description, <i>Ranger 5</i>	13
<b>II. <i>Surveyor</i> Project</b>	25
A. Introduction	25
B. Spacecraft Development	25

### THE PLANETARY-INTERPLANETARY PROGRAM

<b>III. <i>Mariner</i> Project</b>	31
A. Introduction	31
B. Launch and Arrival Date Considerations	32
C. Spacecraft Design	32
D. <i>Mariner</i> Venus 1962 Design Evaluation Vehicle (DEV) Tests	42
<b>IV. <i>Voyager</i> Project</b>	45

### THE DEEP SPACE INSTRUMENTATION FACILITY

<b>V. Introduction</b>	47
<b>VI. Communications Research, Development, and Facilities</b>	48
A. Engineering Development	48
B. Research and Development	49
C. Facilities	53

## Contents (Cont'd)

### OPERATIONAL AND TEST FACILITIES

<b>VII. The Space Flight Operations Facility</b> . . . . .	55
A. Introduction . . . . .	55
B. Scheduling . . . . .	55
C. Facility Description . . . . .	56
<b>VIII. Test and Support Equipment</b> . . . . .	60
A. Environmental Test Laboratory . . . . .	60
B. Ground Support Equipment (GSE) . . . . .	60

### SPACE SCIENCES

<b>IX. Space Instruments Development</b> . . . . .	65
A. Transfer Characteristics and Gray-Scale Reproduction for Space Camera Evaluation . . . . .	65
Reference . . . . .	71
<b>X. Space Instruments Systems</b> . . . . .	72
A. Formulation of Electrical Network Problems for Computer Analysis . . . . .	72
B. Planetary Scan Subsystem for <i>Mariner</i> Mars 1964 . . . . .	75
<b>XI. Lunar and Planetary Studies</b> . . . . .	79
A. Preliminary Results from <i>Ranger</i> 3 Gamma Ray Spectrometer . . . . .	79
B. <i>Surveyor</i> X-Ray Spectrometer . . . . .	80
References . . . . .	81

# THE LUNAR PROGRAM

## I. *Ranger* Project

### A. Introduction

The objective of the *Ranger* Project is to exploit present technology in support of the U.S. manned lunar flight program. Fourteen *Ranger* launchings, using *Atlas-Agena B* rockets, are now planned; five of these flights have been made.

*Rangers 1* and *2* (Block I) were engineering evaluation flights to test the basic system to be employed in later lunar and planetary vehicles. Several scientific experiments were carried, but on a noninterference basis. The *Ranger 3, 4, and 5* (Block II) spacecraft carried a gamma-ray instrument, a radar reflection experiment, a TV camera, and a rough-landing seismometer capsule. All three of these flights failed; as a result, the objectives of future flights have been reviewed, and subsequent spacecraft design modifications are being accomplished.

The over-all functional design of the *Ranger* Block III spacecraft (*Rangers 6-9*) is complete, and the detail design is 98% complete. The basis chosen for the new design was that of the former *Ranger 8*, less nonvisual instruments. Assembly of the Block III proof test model was started in April. Initial buildup will utilize some electrically equivalent electronic equipment so that electrical testing of the Block III design may proceed as soon as possible.

Block IV is in the development stage just prior to the formalization of the design freeze; design reviews are still being held.

### B. *Ranger* Design Modifications

#### 1. Structures

The structural, mechanical, and electromechanical subsystems of the Block III spacecraft system have been reviewed. As a result, the following modifications are being made to these subsystems:

- (1) Change of bus structure from magnesium alloy to aluminum alloy in order to sustain higher spacecraft weight.
- (2) Increase of solar panel substrate area to provide for increased solar power.
- (3) Addition of a hydraulic timer to back up certain vital central computer and sequencer commands.

- (4) Incorporation of dampers to reduce excursion of solar panels during boost phase.
- (5) A series of improvements to the squib firing assembly to improve system and component reliability (see 4. *Pyrotechnics-Squib Firing Assembly*, this section).

## 2. Power Subsystem

*a. Batteries.* In view of the satisfactory performance of the sealed secondary silver zinc batteries in the *Ranger* Block II mission, the same basic designs were selected for use in Block III missions. However, in order to increase the reliability of the battery, changes were made which incorporate the latest in the battery state-of-the-art and alleviate the problems associated with handling of the battery cases. In addition, to further enhance the power subsystem reliability, a decision was made to have two of these batteries on each spacecraft.

*Packaging.* The battery for Block II was permanently potted into one half of a full bay case during manufacture. The booster regulator, power switch and logic, and squib firing assembly modules and the case harness were installed in the remaining half of that case. This made it necessary to remove these units to service the battery, as well as to change these units to the flight battery case just prior to the final system test when the flight battery is first mounted on the spacecraft.

For Block III the battery is installed permanently in a case which is only one half the size of the original full bay case. This is then mounted directly to the spacecraft. The other units, formerly mounted in the battery case, are installed in a similar half-size case which is mounted in the other half of the bay. With this arrangement the battery can be removed or changed without handling any other unit on the spacecraft.

The second battery is mounted in the adjacent bay, but on the side next to the first battery, in order to satisfy spacecraft center-of-gravity requirements. The two batteries supply the power subsystem in parallel with the solar panels through logic isolation diodes, but each battery supplies a separate channel of the squib firing assembly for pyrotechnic events.

*Sealing.* The cell seal has proved to be a problem area in the past. A change has been made in the material used in coating the plate lead wires. This coating is applied to these wires to protect them from local cell action which

would damage the wire and discharge the cell. The new material accomplishes the primary task better and makes a better bond with the epoxy used in the seal. Also, lead wires are being sealed before cell activation to insure that they are not contaminated by either KOH or  $K_2CO_3$ . Such contamination could prevent the formation of a good bond between the epoxy and the silver wire.

Changes have been made to eliminate some of the polystyrene-to-polystyrene cement-joint seals. The remaining ones have a redundant cement joint to enhance their seal.

*Separators.* The inconsistent quality of recent shipments of one of the separator materials used in the Block II batteries made a change in this area necessary. Results of tests indicated another layer of cellophane could be used without degrading performance. One layer of Synpor and three layers of cellophane were used in Block II batteries, and one layer of Dynel, one layer of Polypor, and four layers of cellophane are used in Block III.

*b. Electrical conversion equipment.* The electrical conversion equipment for Block III is presently being reprocedured. This effort was initiated in order to obtain flight equipment which has appreciably improved reliability. Several changes have been made in the design and fabrication of the flight power equipment in order to achieve the increased reliability.

All of the electronic components in the power equipment are either being procured to a high-reliability specification or being 100% screened prior to their installation in the subassemblies. Approximately 30 screening specifications have been generated for those components unique to the power system (primarily, transformers and chokes) for which there were previously no screening specifications.

The booster regulator has been repackaged in order to make the unit easier to fabricate and to permit all of the components to be inspected after assembly. The basic circuitry remains essentially unchanged.

The synchronizer has also been repackaged, primarily for improved ease of inspection. All printed circuits have been placed on the front side of the circuit boards, where the condition of the solder joints with the terminals can easily be evaluated.

The power switch and logic assembly has been redesigned. The number of telemetry signal conditioners has

been increased from 4 to 9 in order to accommodate a greater number of measurements and to provide electrical isolation for several previously existing measurements. The oscillator which provides excitation to the signal conditioners has been fused to prevent an oscillator failure from damaging the remainder of the power system.

### 3. Command Subsystem

The command functions required on Block I consisted of three momentary relay closures to initiate spacecraft roll search, to override the high-gain antenna hinge angle setting, and to switch the radio transmitter output between the low- and high-gain antennas. To fulfill these requirements, a simple subcarrier tone burst system was developed. To initiate any command, the subcarrier tone corresponding to that command was transmitted to the spacecraft over the radio link. The spacecraft command subsystem utilized narrow-band tuning fork filters to selectively detect the subcarrier tones from the broad spectrum communication noise.

The command functions required on Block II were more extensive than those required on Block I. Eight relay closure commands were required; it was also necessary to transfer six 12-bit blocks of quantitative information to the spacecraft. To fulfill these requirements a command subsystem was developed in which digital command words were transmitted to the spacecraft in the form of a modulated subcarrier. The modulated subcarrier was demodulated in the spacecraft command detector. The recovered serial binary information was applied to the spacecraft command decoder, which accumulated each command word in a storage register and decoded the command address, and the required outputs were issued to the designated subsystem.

The data from the Block II flights indicate that the command subsystem operated faultlessly whenever the correct power and input signals were applied.

Considerable logical simplification can be achieved by combining the detector and decoder program control functions and by shortening the decoder storage register. It is planned to incorporate this logical simplification on the first program having a schedule which will permit the design change.

The *Ranger* command subsystem design was briefly re-examined before the Block III equipment was ordered. The following conclusions were drawn:

- (1) The Block II package design is susceptible to damage from sterilization. A minor modification of the cordwood module construction has been incorporated in the units for Block III to decrease the probability of a solder-joint failure.
- (2) The command subsystem timing should not be dependent upon the central computer and sequencer. A redundant clock pulse source has been incorporated into the command subsystems for Block III.

A stress analysis was conducted on the Block II circuits, and the voltage rating of three capacitors was increased for Block III to provide adequate derating. Also, some high-reliability components were substituted where direct interchange was possible. The stress analysis resulted in a predicted probability of total success of 98.6% for a 70-hr mission.

*a. RF command.* The redundant contacts on Real-Time Command 5 (telemetry mode change) are being used to disable the backup timer in the TV subsystem rather than to update the timer as stated in SPS 37-20, Vol. VI, p. 6. The timer, started at spacecraft separation by a newly installed microswitch on Leg E of the bus, will initiate (at the Moon) one half of the TV subsystem independent of the spacecraft. If postlaunch tracking indicates that the prelaunch set time is wrong and command capability still exists, the command system will be used to turn off the timer. Turning off the timer at the latest possible time provides a minimum time period during which a command subsystem failure might cause loss of TV data.

### 4. Pyrotechnics—Squib Firing Assembly

A number of changes were made in the design of the squib firing assembly to improve the subsystem and/or spacecraft system reliability. Perhaps the most significant of these changes in regard to improvement of system reliability was the incorporation of relay circuitry to switch off the return side to all squibs, as well as the "hot" side. The method used in squib firing in the *Ranger* design involves switching power directly from the spacecraft battery. To prevent drawing maintained current from the battery due to postfire pin-to-pin squib shorts, the power-switching relays in the hot side of the line were shut off approximately 1 sec after closure; however, the return side (common to the battery return) was not shut off in the Block II design. With a postfire squib short to frame (a highly probable occurrence), the resulting situation could be one wherein the return side

of the spacecraft battery was hard-grounded to the spacecraft frame; a short from the battery positive side elsewhere in the system (such as in the power subsystem) could then result in a total failure. With the redesigned shutoff circuitry in the Block III squib firing assembly, a squib short to frame would be of a transitory nature only, and the probability of contributing to a gross failure in the system is greatly reduced.

## C. Subsystem and Component Testing

### 1. Antennas and RF Components

RF power handling capability tests were made of the *Ranger* coaxial rotary joint, directional coupler, directional antenna, and associated coaxial cables in vacuums ranging from  $10^{-3}$  to  $10^{-5}$  torr. The test results indicate that RF voltage breakdown, probably due to a mechanism known as multipacting, will occur in the Type-N coaxial connectors used on these components at RF power levels of approximately 70 to 90 w. Such a breakdown results in a large drop (50 to 90%) in the power transmitted through the component and, if sustained, considerable physical damage to the item.

Multipacting depends on secondary emission from the walls of the item under test, and requires that the mean free electron path be long compared to the internal dimensions of the component. This condition is easily met at the pressures being considered. On the other hand, ionization breakdown requires that the mean free path be short compared to component dimensions. When the ambient pressure is  $10^{-3}$  torr or lower, it seems inconceivable that a vented component could maintain sufficient pressure to give this condition.

Since secondary emission is required to sustain multipacting, there must be voids present in the component of a size sufficient to allow a primary electron to accelerate to a velocity sufficient to knock out secondaries when the primary impacts a surface. Thus, the quickest available fix appears to be the elimination of such voids in the components.

At present, the Block III TV package is designed to apply RF power levels of 65 to 70 w to the above components. RF voltage breakdown problems reported by RCA during vacuum testing of the TV package transmitter and associated components led to the conclusion that

the JPL components that would carry the 65 to 70 w of RF power from the TV package should be vacuum-tested for their power handling capability at the transmitter frequency.

Since the Type-N connectors seem to be the weak point, work is presently proceeding on changing these to a dielectric filled connector (a modified Type-SC). Incorporation of the modified RF components in time for Block III flights is planned.

### 2. Propulsion System

During this reporting period systems work has been concerned primarily with qualification of components which will be used in the assembly and testing of two type-approval propulsion systems, TA 1 and TA 2.

*a. Engine.* The rocket engine used in the Block III propulsion system is identical to that used on the previous systems, except for modification of the oxidizer nozzle (2-gal/hr increase) and modification of the oxidizer and fuel line flange design. It is felt that the new nozzle will have a better start transient and, consequently, smoother steady-state combustion.

Type-approval testing on the rocket engine has been completed. The engine was subjected to the environmental tests of shock, static acceleration, and boost-phase vibration. These tests were followed by engine firings of 300-sec duration at nominal chamber pressure and at 1.5 times nominal chamber pressure. The engine was subjected to a humidity test and then statically fired for 100-sec duration. All of the type-approval tests were passed successfully.

*b. Oxidizer start cartridge.* The start cartridge to be used on the Block III propulsion system is a modification of the cartridge used on the *Ranger 5* system.

Type-approval tests on the start cartridge have been completed. Initially, the bellows were functionally cycled 100 times, using water in place of the oxidizer. The cartridge was then filled with water, pressurized with nitrogen, and subjected to the environmental tests of shock, static acceleration, and boost-phase vibration. At the completion of the environmental tests the cartridge was once again functionally cycled 60 times. The start cartridge was then used for three engine ignition tests.

No problems were encountered during any of the type-approval tests.

**c. Visual pressure gage.** The oxidizer start cartridge contains a visual pressure gage used for pre-launch monitoring of the start cartridge pressure. This gage is identical to the one used on previous systems.

Type-approval tests on the gage were initial calibration and leak tests; environmental tests of transportation and handling, vibration, shock, static acceleration, and boost-phase vibration; and vacuum-temperature tests at 14 and 167°F for 116-hr duration. The gage was then subjected to 1000 pressurizing cycles to assure its durability. The gage successfully passed all of the type-approval tests.

**d. Pneumatic regulator.** Type-approval testing on the regulator consisted of initial proof, leak, and flow tests, followed by environmental tests of shock, static acceleration, and boost-phase vibration. Flow tests at 14 and 167°F and lockup tests followed. A failure of a metal-to-metal seal occurred during the high-temperature (167°F) test. This seal was modified by incorporation of a backup O-ring seal. The regulator was then successfully subjected to the above environmental tests.

**e. Fuel tank bladder.** The butyl rubber compound for the bladder has been changed from Fargo Rubber

FR-6-50-3 to FR-6-60-26. Permeability tests with the compound indicated no measurable rates during a 90-hr test period. A compatibility test with the compound was made by immersing a sample in a glass vial of hydrazine and measuring pressure rise as a function of time. After 1 mo the measured pressure rise was only 4 lb/in.<sup>2</sup>, and after 6 mo, 10 lb/in.<sup>2</sup> Additionally, a fuel tank and bladder assembly was filled with hydrazine, pressurized at 260 psig, and stored at ambient conditions with the pressure of the tank being monitored on a daily basis. No pressure rise has been noted after 6 mo of testing.

Type-approval testing on the bladder consisted of initial leak tests, followed by 50 cycles of pressure-vacuum cycling on the bladders. At the end of the 50 cycles the bladder was again subjected to a leak test. No problems were encountered during the type-approval tests.

### 3. Solar Panels

As was stated in SPS 37-20, Vol. VI, p. 6, the rectangular-shaped Mark IV solar panels will be used in place of the trapezoidal panels for the *Ranger* Block III spacecraft. Each Mark IV solar panel is made of three electrically independent sections, which each contain 68 cells in series and 24 in parallel, or a total of 1,632 cells. Type-approval solar panel TA 1 (Fig. 1) has been delivered to JPL from the manufacturer, and is presently undergoing tests.

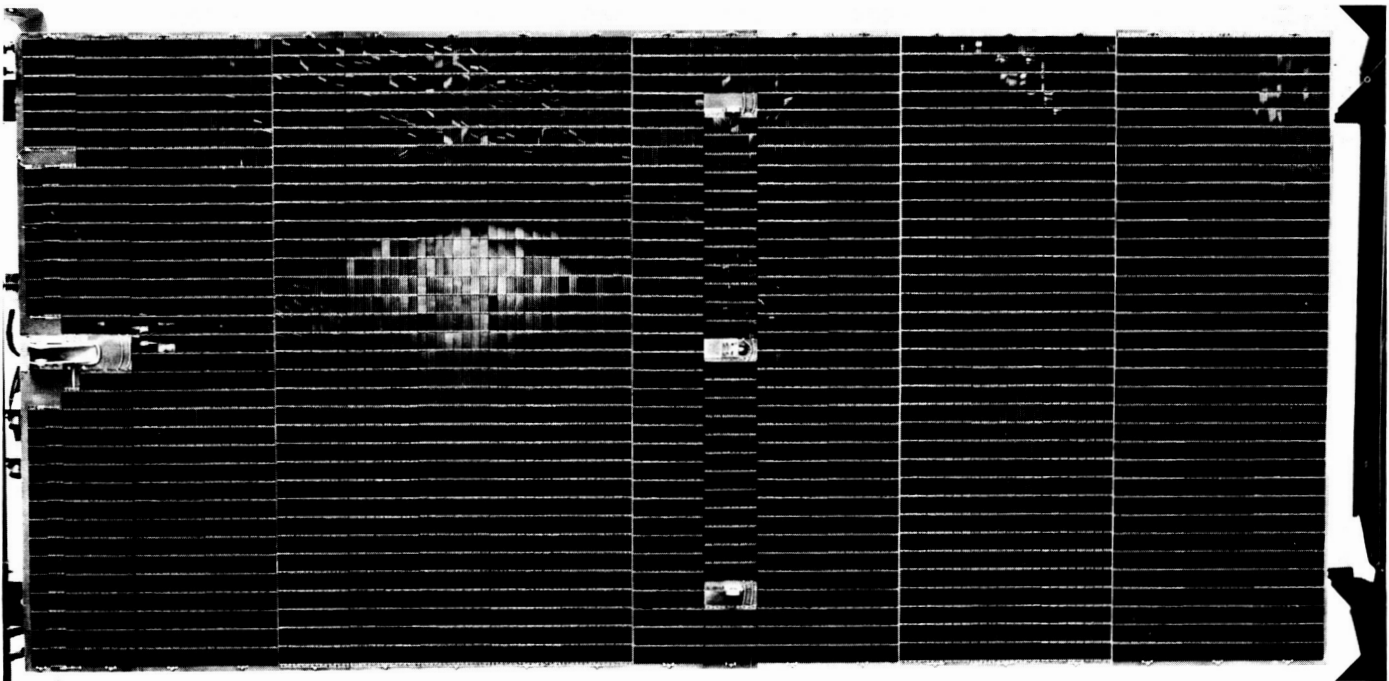


Fig. 1. Solar panel TA 1, front surface

A series of special tests was performed at JPL to determine the effect of different soldering procedures on the output of solar cells of the type used on the Mark IV solar panels. In addition, tests were conducted to determine the effect of using soldering to remove irregularities in the grid contacts to the sensitive surface. For these tests 25 Heliotek solar cells were used. Complete current-voltage characteristics were measured on the solar cells before and after each of the soldering iron tests. All electrical tests were run in tungsten at an intensity of 100 mw/cm<sup>2</sup> and a cell temperature of 28°C. In one of the tests, a large change in the series resistance of the solar cell contact was indicated. A lower open circuit voltage also indicated a slight increase in shunt resistance.

## D. Functional Analyses

### 1. Control Circuit Analysis Program

During the past several months a program to provide comprehensive analyses of all *Ranger* control circuits has been pursued. In performing the studies, a RECOMP II digital computer, leased by JPL from Autonetics Industrial Products Div. of North American Aviation, has been employed to provide the format and carry out the detailed computations necessary in completing the analyses. The SPARC program provided with the RECOMP II is a worst-case circuit analysis program adapted from the MANDEX program originally developed for the IBM 7090. It is available in three parts, enabling the user to perform: (1) worst-case bias stabilization analysis, (2) steady-state analysis in the frequency domain, and (3) transient analysis in the time domain. Regarding these three analyses, the DC program is the only one which automatically performs a worst-case analysis.

To date, only the bias stabilization analysis program has been applied in the control circuits analysis effort. A number of minor examples of component overstressing beyond recommended maximums, performance degradation due to local nonlinearities, and circuit sensitivities to component parameter variations have been disclosed as a result of the analysis program, and corrections for these difficulties have been included in the Block III redesign activity.

### 2. Spacecraft Reliability Study

Phase I of a Block III spacecraft reliability study, performed by the Fairchild Stratos Corp. under JPL contract, was completed the latter part of January 1963. Of special interest in the final report is an analytical reliability model comprised of reliability equations and matrices which define the failure modes for the following 11 subsystems of the Block III spacecraft: power supply, central computer and sequencer, attitude control (includes autopilot), command, antenna, transponder, pyrotechnics, TV, data automation, data encoder, and midcourse motor. Each spacecraft was analyzed for a normal mission and three degraded types of missions.

No numerical reliability predictions were attempted for the Block III spacecraft during the Phase I effort; therefore, a Phase IIA contract was issued primarily for utilizing the Phase I analytical model to estimate the numerical reliability of the spacecraft.

## E. Block IV Design Status

The *Ranger* Block IV (Figs. 2-4) resembles *Ranger* Block III, except for the following significant additions: (1) a gamma ray spectrometer, (2) a science half-case in Bay V, (3) a radar altimeter antenna and its associated electronics box in Bay VI, (4) a data automation system, and (5) a dual attitude control subsystem. The larger Mark IV solar panels will also be incorporated in the Block IV design as on Block III.

### 1. Gamma Ray Spectrometer

The gamma ray spectrometer will sense gamma radiation both in the cislunar environment and in the vicinity of the Moon. The purpose of the spectrometer is to determine the spectrum of the radiation emanating from the lunar surface.

The spectrometer will consist of the detector, high-voltage supply, and pulse height analyzer. The high-voltage supply for the photomultiplier tube will occupy about 10 in.<sup>3</sup> The power supply for the pulse height analyzer, which operates off the 2.4-kc scientific inverter, will be mounted on a separate module.



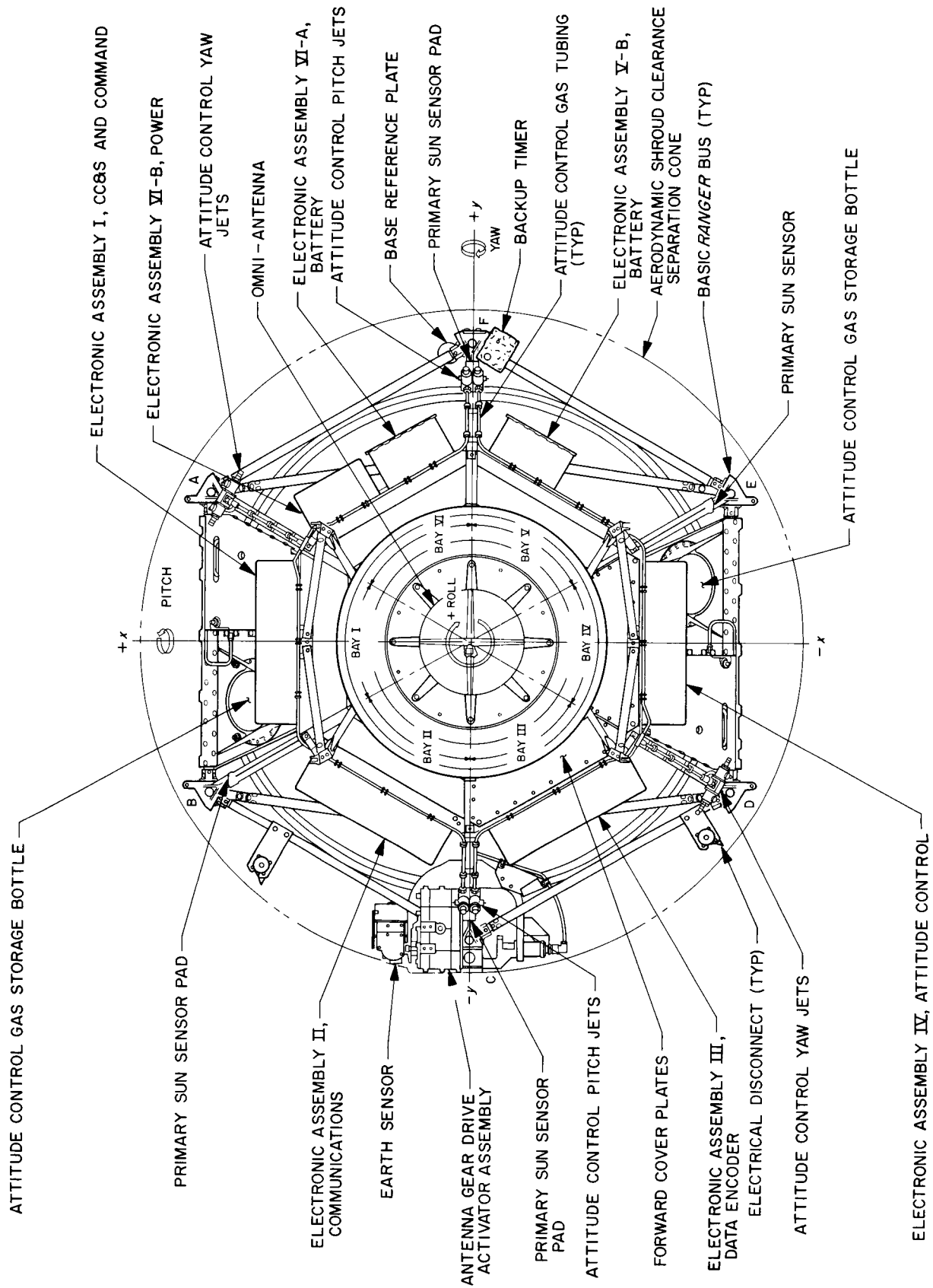


Fig. 2. Ranger Block IV configuration, top view

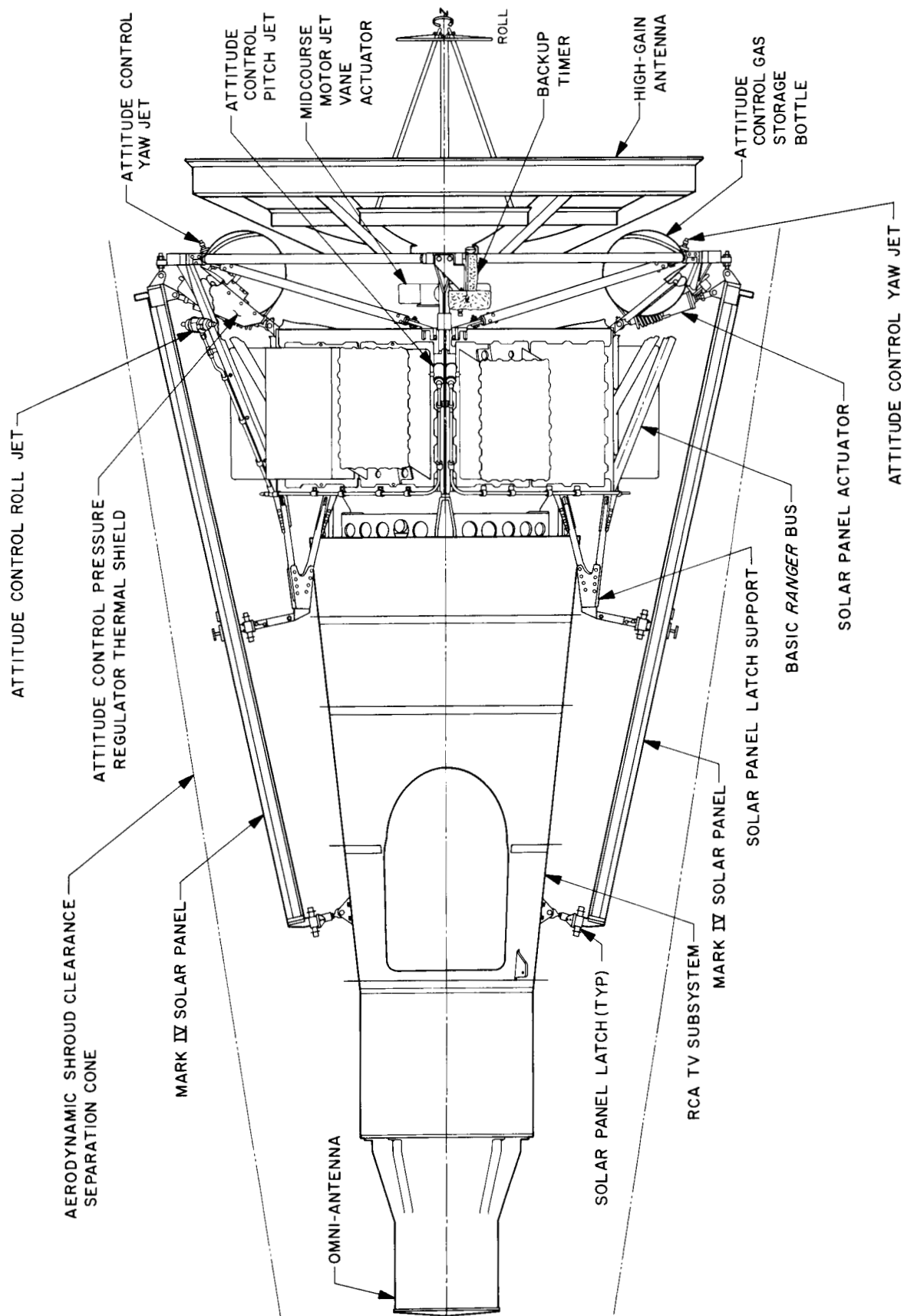


Fig. 3. Ranger Block IV configuration, side view (+y)

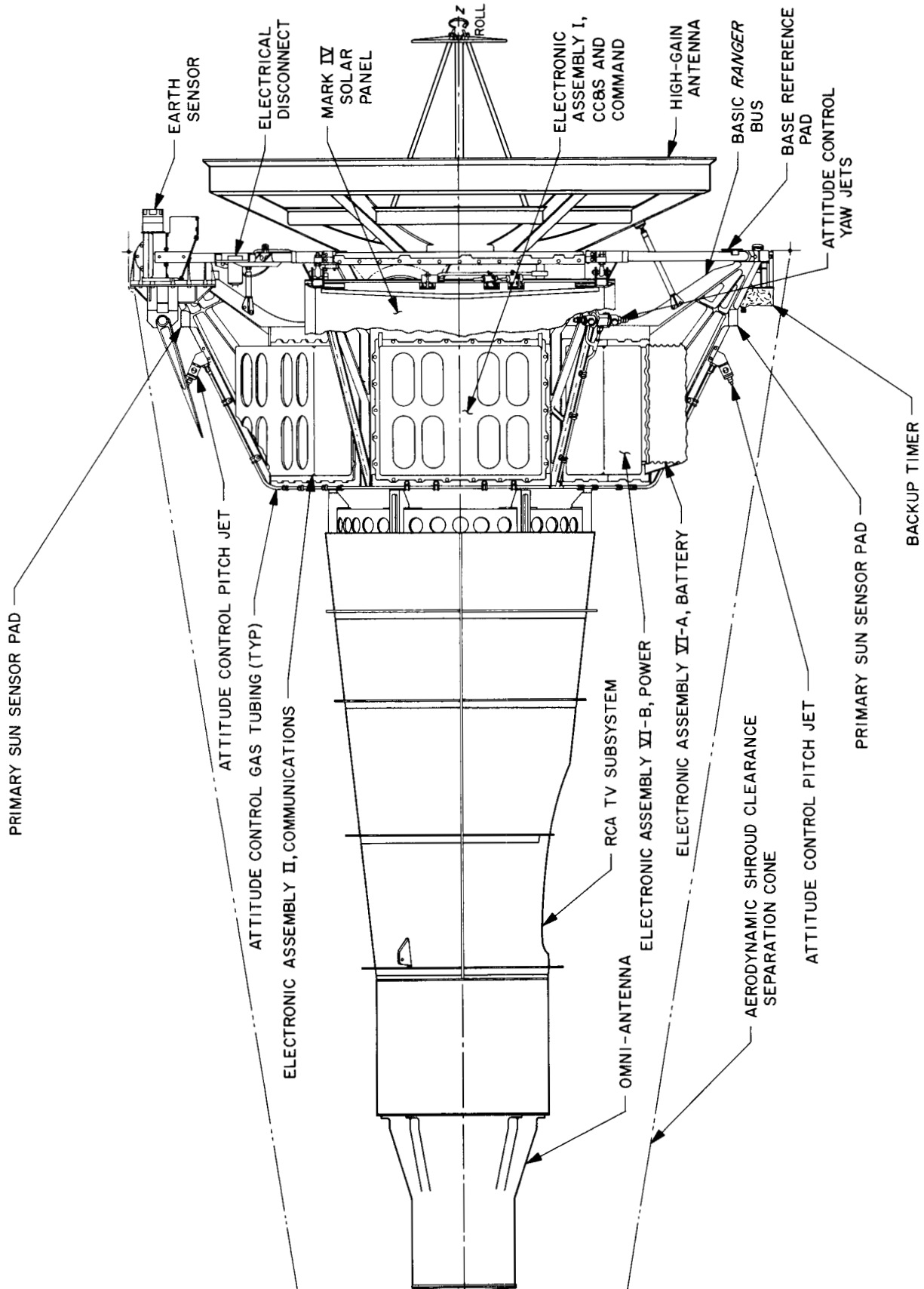


Fig. 4. Ranger Block IV configuration, side view (+x)

## 2. Radar Ranging Altimeter Experiment

This experiment will: (1) make measurements of the lunar surface characteristics, and (2) test ranging techniques for design verification of an altimeter capable of generating a fuzing signal for an ejectable capsule in succeeding *Rangers*.

The radar ranging altimeter will provide a profile of the lunar surface, yielding an average cross section. Significant parameters are roughness, porosity, electrical permeability and permittivity, and conductivity. The engineering information that is useful for future radars involves peak echo returns, average echo, transmitted power needed, and range. A smooth lunar surface should yield an altimeter accuracy of  $\pm 20$  m and a starting altitude of 400 km.

## 3. Electrical Conversion Equipment

Several additional changes are being incorporated into the Block IV electrical conversion equipment in order to improve reliability and performance. All of the converters and inverters are being repackaged in order to simplify the circuit boards and reduce the quantity of circuit boards required. The deletion of approximately 150 components associated with the overload circuits was primarily responsible for the simplification of the circuit boards.

The command converter is being redesigned in order to take advantage of a relaxation of the regulation tolerances of the outputs. The change in the regulation requirements permits a considerable reduction in the complexity of the four series regulators in the unit, resulting in a reduction in the components count and an increase in efficiency.

The single-phase 400-cps inverter is being modified to incorporate increased input filtering. This change will reduce the amount of 800-cps ripple fed back into the booster by a factor of about 3, resulting in a reduction of ripple of this frequency in the outputs of all the remaining converters and inverters.

The synchronizer is being modified to make use of a 19.2-kc input frequency from the central computer and sequencer. This change will eliminate one binary stage from the synchronizer and also about 10 components.

## F. Lunar Facsimile Capsule

### 1. Introduction

Aeronutronic Division of Ford Motor Company (ADF), under JPL contract, is developing major subassemblies of the landing sphere assembly for the lunar facsimile capsule (LFC). The LFC is basically the *Ranger* seismometer capsule with a high-resolution facsimile device replacing the seismometer experiment. The LFC transmits data to reproduce on Earth a complete 360-deg panoramic view of the lunar terrain surrounding the landed capsule. The viewing system scans from 10 deg above the horizon to within 4 ft of the capsule, is in focus from about 4 ft to infinity, and has an angular resolution approaching 0.1 deg. The facsimile picture includes an accurate profile of the entire lunar horizon, as well as resolutions down to 0.1 in. in the near field.

The following material relating to the lunar facsimile capsule was extracted from the ADF document: *Bi-monthly Technical Progress Report No. 2, Lunar Facsimile Capsule Program*, March 1963.

The LFC development is planned in three phases. Effort is currently authorized on Phase I, with the primary objective of demonstrating the ability of the prototype LFC viewing subsystem to survive and function after being subjected to a simulated lunar impact.

Some aspects of the experiment have not as yet been firmly defined. Therefore, effort is being expended to define the limitations and alternate capabilities existing within the facsimile concept. Some possible extended experiments which have been evaluated reveal that the system could be mechanized to provide stereoscopic black and white or monoscopic color facsimiles.

Phase I also includes effort on a breadboard porting mechanism and a prototype solid-state transmitter. Dynamic porting characteristics to produce vital design data will be investigated, with special attention to reaction impulse and tipoff effects which might overturn the landing sphere assembly. The transmitter will be developed to meet the power and efficiency objectives of the LFC design and will be packaged in an assembly compatible with the payload sphere configuration.

### 2. Subsystem Development Status

*a. Top tube assembly.* The advanced development program to demonstrate impact survival of the preprototype

top tube has been completed. The preprototype passed all demonstration tests successfully after surviving two 3000 g impacts.

A sensor for the LFC program has been selected, breadboard testing of the preamplifier has been completed, and sensor/preamp packaging of the preprototype model is nearly complete. Five types of light sensors were tested and initially appeared most promising for this program. A silicon photo device designed to ADF specifications was selected on the basis of temperature characteristics, sensitivity, and physical construction.

The new preamplifier design incorporates a field-effect transistor input stage. This design results in the following improvements over that of the preamplifier used in the high-resolution facsimile study program: higher input resistance, lower input capacitance, and better signal-to-noise ratio.

**b. Extension mechanism.** The extension system selected for Prototype 1 is shown in Fig. 5. The extension force is derived from atmospheric gas sealed within the sphere during assembly. When the porting gun removes the payload cover, the top tube is automatically extended.

An extension system functional model, representative of the Prototype 1 configuration except for having a 4-in. instead of an 18-in. stroke, has been fabricated, assembled, and tested. The model utilizes continuous top tube support, taper-lock snap rings, and gas actuation with O-ring seals. The primary purpose of this model was to determine the relationship between terminal extension velocity and terminal impact shock.

**c. Signal and synchronization electronics.** Portions of the signal and synchronization electronics breadboard have been completed, and design work on the remaining circuits is in progress. A block diagram of the signal and synchronization electronics is shown in Fig. 6.

**d. Motor drive electronics.** A breadboard of the motor drive electronics has been constructed and checked out using a dummy load. Samples of some of the components have been functionally tested and are being prepared for shock test.

**e. Ground reproduction system.** The LFC ground reproducer electronics circuitry has been designed and

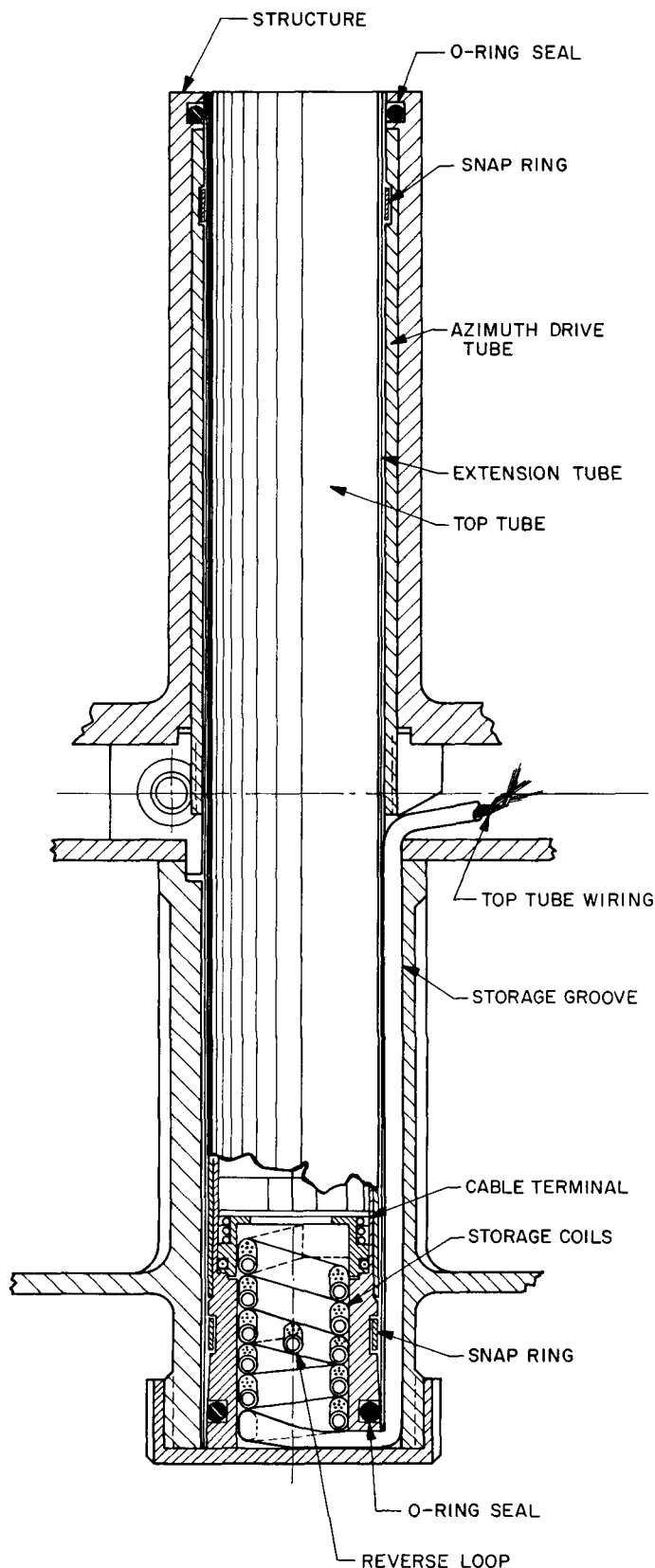


Fig. 5. Extension system, Prototype 1 design

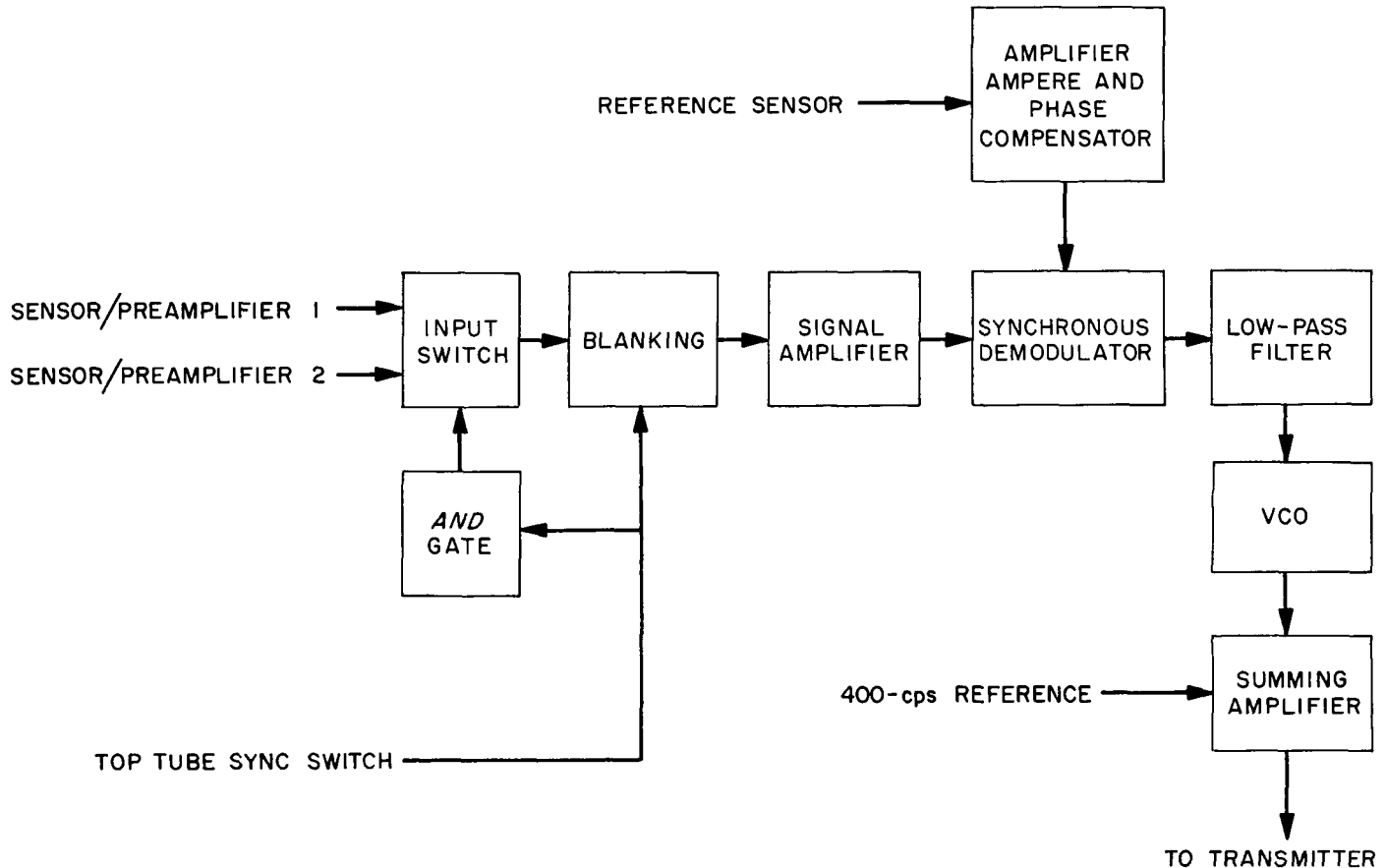


Fig. 6. Signal and synchronization electronics

fabricated into a 19-in. rack-mounted unit. This unit contains a 65-cps, four-pole, low-pass Butterworth filter and pulse-width modulator circuit.

A different circuit technique for accomplishing the modulation process has been devised. This modification allows for deletion of the inverter circuitry that was under development.

**f. Transmitter.** Performance characteristics of the basic transmitter circuit were evaluated for a 26- to 30-v input voltage range, which is representative of the range expected from the LFC battery. The data indicate a drop in efficiency from 11.8 to 9% over the anticipated input voltage range. An additional data point at 28 v indicates that an efficiency exceeding 12% is possible for a circuit configuration optimized for this voltage. An effort will be made to modify the basic circuit to maintain this higher efficiency over the entire input voltage range.

Dimensionally, the transmitter occupies 152 deg of an annular ring of 2-in. depth and inner and outer radii of

2.16 and 4.8 in., respectively. The outer dimension is consistent with possible requirements for a 10½-in. D payload sphere, and was used at this time to minimize redesign in the event the smaller diameter sphere is used.

## G. TV Subsystem

The primary objective of the Block III spacecraft will be to produce high-resolution TV pictures of the lunar surface. To implement this objective, a TV subsystem is being developed by RCA under contract to JPL. The subsystem will mate with the JPL bus, as did the lunar capsule of the Block II series.

The subsystem structure consists of three major assemblies: (1) the central box which houses the main electronic components, (2) the camera subassembly with associated

bracketry and equipment, and (3) the thermal shield. Camera view apertures are provided in the thermal shield.

The following material relating to the subsystem development is extracted from the RCA report: *Ranger TV Subsystem, Tenth Bimonthly Progress Report*, April 15, 1963.

Flight Model (FM) 2 was acceptance-tested and shipped to JPL. FM 2, redesignated as the life test model (LTM), is not a flight model of the split-system configuration. The LTM has undergone a variety of subsystem and assembly tests at JPL in preparation for the life tests, which are to be complete subsystem tests run in vacuum and at various temperatures.

Mechanical Test Model (MTM) 2 with the *Mariner* solar panels was subjected to squib firing tests at JPL. MTM 2 was instrumented to record shock levels and the propagation of the shock impulses through the TV subsystem.

The temperature test model, newly designated as the temperature control model, was tested at JPL in the large vacuum chamber with solar simulation in order to calibrate the chamber, as well as to test the temperature control capability of the TV subsystem.

The split-system configuration described in SPS 37-20, Vol. VI, p. 13, was incorporated in the design of the Block III proof test model subsystem. This incorporation included the addition of a distribution control unit, power control unit, and a second high-current regulator. The redesign to the split-system configuration also involved minor modifications in some units, such as the command switch, and the installation of harnesses modified to the new redundant configuration. After the modifications were completed, the proof test model was assembled, debugged, and then successfully operated during a simulated mission test.

FMs 1, 3, and 4 have been redesignated as Block III-1, -2, and -3, respectively. Extensive development work was performed on the camera components, testing of lenses (in the 25-mm, f/1.0 regions), rapid-scan erase, and the transistorized preamplifier, and work continued on the trajectory effects on *Ranger TV* subsystem performance and over-all camera system analysis.

## H. Trajectory Description, Ranger 5

### 1. Launch Phase

The *Ranger 5* spacecraft was launched at 16:59:07.84 GMT on October 18, 1962, from the Atlantic Missile Range (AMR) using the *Atlas D-Agena B* boost vehicle. After liftoff, the booster rolled to a launch azimuth of 95.6 deg (east of north) and performed a programmed pitch maneuver until booster cutoff. During the *Atlas* sustainer and vernier stages, adjustments in vehicle attitude and engine cutoff times were commanded as required by the ground guidance computer to adjust the altitude and velocity at *Atlas* vernier engine cutoff. After *Atlas-Agena* separation, there was a short coast period prior to the first *Agena* ignition. At a preset value of sensed velocity increase, the *Agena* engine was cut off. At this time both the *Agena* and spacecraft were coasting in a nearly circular parking orbit at an altitude of 188 km and a speed of 7.8 km/sec (space-fixed). After a total coast time of 25.9 min in the parking orbit, the second *Agena* ignition occurred. This parking orbit coast time was determined after liftoff by the ground guidance computer and transmitted to the *Agena* during the *Atlas* vernier stage. The launch phase was nearly nominal with the exception of the parking orbit altitude, which was slightly above nominal (approximately 21 km high at second *Agena* ignition; see Fig. 7). A typical sequence of events is shown in Fig. 8.

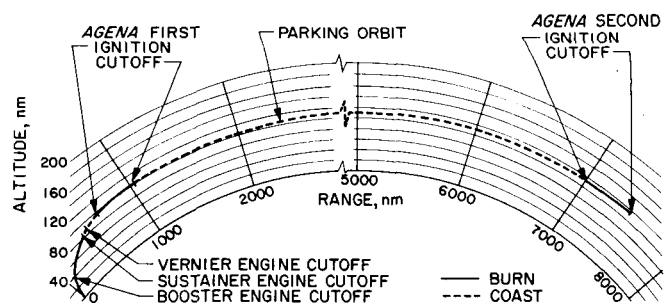


Fig. 7. Ascent trajectory profile

### 2. Cruise Phase

Injection (*Agena* final cutoff) occurred at 17:34:46 GMT, at which time the *Agena* and spacecraft were traveling at a speed of 10.962 km/sec (space-fixed). The geocentric latitude and longitude of injection were  $-21.4$  and  $36.6$  deg, respectively, with injection taking place over the eastern coast of South Africa. The *Agena* and

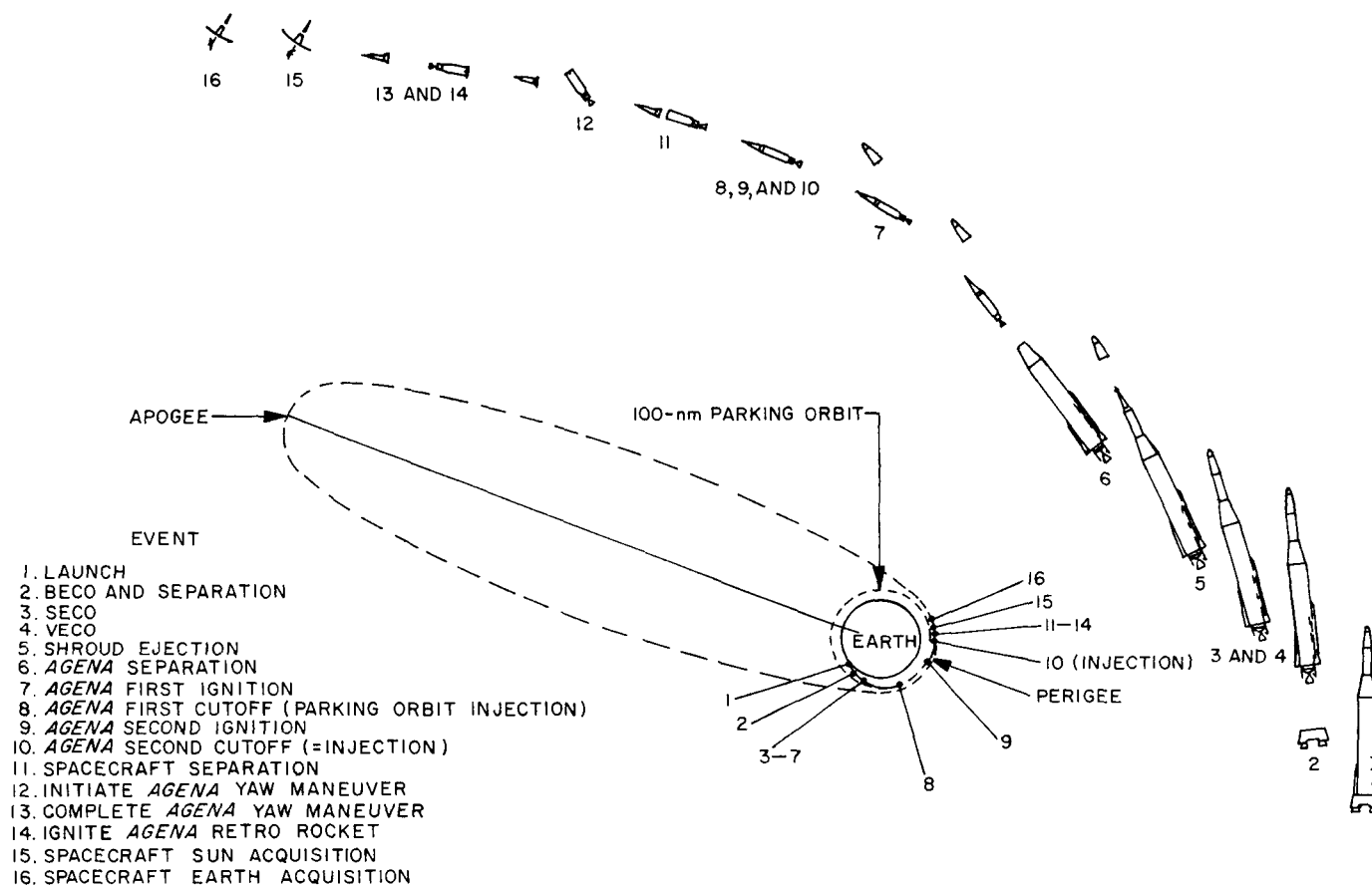


Fig. 8. Sequence of events

spacecraft separated 2½ min after injection occurred. The *Agenda* then performed a programmed 180-deg yaw maneuver and ignited its retrorocket. The retrorocket impulse was designed to eliminate interference with the spacecraft operation and reduce the chance of lunar impact by the *Agenda*. The geocentric characteristics of the *Ranger 5* premidcourse orbit are presented in Table 1. (Definitions of the symbols used in Tables 1, 2, and 3 are given in Table 4.)

Within 1 hr after injection, the spacecraft was receding from the Earth in almost a radial direction with decreasing speed. This reduced the geocentric angular rate of the spacecraft (in inertial coordinates) until, at 1.4 hr after injection, the angular rate of the Earth exceeded that of the spacecraft. This caused the Earth track of the spacecraft to reverse its direction from increasing to decreasing Earth longitude (Fig. 9). Note in Fig. 9 where the spacecraft entered the Earth's shadow during the parking orbit and emerged shortly after injection.

The *Ranger 5* premidcourse orbit, as determined using the limited tracking data available, indicated that the spacecraft would miss the Moon by 631 km on the trailing edge, 7.84 deg below the lunar equator. Only 40% of the spacecraft midcourse maneuver capability would have been required to obtain a lunar impact in the target area if the spacecraft had performed properly. However, 40 min past injection a malfunction in the electrical power distribution system made it necessary for the spacecraft to operate from battery power. Because of the relatively short battery life, a nonstandard midcourse maneuver was attempted. The batteries operated within design limits, but were depleted at 8 hr, 15 min past injection during the execution of the midcourse maneuver sequence before any significant maneuver was performed. The midcourse motor burn would have been completed at 8 hr, 21 min past injection.

After the midcourse maneuver attempt, some perturbations due to unbalanced attitude control torques or



Table 1. Ranger 5 trajectory characteristics, geocentric

Event	Orbit	Epoch			z θ	x v	y γ	z σ	Epoch of pericenter passage			Period Apogee Perigee
		x r	y φ	z θ					a e	i Ω	ω P	
		Central body										
Injection <sup>a</sup>	Premidcourse	10-18-62	17 h 34 m 49.000 s			Earth			10-18-62	17 h 34 m 14.222 s		25318.884
		5160.3084	—3337.6059	—2408.5288	4.7676745	9.2194782	—3.4133226	285621.50	28.277414	227.07382	564647.70	
		6600.7121	—21.400765	36.678061	10.503421	1.6966992	109.72965	0.97690894	100.34123	3.3006440	6595.3013	
Midcourse	Postmidcourse	10-19-62	01 h 56 m 08.000 s			Earth			10-18-62	17 h 34 m 17.998 s		24359.324
		—50885.925	91512.070	18173.407	—1.6380212	1.6998046	0.70499460	278358.62	28.324781	227.12511	550131.92	
		106273.74	9.8462939	62.976418	7.4244739	18.603799	272.47972	0.97634232	100.29226	154.00054	6585.3187	
Closest approach to Moon (CAM)	Postmidcourse	10-21-62	15 h 53 m 43.304 s			Earth						
		—266515.31	267754.70	120687.60	—1.9612392	1.0016941	0.85827341					
		396596.12	17.716569	226.82526	26.960412	4.7987901	270.38492					
Postencounter with Moon	Postmidcourse	11-8-62	00 h 00 m 00.00 s			Earth						
		—2285918.0	—594768.00	120984.50	—1.2436209	—0.63197970	—0.05552590					
		2365122.6	2.9321643	147.88415	171.94860	0.45252991	269.95828					
Prior to encounter with Earth	Postmidcourse	7-6-63	15 h 16 m 00.290 s			Earth						
		10426178.	—2058456.0	—2053722.5	—1.4372225	1.2795127	0.52914947					
		10824057.	—10.937427	195.94791	773.98998	—0.12792773	270.01517					
Closest approach to Earth	Postmidcourse	10-11-63	7 h 39 m 51.700 s			Earth			10-11-63	7 h 39 m 51.709 s		N.A.
		—45776.764	—1428105.8	—627678.08	—0.94190025	—0.077877562	0.24588169	—900035.69	151.67291	302.04708	N.A.	
		1560628.5	—23.715514	134.02097	105.13186	—0.44868407E-6	270.14636	2.7339629	213.58348	—0.68301891E-5	1560628.5	
Postencounter with Earth	Postmidcourse	11-5-63	7 h 1 m 49.025 s			Earth						
		—2181309.0	—1320464.0	—27853.000	—1.0778708	0.055039643	0.24680448					
		2550000.8	—0.62583913	61.941898	186.54547	0.27361225	270.07880					

<sup>a</sup>Injection here refers to the injection epoch utilized by orbit determination; actual flight injection occurred 2.72 sec earlier.

<sup>a</sup>Injection here refers to the injection epoch utilized by orbit determination; actual flight injection occurred 2.72 sec earlier.

Table 2. Ranger 5 trajectory characteristics, selenocentric

Event	Orbit	Epoch			Central body			Epoch of pericenter passage			Period Apogee Perigee
		x r	y $\phi$	z $\theta$	x v	y $\gamma$	z $\sigma$	a e	i $\Omega$	$\omega$ $\nu$	
	Postmidcourse	10-21-62	15 h 53 m	43.304 s	Moon			10-21-62	15 h 53 m	43.304 s	N.A.
		2052.2628	1349.3020	291.63757	-1.2036515	1.6114737	1.0284994	-4278.6450	28.039962	14.526639	N.A.
		2473.3477	-7.7901465	87.497032	2.2536799	0.87605676E-6	82.230661	1.5780681	20.441792	0.25613208E-5	2473.3481

Table 3. Ranger 5 trajectory characteristics, heliocentric

Event	Orbit	Epoch			Central body			Epoch of pericenter passage			Period Apogee Perigee
		x r	y $\phi$	z $\theta$	x v	y $\gamma$	z $\sigma$	a e	i $\Omega$	$\omega$ $\nu$	
Postencounter with Moon	Postmidcourse	11-8-62	00 h 00 m	00.00 s	Sun			1-4-63	13 h 43 m	26.125 s	368.97689
		0.10232351E9	0.10450206E9	347960.50	-22.833730	20.303836	0.20121676	0.15061302E9	0.40782426	81.242884	0.15905268E9
		0.14625629E9	0.13631521	45.603487	30.555939	-2.7519310	89.615704	0.056035391	26.073687	-61.712637	0.14217336E9
Prior to encounter with Earth	Postmidcourse	7-6-63	15 h 16 m	00.290 s	Sun			1-4-63	17 h 48 m	25.415 s	365.78834
		46809173.	-0.15038849E9	-1065399.0	26.987741	8.4002281	-0.022421241	0.14974407E9	0.39010680	83.311208	0.15750853E9
		0.15750851E9	-0.38755603	287.28902	28.264863	0.77496631E-6	90.045452	0.051851512	23.977965	179.99998	0.14197961E9
Closest approach to Earth	Postmidcourse	10-11-63	7 h 39 m	51.700 s	Sun						
		0.14256443E9	42783742.	-7764.1249	-10.264214	28.371872	0.25552642				
		0.14884577E9	-0.29886746E-2	16.704556	30.172546	-3.1841736	89.514181				
Postencounter with Earth	Postmidcourse	11-5-63	7 h 1 m	49.025 s	Sun			12-8-63	23 h 35 m	29.025 s	378.91262
		0.10779746E9	98298109.	499914.50	-21.539619	22.129911	0.20338929	0.15330481E9	0.43120386	62.862038	0.16223837E9
		0.14588715E9	0.19633720	42.360993	30.882512	-1.8632269	89.616064	0.058273201	15.277130	-35.777527	0.14437125E9

Table 4. Legend for Tables 1, 2, and 3

Parameters	Definition		
	Earth as central body	Moon as central body	Sun as central body
$x, y, z$	Vernal equinox cartesian coordinates in a geocentric equatorial system. The origin is the center of the central body. The principal direction $\hat{x}$ is the vernal equinox direction of date, and the principal plane $(x, y)$ is the Earth equatorial plane of date. $\hat{z}$ is along the direction of the Earth's spin axis of date, km.	Vernal equinox cartesian coordinates in a geocentric equatorial system. The origin is the center of the central body. The principal direction $\hat{x}$ is the vernal equinox direction of date, and the principal plane $(x, y)$ is the Earth equatorial plane of date. $\hat{z}$ is along the direction of the Earth's spin axis of date, km.	Vernal equinox cartesian coordinates in a heliocentric equatorial system. The origin is the center of the Sun. The principal direction $\hat{x}$ is the vernal equinox direction of date, and the principal plane $(x, y)$ is the ecliptic plane of date. $\hat{z}$ is normal to the ecliptic plane of date, km.
$\dot{x}, \dot{y}, \dot{z}$	First time derivatives of $x, y$ , and $z$ , respectively; i.e., cartesian components of the probe space-fixed velocity vector, km/sec.	First time derivatives of $x, y$ , and $z$ , respectively; i.e., cartesian components of the probe space-fixed velocity vector, km/sec.	First time derivatives of $x, y$ , and $z$ , respectively; i.e., cartesian components of the probe space-fixed velocity vector, km/sec.
$r$	Probe radius distance, km	Probe radius distance, km	Probe radius distance, km
$\phi$	Probe geocentric latitude, deg	Probe selenocentric latitude, deg	Probe celestial latitude, deg
$\theta$	Probe east longitude, deg	Probe selenocentric east longitude, deg	Probe celestial longitude, deg
$v$	Probe Earth-fixed velocity, km/sec	Probe selenocentric-fixed velocity, km/sec	Probe heliocentric inertial velocity vector, km/sec
$\gamma$	Path angle of the probe Earth-fixed velocity vector with respect to the local horizontal, deg	Path angle of the probe selenocentric-fixed velocity vector with respect to the local horizontal, deg	Path angle of the probe heliocentric inertial velocity vector with respect to the local horizontal, deg
$\sigma$	Azimuth angle of the probe Earth-fixed velocity vector measured east of true north, deg	Azimuth angle of the probe selenocentric-fixed velocity vector measured east of the Moon's mean spin axis, deg	Azimuth angle of the probe heliocentric inertial velocity vector measured east of the celestial north direction, deg
$a$	Semi-major axis, km (negative for hyperbolic orbit)	Semi-major axis, km (negative for hyperbolic orbit)	Semi-major axis, km
$e$	Eccentricity	Eccentricity	Eccentricity
$i$	Inclination of the orbit plane to the Earth equatorial plane, deg	Inclination of the orbit plane to the Earth equatorial plane, deg	Inclination of the orbit plane to the ecliptic, deg
$\Omega$	Longitude of the ascending node, deg	Longitude of the ascending node, deg	Longitude of the ascending node, deg
$\omega$	Argument of pericenter, deg	Argument of pericenter, deg	Argument of pericenter, deg
$\nu$	True anomaly, deg	True anomaly, deg	True anomaly, deg
Period	Measured in sec	Measured in sec	Measured in days
Apogee	Measured in km	Measured in km	Measured in km
Perigee	Measured in km	Measured in km	Measured in km
N.A. = Not applicable			

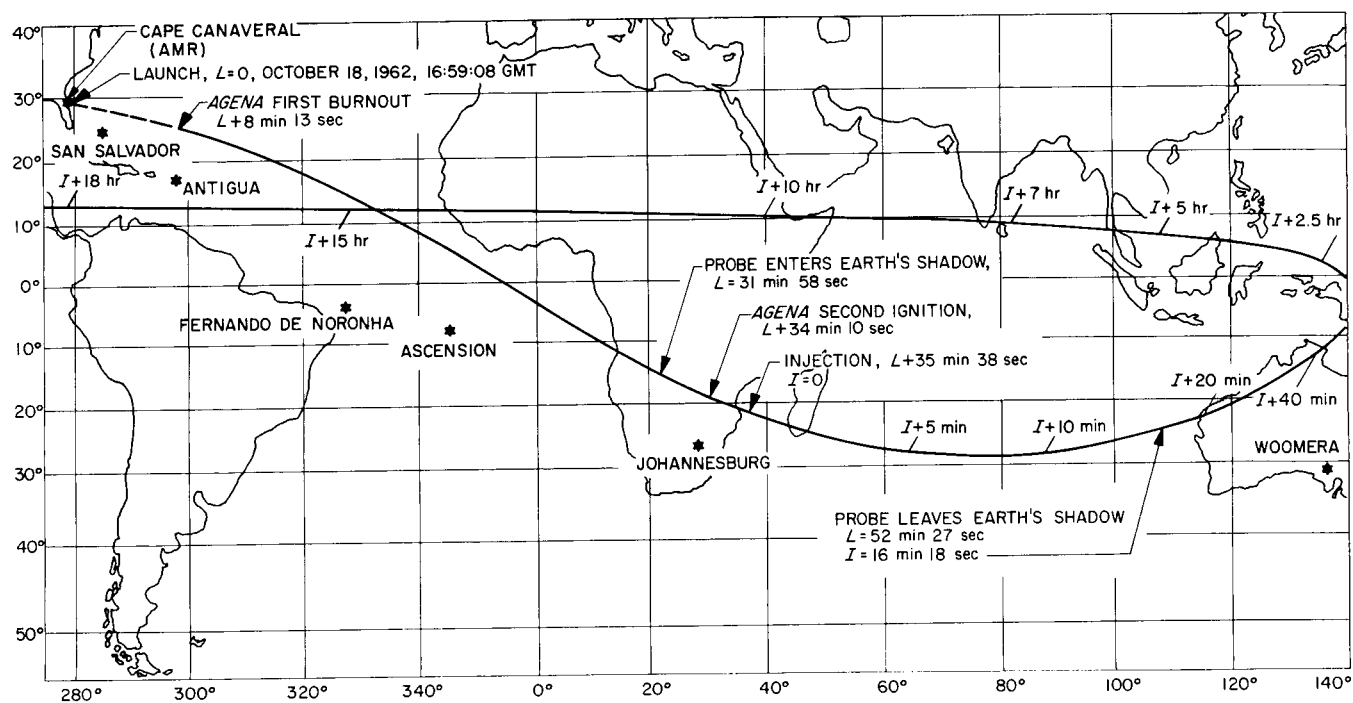


Fig. 9. Earth track of Ranger 5

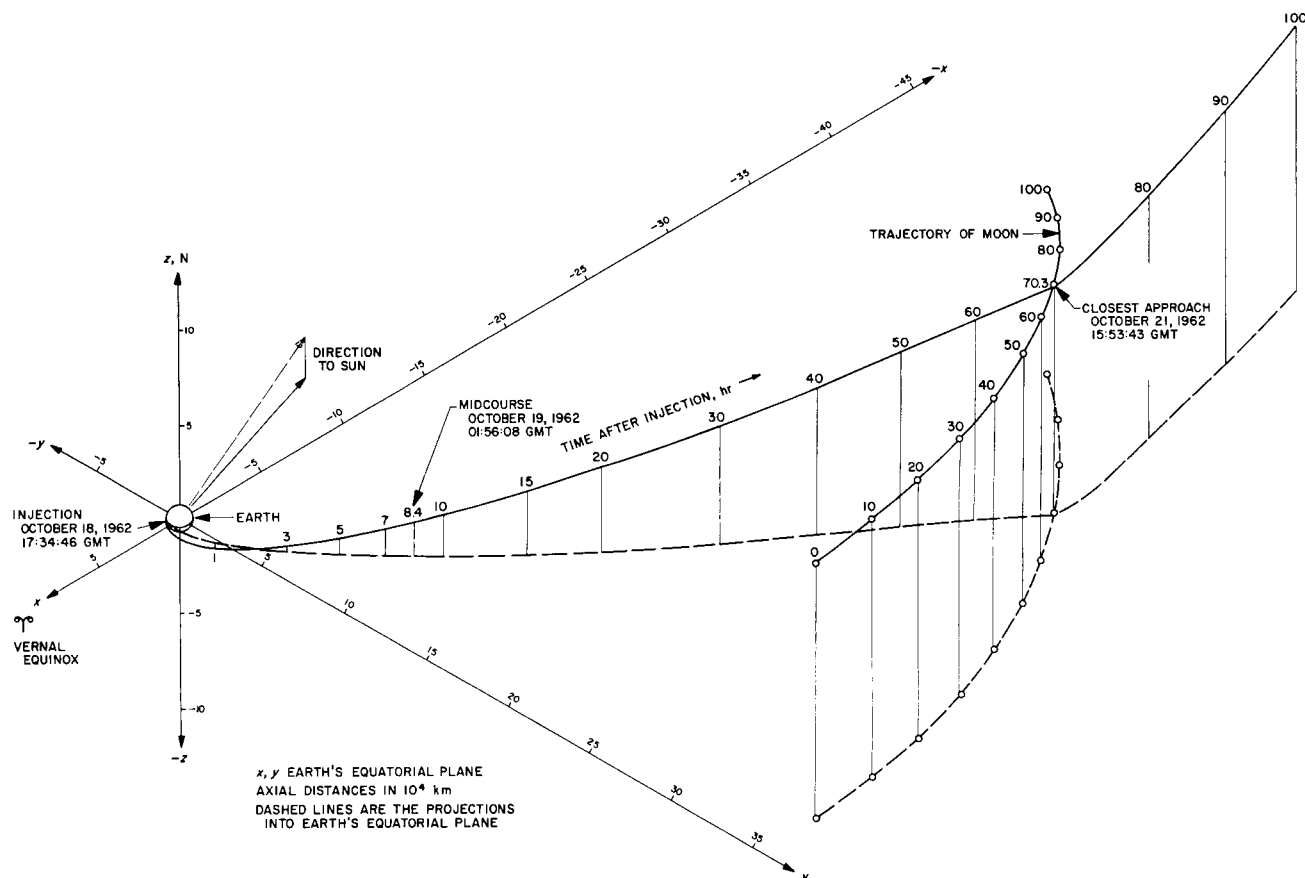


Fig. 10. Ranger 5 Earth-Moon transit geometry

sources connected with the midcourse rocket system are presumed to have slightly altered the trajectory. Subsequent tracking of the capsule beacon through lunar encounter provided data to determine the postmidcourse orbit. This orbit indicates that the spacecraft missed the Moon by 735 km on the trailing edge, 7.79 deg below the lunar equator. At the time the midcourse maneuver

was attempted, the spacecraft was at a distance of 106,000 km and traveling at a speed of 2.46 km/sec relative to the Earth. The spacecraft continued moving primarily under the gravitational influence of the Earth in a highly elliptical geocentric orbit on its transit to lunar encounter. Fig. 10 illustrates the geometrical relations of the trajectory through lunar encounter. Figs. 11

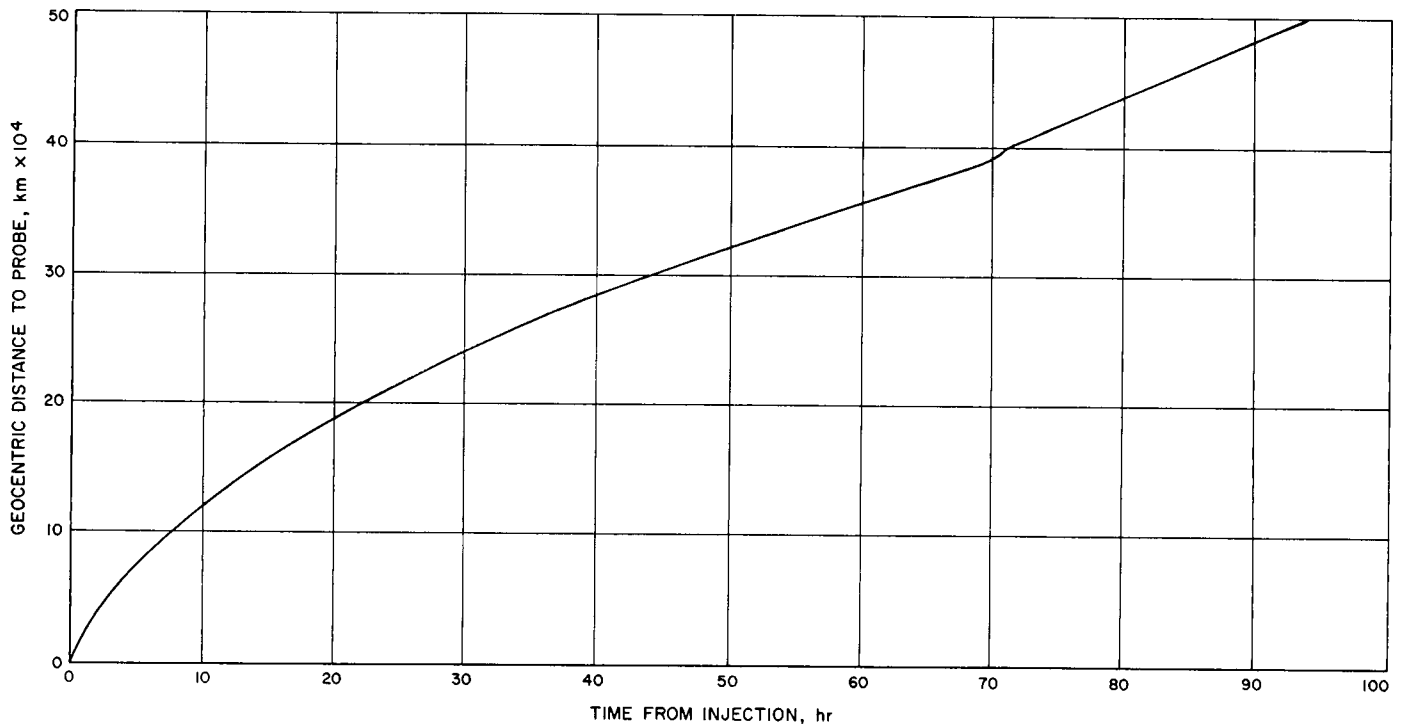


Fig. 11. Geocentric distance to probe versus time from injection

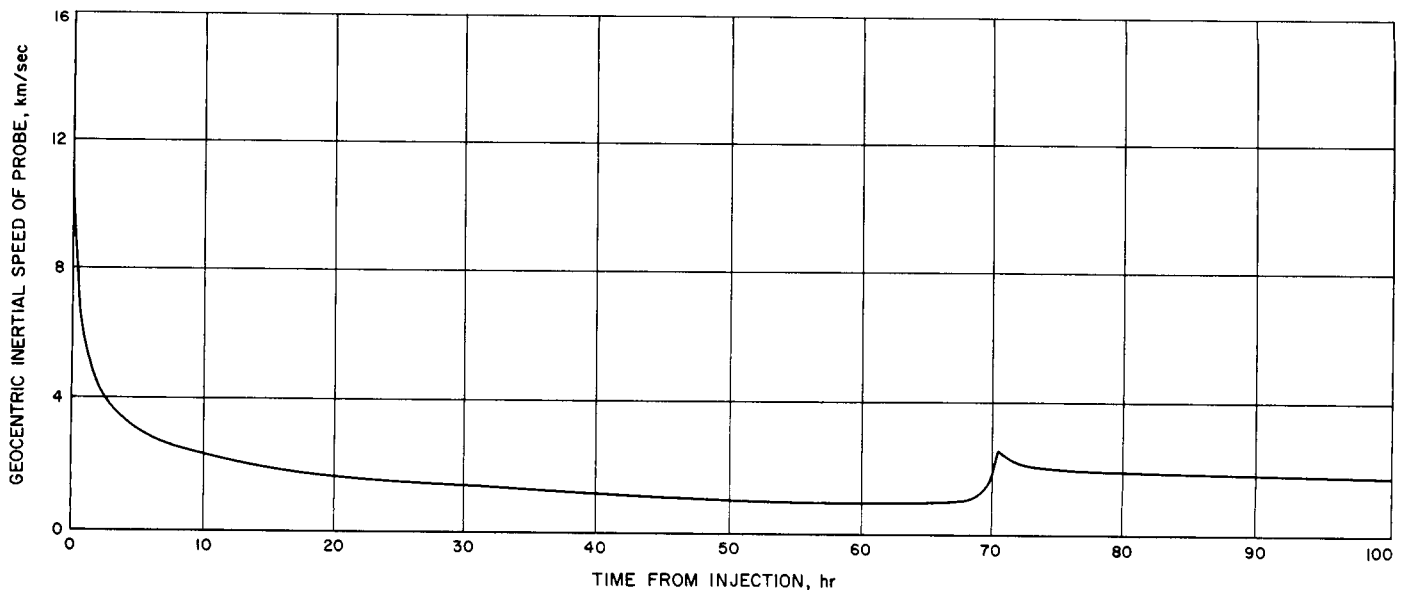


Fig. 12. Geocentric inertial speed of probe versus time from injection

through 15 show geocentric radii (distance to probe), geocentric inertial speed, Earth-probe-Sun angle, Earth-probe-Moon angle, and Sun-probe-Moon angle versus

flight time from injection to lunar encounter. At 63 hr past injection and 370,000 km from Earth, the speed of the spacecraft reached a minimum of 0.92 km/sec with

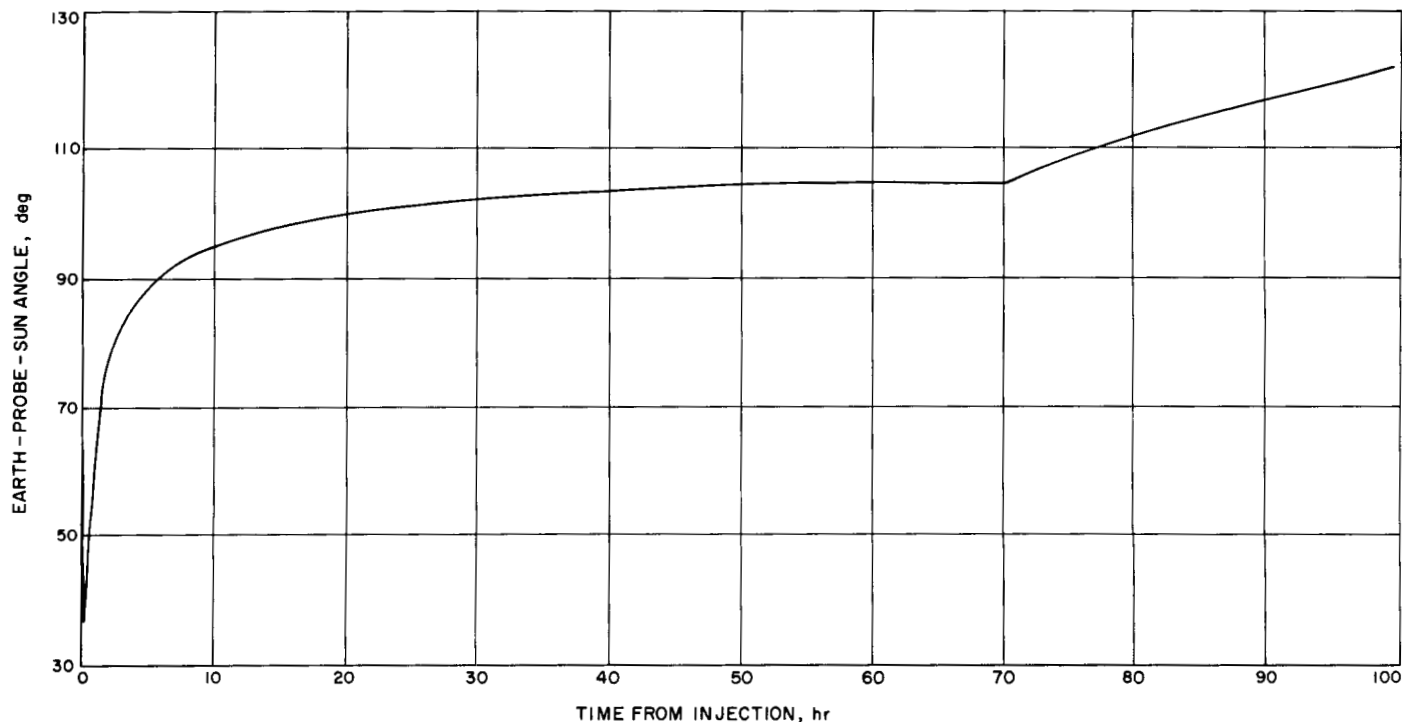


Fig. 13. Earth-probe-Sun angle versus time from injection

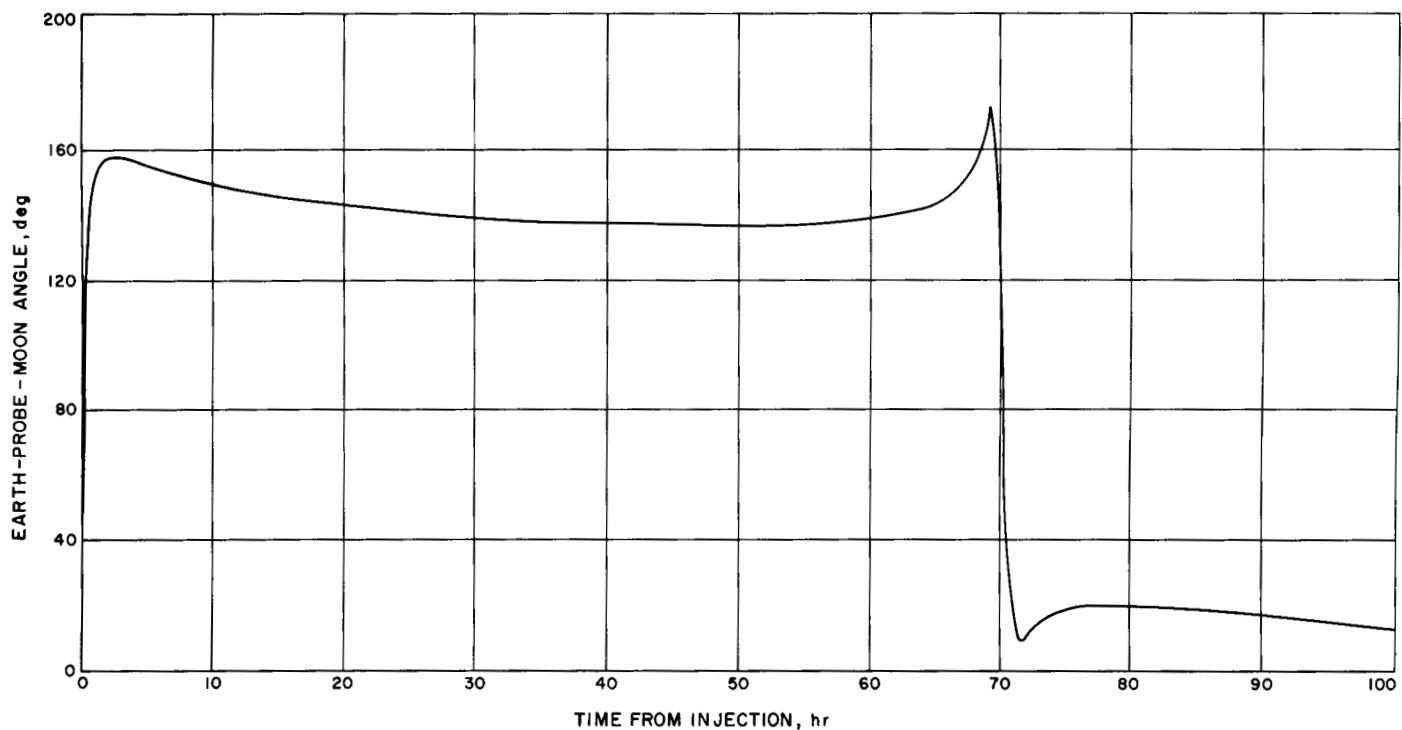


Fig. 14. Earth-probe-Moon angle versus time from injection

respect to Earth (Fig. 12). The spacecraft accelerated thereafter due to the gravitational influence of the Moon.

The geocentric postinjection orbit characteristics before and after lunar encounter are given in Table 1.

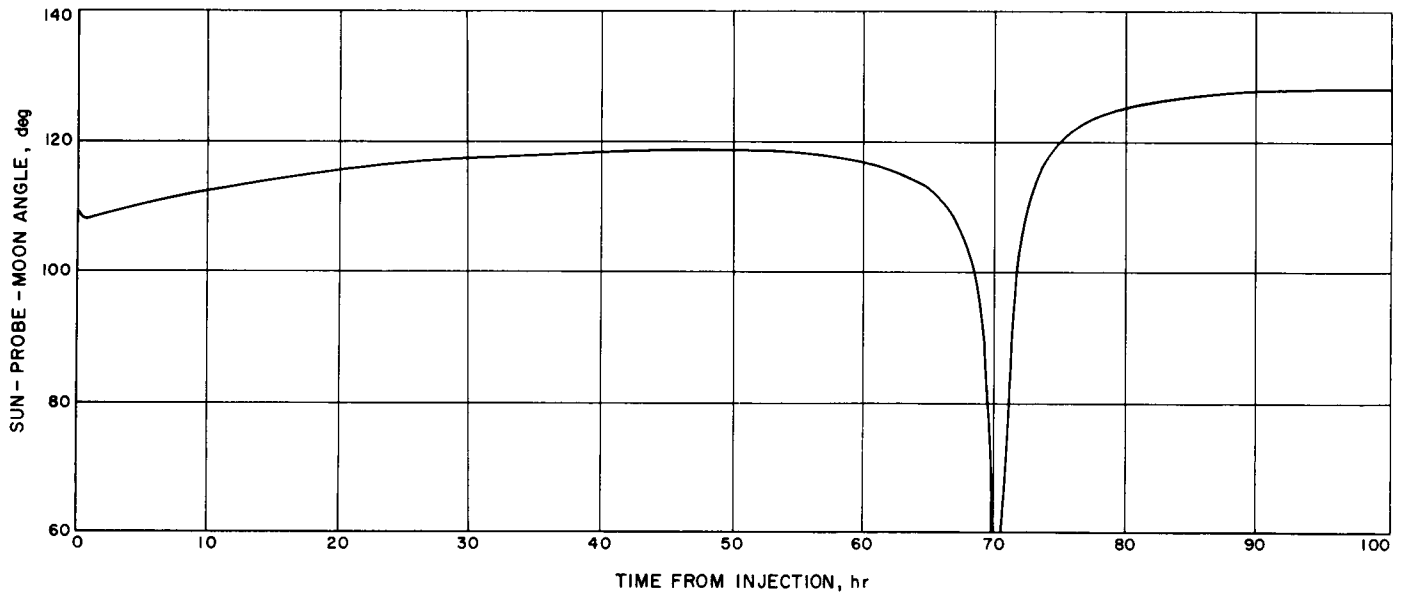


Fig. 15. Sun-probe-Moon angle versus time from injection

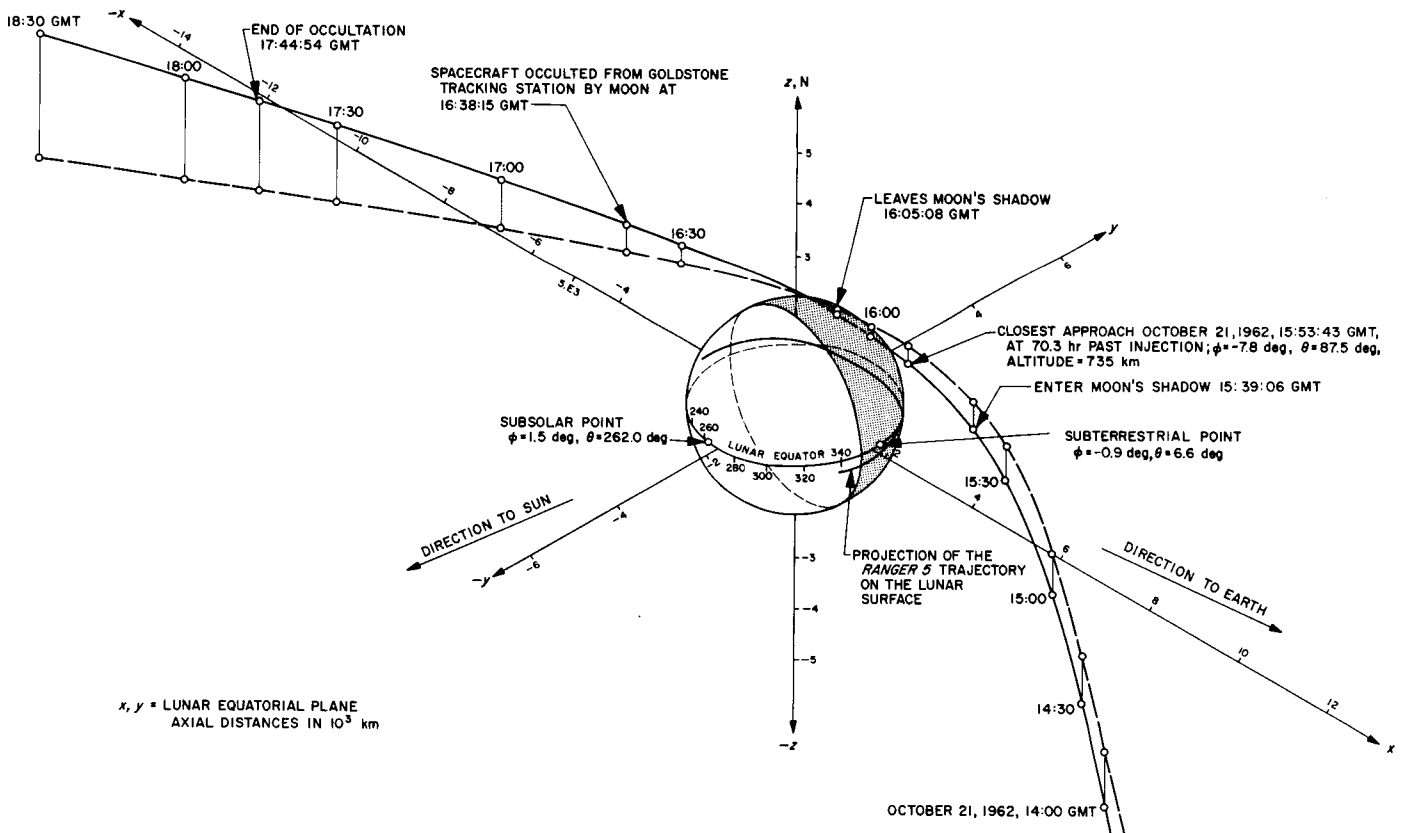
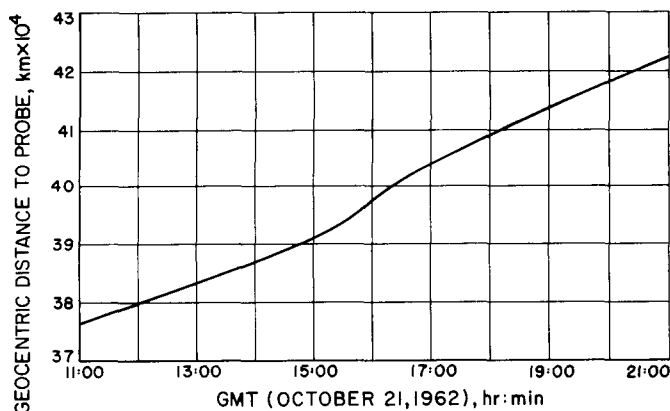


Fig. 16. Ranger 5 lunar encounter

### 3. Encounter Phase

On October 21, 1962, the spacecraft encountered the Moon, approaching in a hyperbolic selenocentric orbit with closest approach near the Moon's trailing edge. Fig. 16 shows the selenocentric geometry of the flight past the Moon and illustrates the position of the spacecraft as it passed through the Moon's shadow and later was occulted from Earth by the Moon. Closest approach occurred at 15:53:43 GMT, some 70.3 hr past injection, at a distance of 2473 km from the center of the Moon or



**Fig. 17. Geocentric distance to probe versus GMT time during lunar encounter**

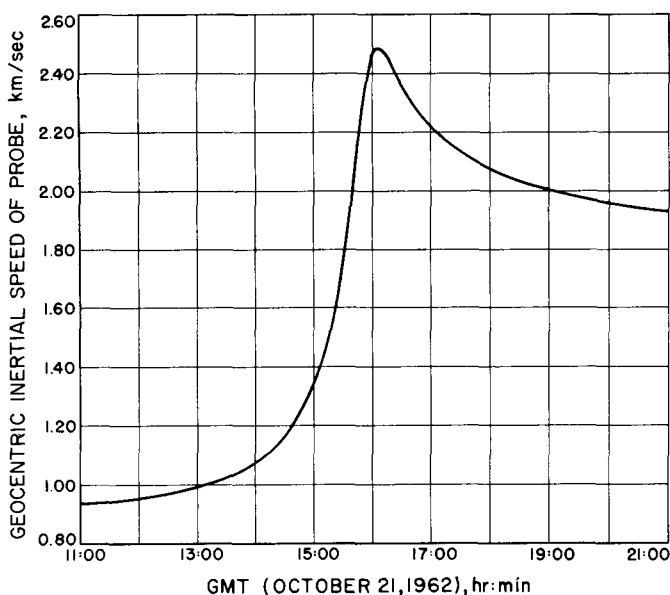


**Fig. 18. Geocentric inertial speed of probe versus GMT time during lunar encounter**

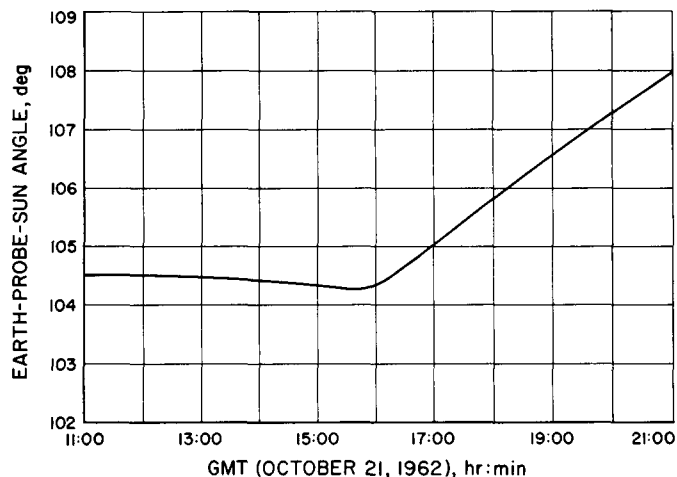


**Fig. 19. Earth-probe-Sun angle versus GMT time during lunar encounter**

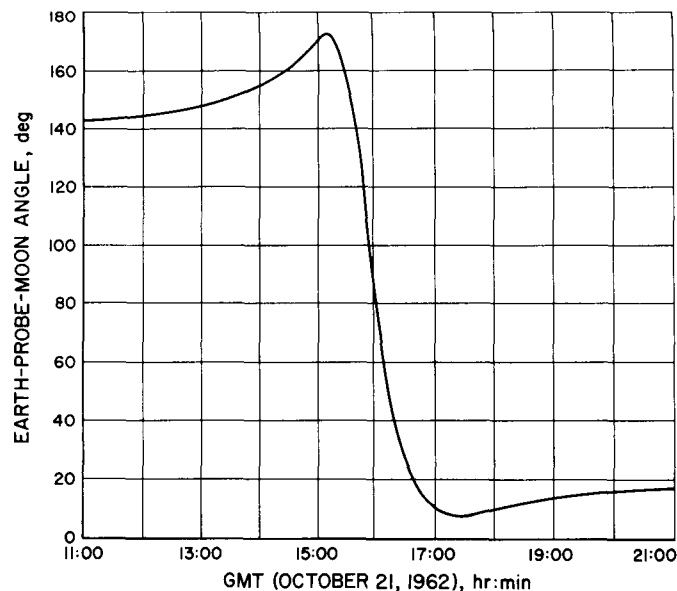


**Fig. 20. Earth-probe-Moon angle versus GMT time during lunar encounter**

735 km from its surface. Figs. 17 through 23 show the trajectory characteristics during lunar encounter, including geocentric radii (distance to probe), geocentric inertial speed, Earth-probe-Sun angle, Earth-probe-Moon angle, Sun-probe-Moon angle, selenocentric altitude, and selenocentric inertial speed versus GMT. Fig. 24 shows the time derivative of the range rate of the spacecraft as seen at the Goldstone Tracking Station. Because the Goldstone Tracking Station was recording the doppler



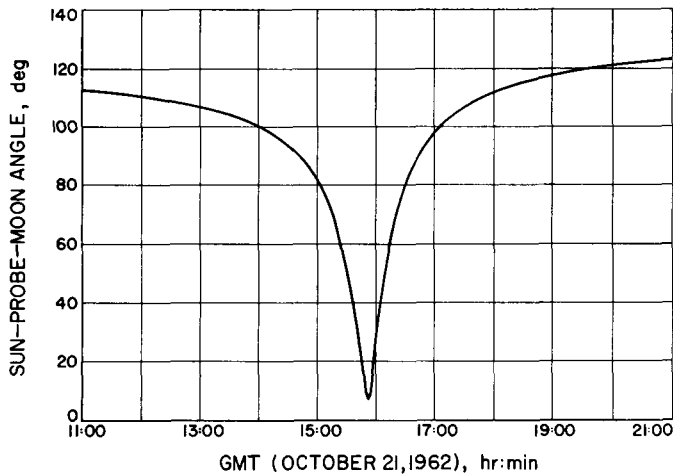


**Fig. 21. Sun-probe-Moon angle versus GMT time during lunar encounter**

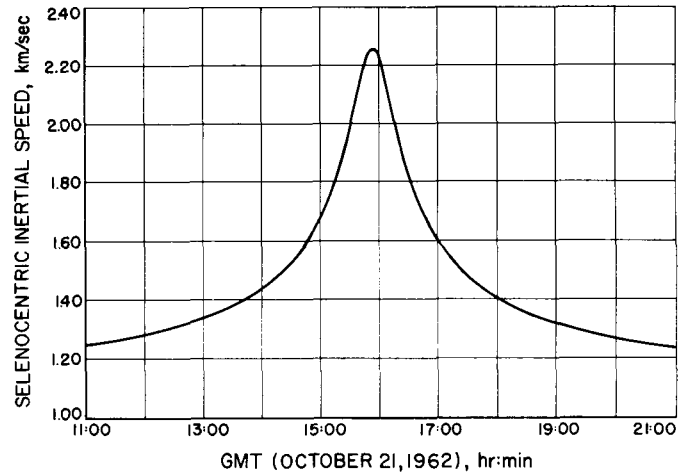


**Fig. 23. Selenocentric inertial speed of probe versus GMT time during lunar encounter**

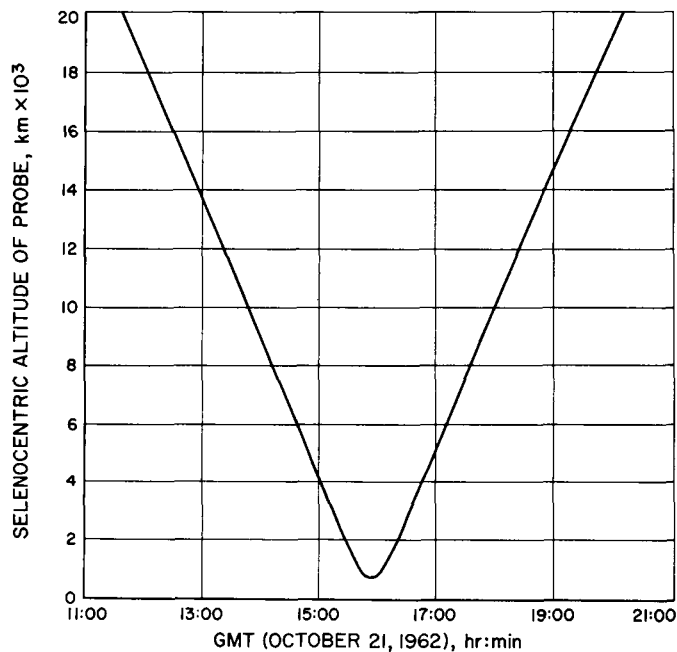


**Fig. 22. Selenocentric altitude of probe versus GMT time during lunar encounter**

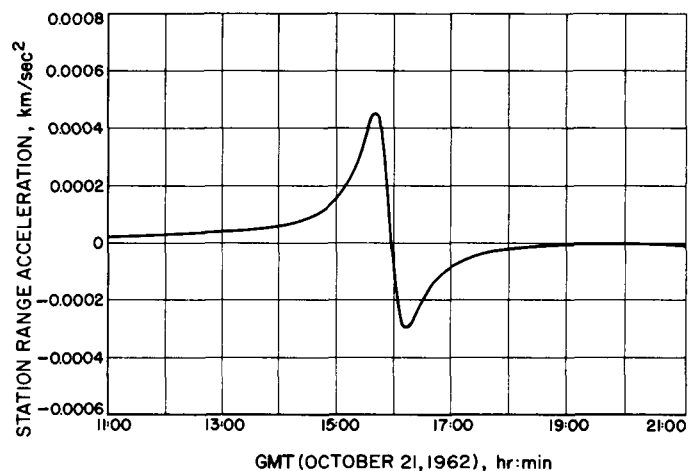


**Fig. 24. Range acceleration at Goldstone for the probe versus GMT time during lunar encounter**

signal from the capsule beacon during lunar encounter, the range rate derivative could be derived in spite of slow frequency drift of the capsule transmitter. The beginning and end of spacecraft occultation by the Moon were also observed. The capsule beacon was tracked until its signal reached DSIF threshold 11 days after launch. These data were most useful in determining the postmidcourse orbit. The selenocentric characteristics of the trajectory are shown in Table 2.

#### 4. Postencounter Phase

The Moon's gravitational influence altered the spacecraft's initial geocentric orbit during lunar encounter. This resulted in an increase in energy of the spacecraft relative to Earth, so that after lunar encounter the spacecraft's orbit became hyperbolic with respect to Earth. Note in Fig. 18 that an increase in geocentric inertial speed was effected by encounter. After lunar encounter the spacecraft was able to escape from the gravitational influence of the Earth-Moon system and become a satellite of the Sun in an elliptical orbit similar to the Earth's, but with greater eccentricity. The heliocentric elliptical orbit characteristics after lunar encounter are given in Table 3. The spacecraft reached a perihelion distance of

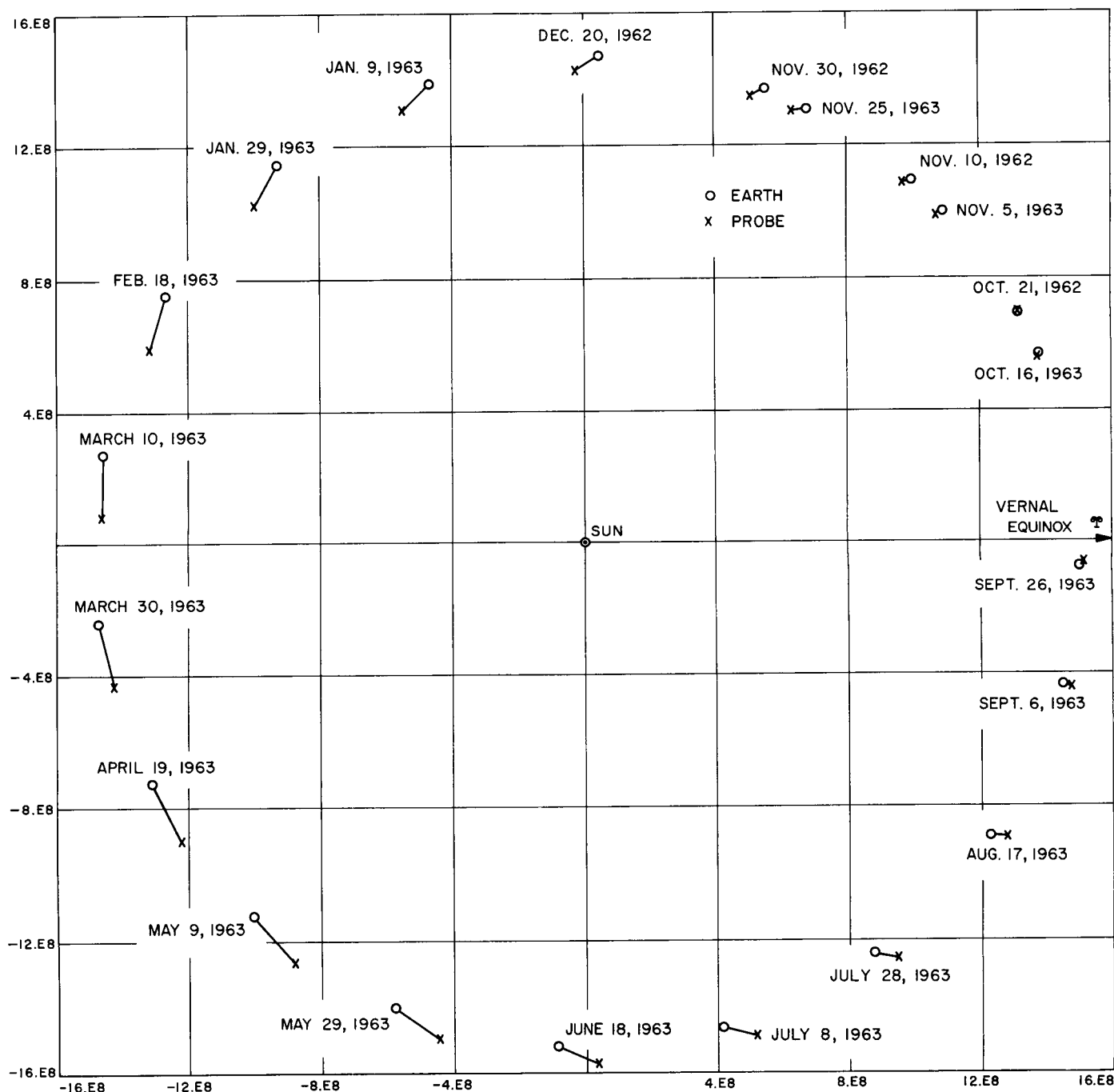


Fig. 25. Heliocentric orbits of Earth and Ranger 5

1,420,000 km on January 5, 1963. Fig. 25 shows the relative positions of the spacecraft and Earth through November 25, 1963, in their respective orbits about the Sun. In March 1963 the spacecraft was at its maximum distance of 20 million km from the Earth. Its geocentric distance will decrease until October 11, 1963, at which time the spacecraft will encounter the Earth with a

closest approach distance of 1.5 million km. The geocentric characteristics of the trajectory at encounter with Earth are listed in Table 1. Just as the geocentric orbit was altered by lunar encounter, the heliocentric orbit will be altered by the October 1963 geocentric encounter. The heliocentric orbit characteristics before and after encounter with Earth are given in Table 3.

## II. *Surveyor* Project

### A. Introduction

The objective of the *Surveyor* Project is to take the next step in advancing lunar technology by making soft landings on the Moon. Seven flights using *Centaur* launch vehicles are scheduled for 1964 and 1965. The objective within this period is to demonstrate successful soft-landing techniques by spacecraft operations subsequent to landing. The primary objective after 1965 will be to perform operations on the Moon which contribute new scientific knowledge and basic data in support of manned lunar landings.

The seven flights are divided into four test missions and three operational missions. The test missions carry engineering payloads and are directed towards progressive demonstration of the *Surveyor* capability up to and including soft landing. The three operational missions will carry a scientific payload of: two TV cameras, soil mechanics experiment, micrometeorite ejecta detector,

and the soil analysis group, which includes surface sampler, sample processor, X-ray diffractometer, and alpha-particle-scattering device.

Mechanical assembly of the prototype spacecraft has been completed, and testing of the installed components has begun.

### B. Spacecraft Development

Studies by Hughes Aircraft Company, the spacecraft development contractor, of the engineering payload to be flown on the four test missions are nearly complete, and the payload list is expected to be finalized in early June.



Fig. 1 (a). Match-mate test operations

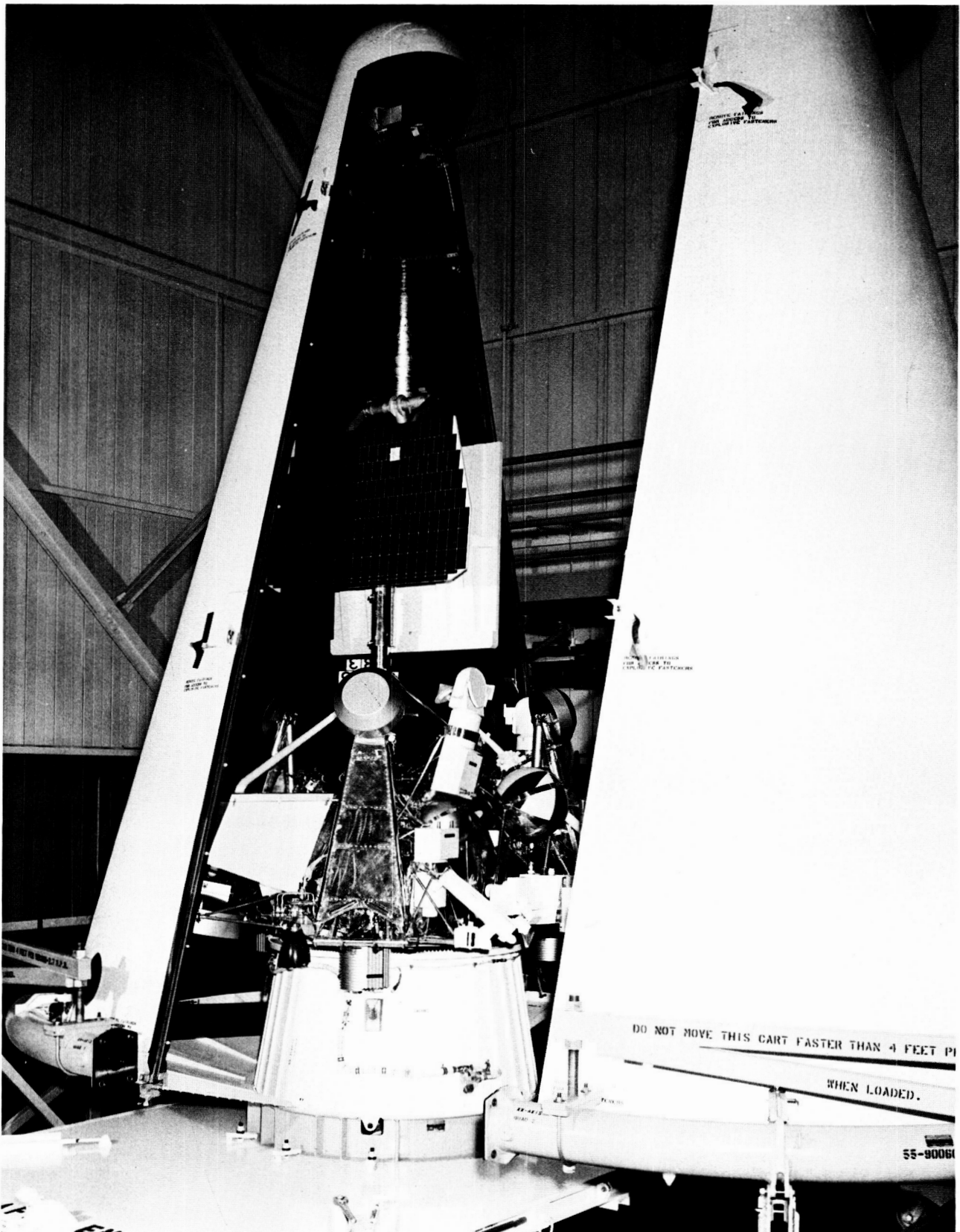


Fig. 1 (b). Match-mate operations showing engineering mockup spacecraft

Group testing of subsystems on the prototype spacecraft was suspended in mid-May to allow for preparation of the spacecraft for match-mate tests with *Centaur* hardware. The test, comprising a gross fit and compatibility check and a general simulation of preflight assembly and encapsulation operations, was first conducted using the full-scale spacecraft mockup (Fig. 1) and subsequently run with the prototype.

Helicopter flight tests of the radar altimeter and doppler velocity sensor, to be used in the descent-dynamics test program and, ultimately, in the controlled-descent phase of the *Surveyor* lunar approach, commenced late in April with promising results (Fig. 2). Operations at AFMTC with the descent-dynamics test spacecraft (see *SPS 37-19*, Vol. VI, pp. 19-21) are ex-

pected to resume in mid-June. The vernier engine system continues to be in the redesign phase of development by the subcontractor, using a new throttle valve developed at Hughes. A contract has been let by JPL to Space Technology Laboratories for development of a backup thrust chamber assembly, which will include the valve system.

The landing-dynamics drop test program has been successfully concluded, and the test spacecraft has been modified and shipped to General Dynamics/Astronautics for *Centaur*/spacecraft separation tests.

The spacecraft thermal mockup, Sector II (Compartment B, flight control sensor group), has completed initial tests in the JPL 25-ft Space Simulator with solar simulation. Measured temperatures in some areas were higher than predicted. The test setup is shown in Fig. 3.



Fig. 2. Helicopter flight test of landing radar for descent-dynamics test spacecraft

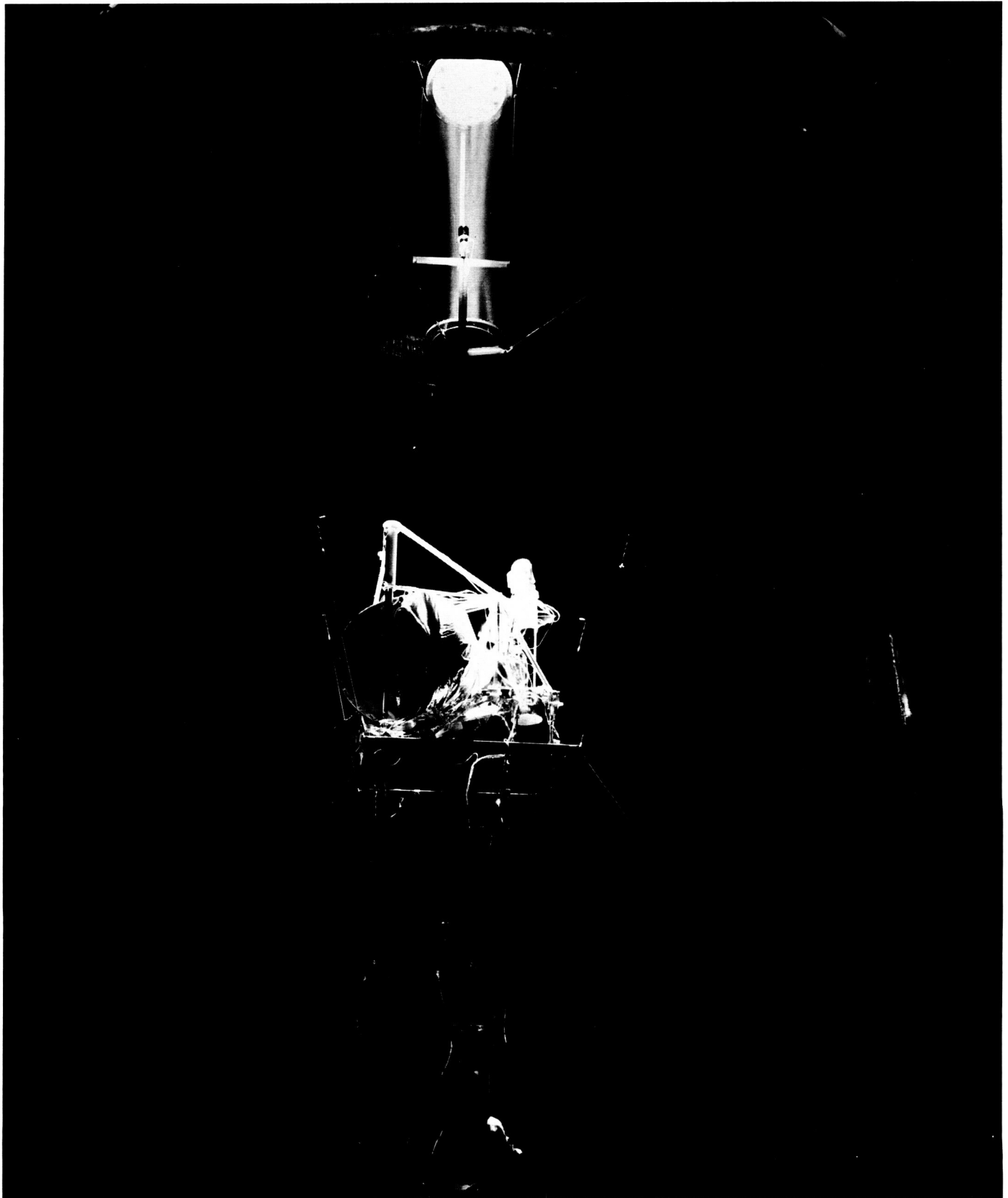


Fig. 3. Thermal mockup (Sector II) in JPL environmental test chamber

# THE PLANETARY-INTERPLANETARY PROGRAM

## III. *Mariner* Project

### A. Introduction

The decision to terminate the *Mariner* Venus 1962, 1964 efforts was made in January 1963. This decision was based upon the high degree of success obtained by *Mariner* 2. Much of the work being performed at that time was directly or partially applicable to the *Mariner* Mars 1964 or *Ranger* Projects, and transfer of efforts has been made. Presently, the only activity directly applicable to *Mariner* Venus is analysis of data resulting from the *Mariner* 2 flight; this work will continue into 1964. Work which had no application to other projects was cancelled.

The primary purpose of the *Mariner* Mars 1964 mission is to permit a biology-oriented scientific investigation of the planet Mars during the 1964 opportunity. Secondary purposes in order of priority are: (1) to make interplanetary scientific investigations in the region between the Earth and Mars orbits, (2) to develop additional experience in the design of spacecraft capable of conducting specific interplanetary missions, and (3) to provide experi-

ence and knowledge which will permit continued development of attitude stabilized spacecraft of the more advanced *Mariner* and *Voyager* types. The *Mariner* Mars spacecraft will be injected into Mars planetary transfer orbit by the *Atlas D* space booster/*Agna D* launch vehicle. Three identical spacecraft will be launched during the launch opportunity.

The *Mariner* Mars 1964 spacecraft detail design is being firmed with most decisions having been made regarding subassembly configuration, location, and electrical interfaces. Design specifications and control drawings are being released to detail these interfaces. The spacecraft estimated weight increased to an unacceptable limit requiring action to establish a maximum allowable weight of 570 lb. It was necessary to make some changes in the spacecraft configuration, including the interchange of some science experiment packages.

A meeting of the potential experimenters for the 1964 Mars mission was held at NASA Headquarters. This



resulted in recommendations for changes in the *Mariner* Mars 1964 science payload. These recommendations were carefully studied at JPL with regard to their influence on the spacecraft design schedule and configuration.

On November 5, 1962, a formal series of design evaluation vehicle (DEV) tests was begun using a *Mariner* Venus 1962 spacecraft. These tests were designed to provide additional information on anomalous operating conditions encountered on the *Mariner 2* flight and to investigate selected *Mariner* Venus 1962 design characteristics. (In addition, the tests are providing invaluable data needed for the *Mariner* Mars 1964 project.)

## B. Launch and Arrival Date Considerations

In 1964 at least two attempts will be made to launch a *Mariner* spacecraft on a flyby path to the planet Mars. The spacecraft will be launched by an *Atlas D-Agena D* booster. The purpose of the mission is to gather scientific data on the interplanetary environment between Earth and Mars as well as to take scientific measurements, including TV pictures, of the planet itself.

To increase the probability of a successful launch, a total launch period of 28 days, using Type I trajectories only, is being used for planning purposes.<sup>1</sup> The actual launch period utilized for the mission will probably be somewhat less than this, being ultimately determined by the final spacecraft weight and launch vehicle performance capability. During the launch period, two shots will be attempted from two separate launch pads. On the first available launch day, countdowns will be conducted simultaneously on both vehicles.

At a predetermined time in the simultaneous countdowns, probably a few hours before lift-off, and if both vehicles are still in a ready condition, one of the countdowns will be suspended. Two days after launch of the first vehicle, the countdown on the second vehicle will begin again.

<sup>1</sup> At the present, Type II trajectories are being considered for inclusion in the mission. If they prove to be feasible, the launch period will be extended to 35 days or more, and a third launch will probably be utilized. Type I trajectories are those along which the spacecraft traverses less than 180 deg in heliocentric space from launch to encounter. For Type II trajectories the spacecraft traverses more than 180 deg but less than 360 deg from launch to encounter.

Since either launch may occur on any day of the launch period, two trajectories will be provided for each launch date with fixed arrival dates separated by 5 days. The 5-day separation at encounter is necessary to simplify the operations during the critical encounter portion of the flight. On the first attempted launch date, when simultaneous countdowns are being conducted, each vehicle will utilize the same arrival date trajectory so that the same injection loci will be used no matter which vehicle is launched. If the first launch is successful, the second launch will use the remaining arrival date for the duration of the launch period. If the first shot is unsuccessful, the second launch will use whichever arrival date is most suitable.

## C. Spacecraft Design

### 1. Configuration

A major change in the complement of scientific experiments aboard the *Mariner* Mars 1964 spacecraft has occurred since the reporting in SPS 37-20, Vol. VI. This has resulted in some rather significant changes to the over-all spacecraft configuration. In addition, the continued evolution of the detail design of the spacecraft has permitted better definition of the location of some of the smaller spacecraft components.

The *Mariner* Mars 1964 spacecraft configuration is currently shaped to accommodate the following scientific experiments:

- (1) Helium vapor magnetometer.
- (2) Cosmic dust detector.
- (3) Ion chamber.
- (4) Trapped radiation detector.
- (5) Low energy plasma detector.
- (6) Cosmic ray telescope.
- (7) Television camera.
- (8) Ultraviolet photometer.

Of this list, the trapped radiation detector and the cosmic ray telescope are additions to the previously considered complement of experiments. Of the remainder, the ultraviolet photometer is being accommodated in

place of the infrared grating spectrometer, and a low energy plasma experiment, developed by MIT, will be flown in place of the JPL plasma probe.

The trapped radiation detector will consist of four detector tubes mounted to an electronic package. In order to accommodate view requirements and package size, this instrument will be mounted on the upper octagonal ring of the basic spacecraft structure in Bay IV as close as possible to Bay III, which contains the scientific data system.

The cosmic ray telescope will consist of a counter telescope attached to a standard size electronic subassembly. The subassembly will be located in the science bay (Bay III) immediately adjacent to the lower octagonal structural ring. An opening in the octagon support ring will provide an unobstructed view for the counter telescope.

The MIT low energy plasma detector cup will be mounted on the upper octagonal ring directly above Bay III. A pigtail from the cup will be routed directly to the associated electronic package immediately below the instrument.

The ultraviolet photometer will be mounted on the planet science scan platform in the position previously provided for the infrared instrument. The ultraviolet instrument is generally less restrictive, mechanically, than the infrared instrument and presents no special spacecraft configuration problems.

As reported previously, the magnetometer sensor and ion chamber are located on the low-gain antenna waveguide. Pattern tests on both the low- and high-gain antennas have progressed sufficiently to allow the determination of the tube elevations at which these instruments may be mounted.

Detailed design of the pedestals required to support the square root Sun sensors on the top of the spacecraft has permitted detailed definition of mounting locations for the Earth detector and Sun gate. The Earth detector will be mounted to the side of the pedestal located above Bay VI. The Sun gate will be mounted to the back of the pedestal above Bay II.

In the interest of minimizing weight a new approach will be used to actuate the four solar panels. This scheme utilizes a separate spring on each panel to provide the opening torque and a central speed retarder to control

the opening speed of all four panels. The central retarder will be mounted at the top of the superstructure truss on the spacecraft centerline. A cable will connect the retarder to each solar panel for transmitting the retarding force.

## 2. Booster Interface

Final design of the items in the spacecraft/*Agna D* interface area has begun. The interface configuration remains essentially as shown in Fig. 1. Both the clam-shell shroud and the over-the-nose shroud are being designed; only the former is shown in the figure.

With the exception of the shroud design, the only significant problem areas as yet unresolved are the low-gain antenna coupler, spacecraft umbilical and inflight disconnect connectors, and the *Agna* diaphragm. Lockheed Missiles and Space Company, Sunnyvale, California, has developed a beam-supported diaphragm design which appears adequate except for its high weight of approximately 12 lb. Another minimum weight design is being evaluated which would have the diaphragm tied down to both the center and outer edge of the *Agna D* forward equipment rack.

## 3. Structural Problems

A major *Mariner* Mars 1964 structure design goal was to achieve a significant structural weight reduction. By pursuing a more integrated design and utilizing point damping, the structural weight fraction has been reduced to approximately 15% of the gross spacecraft weight (from approximately 25% on *Mariner 2*).

This reduction in weight has been obtained in many cases by utilizing thin-gage material. This has produced two major nonstructural problems: (1) the heat conducting capability of these structures has been reduced, and (2) improper handling of these structures can cause severe damage. The first problem has necessitated adding more material in certain areas to restore adequate heat conducting capacity. The second problem has required that special handling techniques be developed and special storage and shipping fixtures be fabricated.

The integration of gas system into the structure is an example of another type of operational and handling problem. The attitude control system will include a welded plumbing system which must be installed in the spacecraft as a unit. The gas weight requirements have been reduced by locating the jets as far as possible from the center of gravity on the solar panel tips. Because the

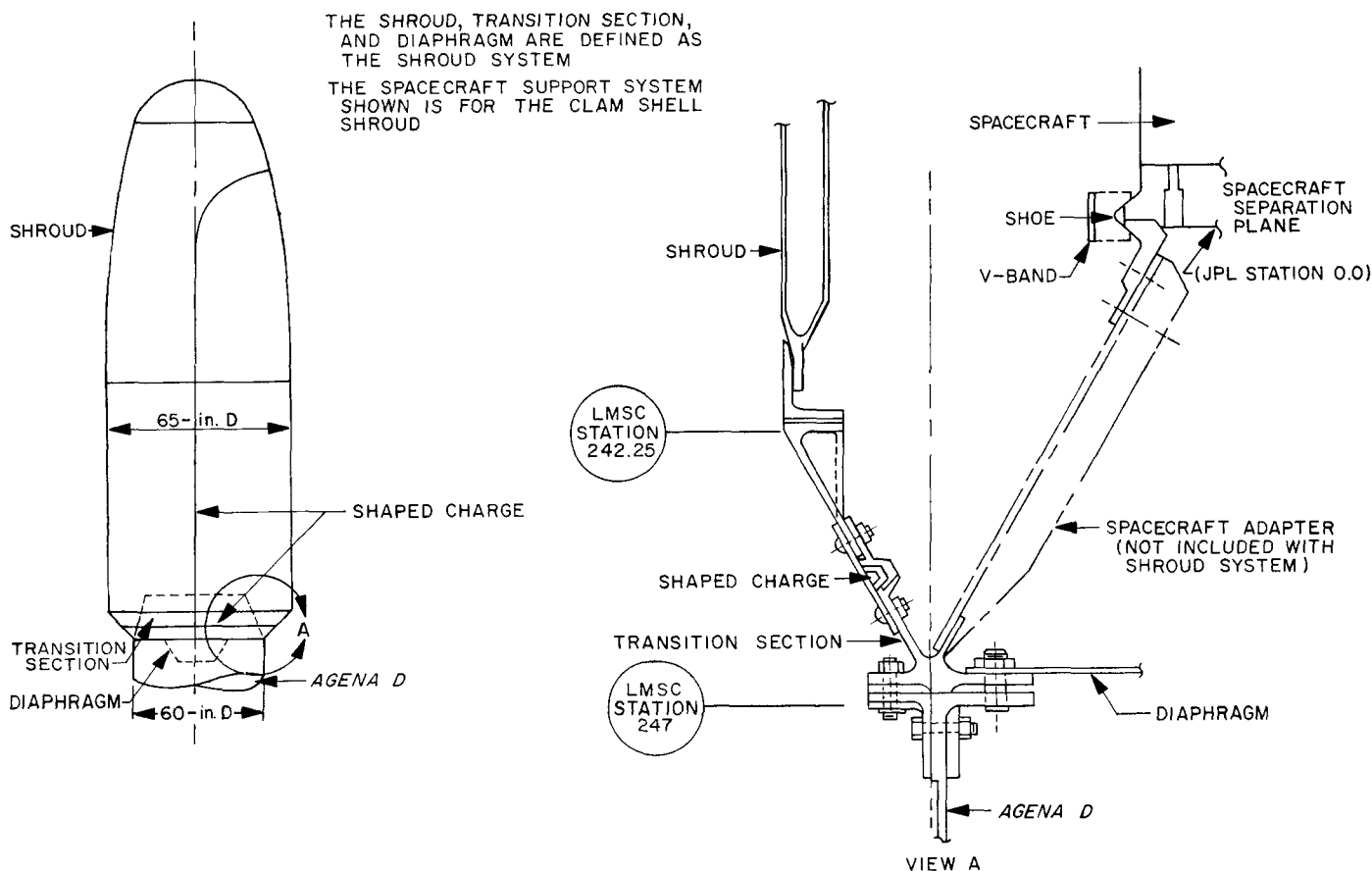


Fig. 1. Spacecraft support system nomenclature

panels are not on the spacecraft at all times, auxiliary support structures must be provided to support the plumbing and jets during the JPL Spacecraft Assembly Facility test operations and when shipped to the Atlantic Missile Range.

#### 4. Temperature Control

Extensive testing of the *Mariner* Mars 1964 temperature control model is planned during the last quarter of 1963.

Since these tests will provide the principal data for the determination of the adequacy of the *Mariner* Mars 1964 thermal design, the sources of experimental errors are of concern. The recognized errors in the solar simulation can be classified as those errors associated with: (1) the less-than-solar collimation or parallelness of the light, (2) the uniformity of the intensity of the light over the test volume, including reflections from the chamber optics, and (3) a non-solar spectral distribution of the light's energy. It is this third source of error that led to the

design of an absorptance standard to be flown on *Mariner* Mars spacecraft.

Four of the *Mariner* Mars 1964 flight temperature measurements have been modified to secure the absorptance of selected surfaces used on the spacecraft. This data will contribute to the interpretation of thermal flight data as well as solar simulator data. The variations in the absorptance resulting from long-term exposure of surface coatings to the solar spectrum and high vacuum conditions also may be deduced from these measurements.

The design of the flight standard is similar in principle to an instrument used to measure the absorptance of surface coatings to various arc sources. A cross section of the absorptance standard is shown in Fig. 2. The standard consists of a sample surface which envelops a temperature transducer and two thermostatic switches. The sample is supported and partially encased in a plastic shell which is fastened to a base plate. Internal radiation energy exchange is reduced by reflective shielding.

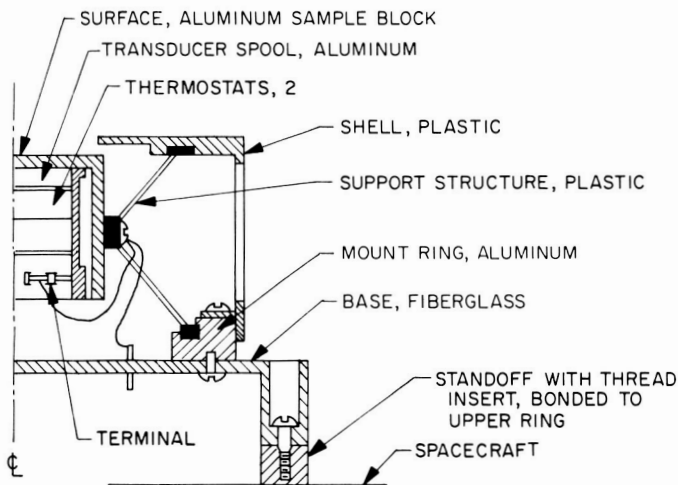


Fig. 2. Temperature control absorbance standard

The thermostatic switches are for the purpose of providing a more accurate in-flight temperature calibration than can be obtained through the telemetry system. The standard requires no electrical power and appears as a typical temperature measurement to the telemetry system. The sample temperature will drop during transit to Mars due to a decrease in the solar intensity. At pre-set temperatures the thermostats will switch the signal level of the platinum wire transducer, thus providing the required in-flight calibration. The design of the standard is complete and prototype hardware is being fabricated.

### 5. Power Subsystem

The *Mariner Mars 1964* power subsystem represents an extension of the technology developed on the *Mariner 2* program. Considerable effort is being expended in the improvement of the design features and fabrication techniques for the solar panels. Extensive prototype panel testing is now planned. For the same weight as the *Mariner 2* battery, the *Mariner Mars 1964* battery should have 33% greater capacity. The major difference between *Mariner 2* and *Mariner Mars 1964* will be in the mechanization of the power subsystem. As was discussed in SPS 37-20, Vol. VI, the *Mariner Mars 1964* will use a redundant booster-regulator and two 2.4-kc inverters. The power subsystem will also incorporate switching and logic functions both for the effective management of spacecraft loads and the proper utilization of the redundant booster-regulator. The power subsystem telemetry measurements have been selected to provide the necessary intelligence for the management of spacecraft system loads by ground command, if required.

*a. Solar panels.* Space Technology Laboratories (STL) has been selected to manufacture the *Mariner Mars 1964* flight solar panels. It is planned that two prototype and four type approval panels will be constructed and tested prior to the fabrication of flight solar panels. Two of the type approval panels, T/A-3 and T/A-4, will be constructed by STL.

Presently, three types of cell interconnection techniques are under evaluation for the first prototype panel. These are shown in Fig. 3. The lower group of cells are of the Mark IV configuration in which connection to the P-contact of the cells is made after the cells have been mounted on the panel. In the two groups of cells labelled B and A, the P contacts are paralleled prior to mounting the module on the panel. These two groups have exhibited a decided advantage: it is possible to reduce the number of operations necessary after the submodules are mounted on the panel when cleaning and cell repairs are relatively difficult.

A prototype structure of the *Mariner Mars 1964* panel has been delivered to JPL by the manufacturer, Ryan Aerospace Corporation. Two  $7 \times 21$  cell assemblies of each of the three types of submodules have been mounted on this panel, including a mock-up of the required panel harnessing. Pieces of aluminum, simulating the weight and size of solar cell assemblies, were bonded to the remainder of the panel surface. The completed panel is shown in Fig. 4.

The power input to the power regulator assembly from the solar panels will be maintained below 50 v dc by a zener diode shunt regulator. The Dickson Electronics Corporation zener 50SZ7.5D has been tentatively selected

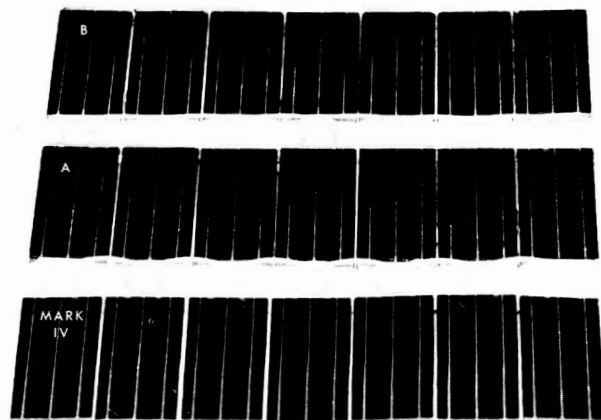


Fig. 3. *Mariner C* solar panel cell interconnection evaluation submodules

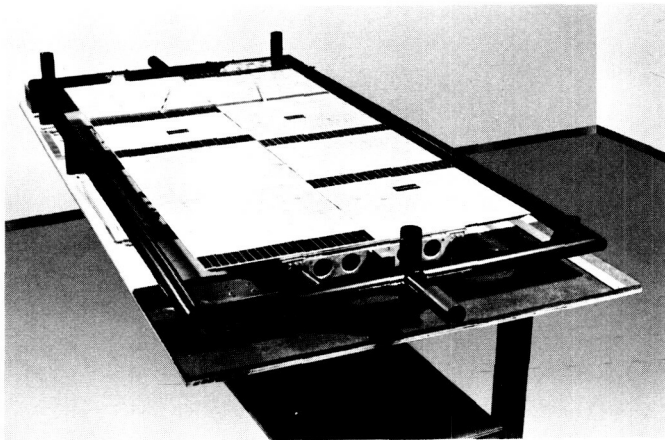


Fig. 4. Mariner Mars 1964 prototype solar panel

for use in the *Mariner* 1964 shunt regulator. Six of these units would be connected in series across each section of the power source. The zeners will be mounted on the underside of the spar assemblies of the panels and will depend upon heat sinking to the panel and radiation to space of the power dissipated in the diodes for temperature control.

**b. Battery.** Table 1 lists *Mariner* Mars 1964 battery characteristics in comparison to the battery flown in *Mariner* 2.

The temperature profile of the battery for the *Mariner* Mars 1964 mission is shown in Fig. 5. Fig. 6 shows how

Table 1. Battery characteristics

Detail	<i>Mariner</i> 2	<i>Mariner</i> Mars 1964
Weight, lb	33	33
Number of silver-zinc cells	18	18
Voltage regulation, v	25.8–33.3	25.8–33.3
Maximum voltage on charging, v	36.0	36.0
Minimum capacity, w-hr	900	1200
Maximum load current, amp	18	10
Maximum charging current (flight), amp	1.0	1.0
Maximum charging current (GSE), amp	2.0	2.0
Expected operating temperature, °F	50–140	40–120
Storage life at 30–50°F, yr	1	1
Charge/discharge cycles	5 or more	5 or more
Battery isolation	Diodes and fuse	Diodes and fuse
Orientation of cells on Earth	9 cells inverted	None inverted
Cells per molded unit	5	3
Capacity loss per month at 90°F, %	4	1

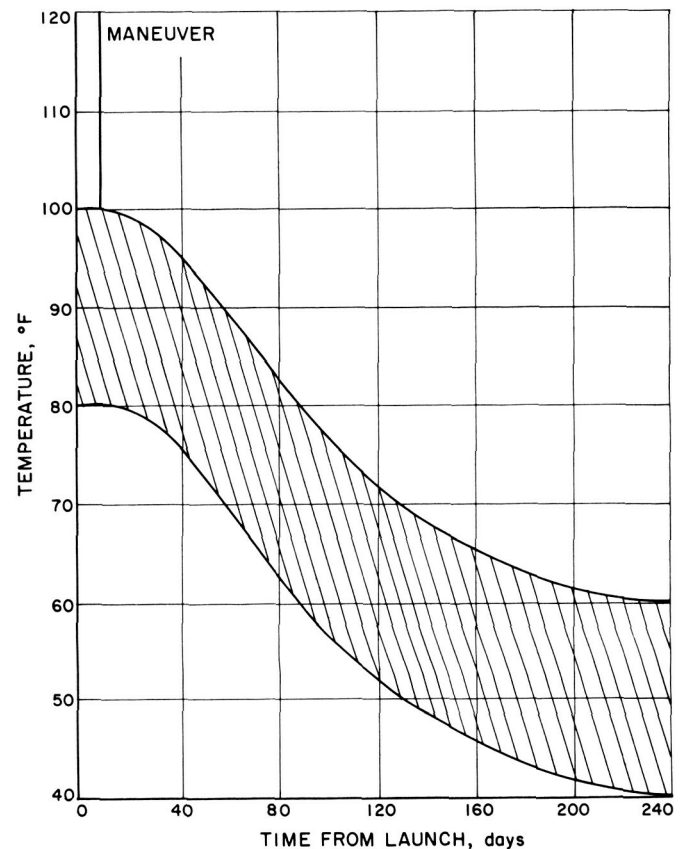


Fig. 5. Mariner Mars 1964 battery temperature estimate

retention of battery capacity varies with temperature under storage conditions. Thus, during the last months of the flight, the battery charger may be turned off, if this power is needed for other purposes, without losing more than 1 or 2% of the battery capacity.

Since the *Mariner* Mars 1964 battery is quite similar to the one flown on the *Mariner* 2 with regards to its temperature characteristics, a 9-cell *Mariner* 2 type monoblock is being tested under a *Mariner* Mars 1964 temperature profile. The purpose of this experiment is not only to observe the temperature responses during the 240-day simulated flight but also to determine the power sharing capabilities at planet encounter. The monoblock has performed normally through the launch, acquisition, and midcourse phases, and is now in cruise mode. As of April 24, 117 days of flight had been completed. The upper limits of the temperature band of Fig. 5 are being followed for this flight. At the end of an 8-month simulated mission, the monoblock temperature will be dropped from 60°F to a worst case condition of 40°F, and the battery will be discharged to depletion in the share mode.

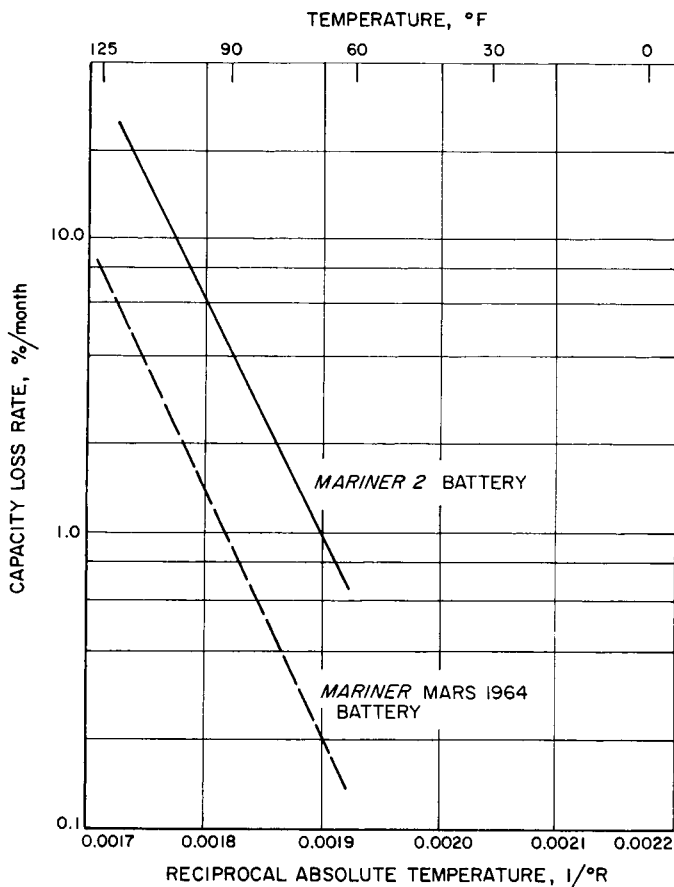


Fig. 6. Preliminary estimate of storage loss for Mariner Mars 1964 batteries

**c. Electrical conversion equipment.** The electrical conversion equipment for the Mariner Mars 1964 spacecraft is contained in two assemblies. The primary input power from the solar panels and battery is first routed to the power regulator assembly, Case VIII. Regulated DC power from Case VIII is then routed to Case I, the power assembly, so that the inverters will provide the various types of power used on the spacecraft.

**Booster characteristics.** The booster regulator is a switched-mode feedback regulator. A magamp operating from an amplified error signal is used to control base drive pulse width to a pair of power transistors. These transistors, which operate in a push-pull amplifier circuit, boost the input voltage when switched on. The resulting quasi-square wave is added to the input voltage. This wave shape is filtered to yield a constant 52 v dc.

**Booster switching.** Under normal flight conditions the main booster will handle all cruise and encounter loads while the maneuver booster supports maneuver loads. If the main booster fails, the maneuver booster will be

switched to handle all spacecraft loads as indicated in Fig. 7. The switching action is initiated by a tolerance detector. If, for a period of 10 sec, the output of the main booster is greater than 58 v or less than 43 v, the tolerance detector will energize relays which remove the main booster from the circuitry and replace it with the maneuver booster.

## 6. High-Gain Antenna

The high-gain antenna is attached to the spacecraft in a fixed position such that its maximum gain is in the direction of Earth at planet encounter. The antenna will be a 46- by 21.2-in. paraboloid, elliptical in planform. The parabolic sector was chosen in preference to a circular parabola of the same gain because of improved performance both at the low-gain antenna-high-gain antenna switch over portion of the spacecraft flight and at the post-encounter region.

A dual cup turnstile feed (Fig. 8) is used to illuminate the sector. The dual cup ground plane establishes very low ellipticity over the illuminating region, which consequently produces low ellipticity over the sector's main beam. The illumination taper, including space loss correction around the edge of the sector, is a nearly constant 11 db.

Gain optimization of the feed reflector combination was accomplished by pattern and gain comparison methods in conjunction with feed focal position adjustments. Fig. 9 shows the prototype sector and standard gain horn mounted in test position.

Two identical prototype sectors are presently under construction using flight configuration feed support structure and dual cup ground plane. A confirmation of the measure gain will be made by an identical antenna gain measurement setup. Delivery of a type approval feed for assembly in the sector is scheduled for July 1963.

## 7. Celestial Sensors

**a. Canopus tracker.** The Mariner Mars 1964 Canopus tracker has two basic functions. The first is to provide roll error signals on Canopus during the cruise mode. Canopus must be acquired for pointing the high-gain antenna back to Earth. The second function is to provide a celestial reference upon which to base the midcourse maneuver.

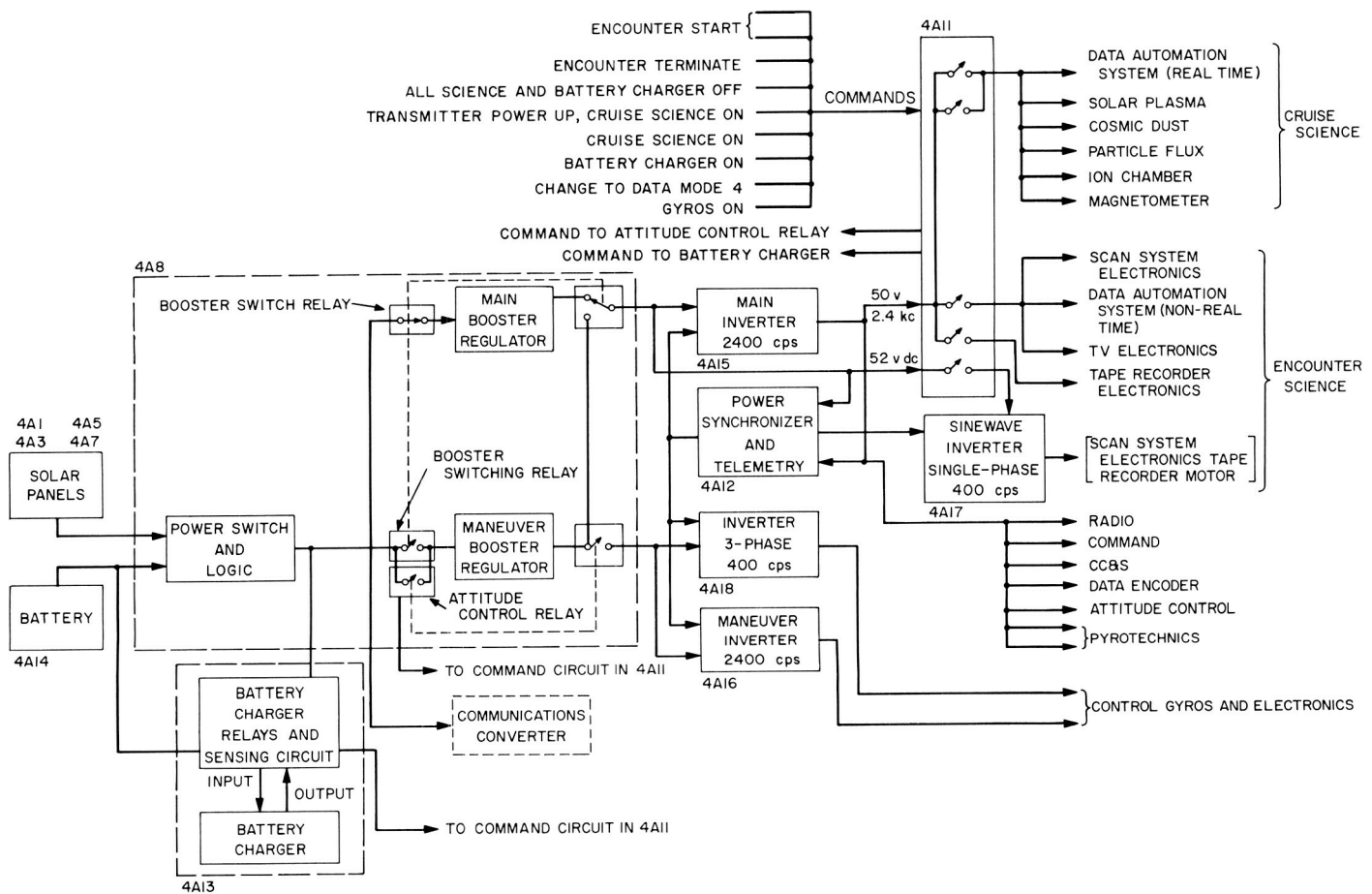


Fig. 7. Mariner Mars 1964 power subsystem functional block diagram

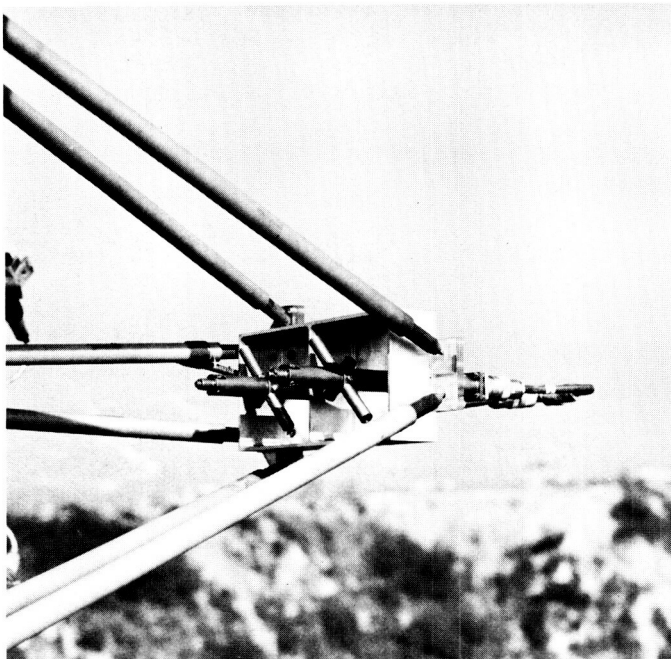


Fig. 8. Dual cup turnstile feed

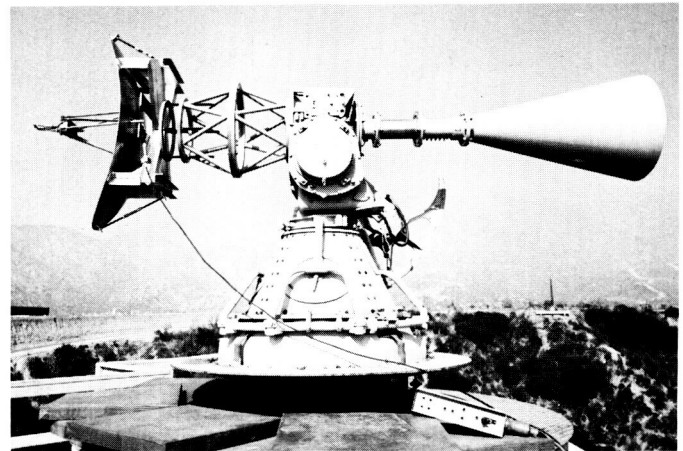


Fig. 9. Prototype sector and standard gain horn in test position

The most difficult problems involved in building the Canopus tracker system are the problems of acquisition and recognition. The problem of acquisition is intimately involved with the whole roll attitude control system.



The position of Canopus is described by its cone angle from the Sun and its clock angle about the probe-Sun line (which is defined as zero with the clock angle of all other objects measured from Canopus; Fig. 10). The field of view of the tracker is limited in cone angle to approximately 11 deg. Therefore, as the spacecraft rolls about the Sun line many stars are excluded as possible targets for acquisition. The 11-deg field of view is gimballed electronically to follow Canopus through a total excursion of 28 deg in cone angle. Decreasing the field of view decreases the length of time a given star has the proper cone angle. Fig. 11 is a bar graph comparing the number of acquirable targets other than Canopus as a function of time for a 32-deg field of view with the 11-deg one used.

The 11-deg field-of-view plot in Fig. 11 serves to illustrate that automatic acquisition and recognition will not be achieved by the Canopus tracker. The star Achernar (illuminance =  $0.43 \times$  Canopus, clock angle 40 deg) is the one object preventing automatic initial acquisition. Achernar has been accepted as a target which cannot be discriminated against without compromising reliability and unduly increasing complexity. A clockwise roll search will be used to make the probability of acquiring Achernar before Canopus equal to approximately 0.1. Two telemetry channels will be prime factors in deciding what target has been acquired. First will be the star brightness readout which will be calibrated to our laboratory standard. As the spacecraft searches for an acquirable target, the brightness of objects in the field of view will be recorded on the ground approximately every 1.2 deg. From this a star map can be made which will be extremely useful in deciding what target has been acquired even if the absolute brightness calibration is not perfect. The second is a channel which monitors the output of a photoconductive Earth gate. The field of view is such that the Earth will be detected only if Canopus is the target acquired by the tracker. Once a target has been acquired, recognition will be a ground-based decision.

The acquisition gate provides a logic signal which discriminates against objects that differ markedly from Canopus in brightness. However, false acquisition signals occur over an off-null angular region for a very bright object because the apparent brightness falls within Canopus brightness range. Extremely bright objects may also cause inverted phase error signals. If this is left uncorrected, the resultant roll motion may be a high-velocity limit cycle with very rapid gas consumption.

To avoid the problems presented by very bright objects causing inverted error signals, logic in addition to the ac-

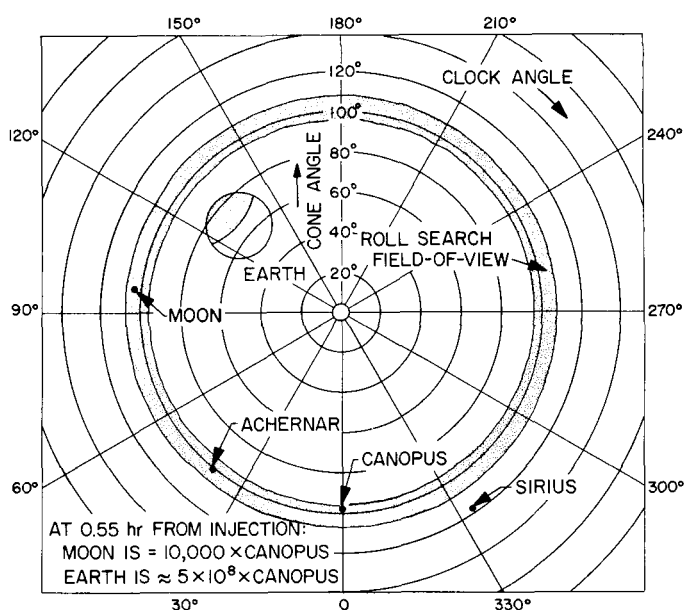


Fig. 10. Trajectory geometry at time of acquisition

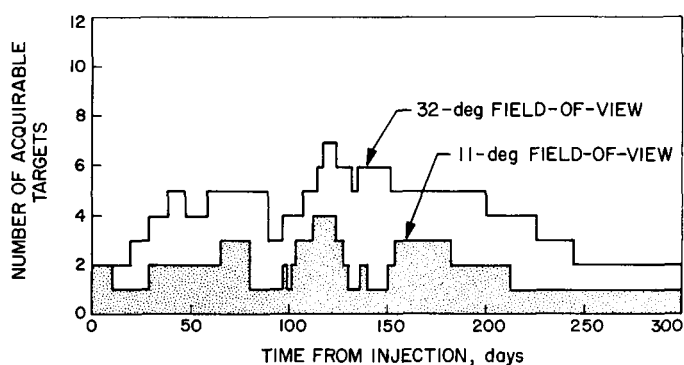


Fig. 11. Star tracker acquirable targets for the Mars mission

quisition signal is required. The additional logic is based on inhibition of the acquisition signal by a roll error signal polarity detection. The mechanization is relatively simple and reliable if unidirectional roll search is employed. Unidirectional roll search has inherent noise rejection properties, i.e., spurious acquisition signals and very narrow field-of-view objects are automatically rejected.

The electronic circuitry of the Canopus star tracker has been designed to take full advantage of the unique characteristics of the image dissector tube. The image dissector tube (Fig. 12) consists of a spherical S-11 photocathode surface followed by an electrostatic focusing electrode and a set of spherical electron optics orthogonal deflection plates and a precision aperture. The deflection system is in a vacuum envelope with a con-



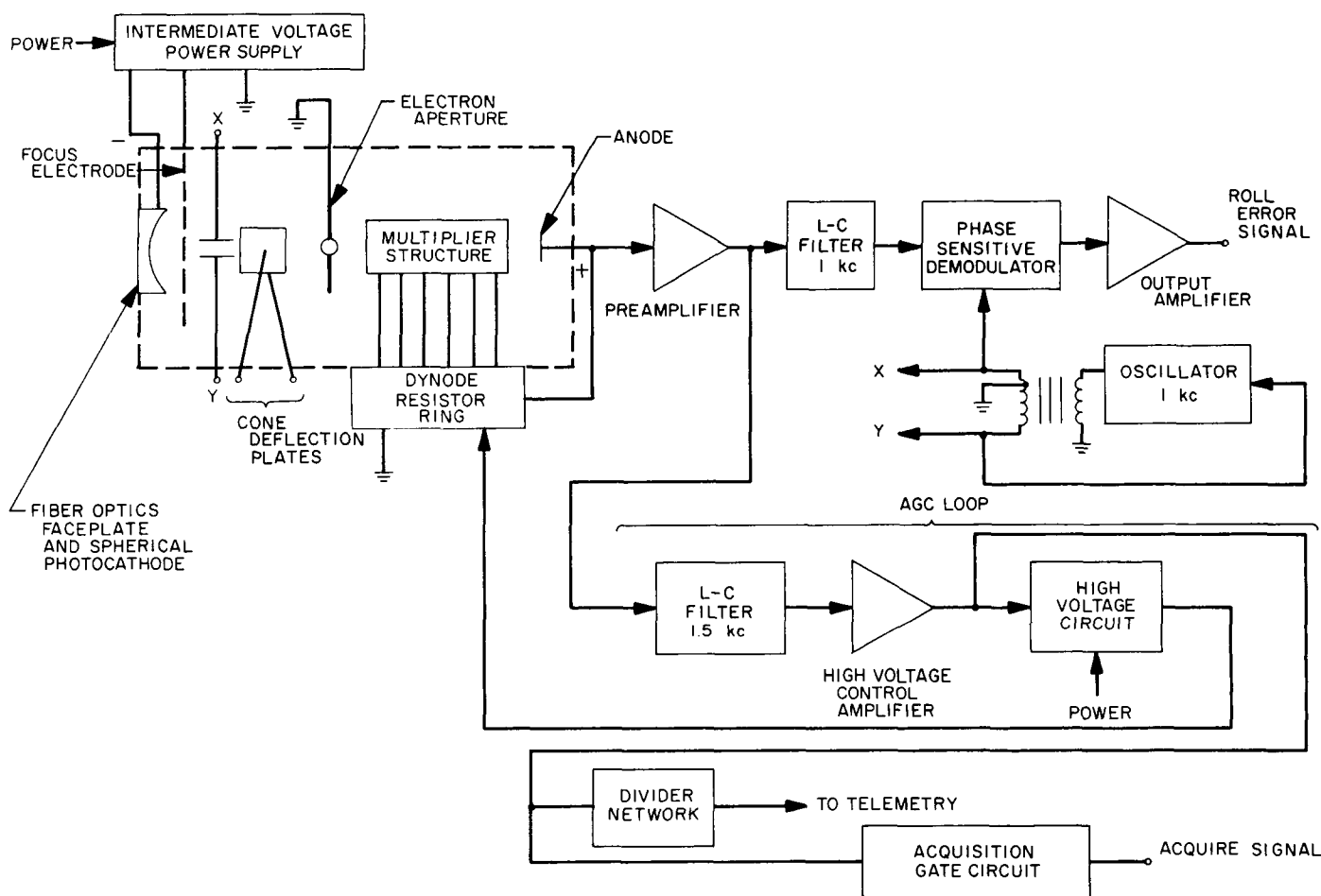


Fig. 12. Image dissector and roll electronics

ventional electron multiplier section. A fiber optics faceplate transfers the image from the optical system's image plane to the curved photocathode surface. The electrons emitted from the photocathode are imaged in the plane of the aperture. The image of electrons is swept sinusoidally at 1 kc across the aperture. Fig. 13 shows the pulse trains generated for various star positions.

The magnitude of the generated pulses is proportional to the brightness of the object in the field of view. The roll error signal is generated from the phase and magnitude of the 1-kc component, and the AGC loop is controlled by the magnitude of both the 1-kc and 2-kc components.

The tracker is equipped with a mechanical Sun shutter that automatically shields the photocathode from the physically damaging effects of imaging extremely bright objects. The power for the shutter is switched on by a logic network in the attitude control system whenever the spacecraft is not positioned along the Sun line.

The optical system of the tracker consists of a shade, a catadioptric lens, and an aperture compensator.

The tracker is integrated into a single unit. It houses the shade, the optics, the image dissector, and all the electronics.

Breadboard and prototype trackers have been in operation for several weeks exceeding all the functional requirements and without any operational failures. An environmental prototype is in construction, and the full range of environmental tests will be conducted with this model.

**b. Square root Sun sensor.** This Sun sensor was developed to allow Sun acquisition without the use of pitch and yaw gyros. The name "square root sensor" was used because the original requirement specified an output which was proportional to the square root of the angle from the null position for both the pitch and yaw axes.

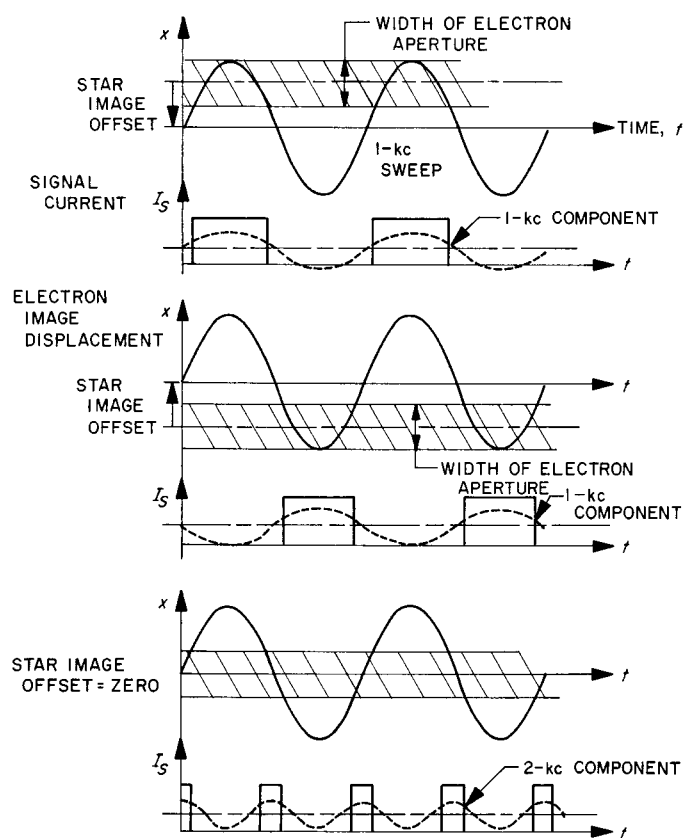


Fig. 13. Pulse trains generated for various star positions

This requirement has since been changed to provide a greater scale factor near null and saturation of the signal near 100 deg. A modified output curve of the Sun sensor system is shown by Fig. 14.

Four nearly identical assemblies, each containing four Clairex 605 photodetectors, are required for the square root Sun sensor system. Two primary assemblies are mounted on the sunlight side of the spacecraft bus and contain four photocells which serve the same function as the primary cells on *Mariner 2*. The remaining four cells (two per assembly) and all eight cells of the secondary assemblies serve the same function as the secondary cells on *Mariner 2*. The secondary assemblies are mounted on the dark side of the spacecraft bus. Two different excitation voltages are supplied to the primary assemblies,  $\pm 16$  v to the primary cells and  $\pm 26$  v to secondary cells. Since the secondary assemblies contain only secondary cells, only the  $\pm 26$ -v excitation is required.

**c. Reset Sun sensor.** The reset Sun sensor is required to indicate when the spacecraft is 180 deg from Sun acquisition about the  $x$  and/or  $y$  axis. This output is used in

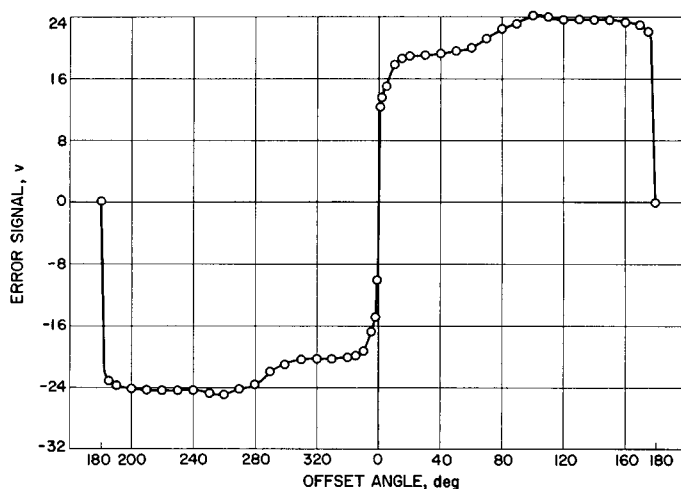


Fig. 14. Square root Sun sensor system characteristics

the attitude control logic to reduce gas consumption and the time required for acquisition. This is done by controlling the gas jets so that the spacecraft's angular rate is reduced as it approaches the Sun-acquired position from 180 deg out.

The sensor is built around two Clairex 605 photocells connected in parallel. One elongated aperture serves both cells, providing a total field of view of  $20 \times 180$  deg. The assemblies are mounted on the dark side of the spacecraft bus. Two assemblies are oriented to sense the Sun position about the  $x$  axis and two more are used for the  $y$  axis. In this way, redundant outputs in both axes are provided to the attitude control system logic.

**d. Sun gate.** The Sun gate used on *Mariner Mars 1964* is a modified version of the one used on *Mariner 2*. For *Mariner Mars 1964* each of the two detectors is masked and shadowed so that it has a uniform response curve to cone angle offsets and is insensitive to clock angle changes. One assembly, therefore, provides two independent outputs instead of one as in *Mariner 2*. The redundant output is used to improve the reliability of the attitude control system.

The output signal is used to terminate the Sun acquisition mode whenever the spacecraft roll axis is within a predetermined angle of the Sun line. The excitation voltage to the secondary Sun sensor's cells is removed upon acquisition. This prevents degradation of null characteristics generated by the primary cells.

**e. Earth detector.** The Earth detector is used to verify the acquisition of Canopus after the roll search is completed. If Sun and Canopus acquisition are accomplished,

the Earth detector will sense reflected sunlight from the Earth. Its field of view is  $\pm 25$  deg in cone and  $\pm 17$  deg in clock, which will cover the change in direction from the spacecraft to Earth due to differences in individual trajectories.

The Earth detector consists of a one-element lens which images the Earth on a cadmium sulphide photocell. The detector strip is in the form of a grid pattern which is large enough to receive the Earth image as the Earth angle changes within the field of view. A DC voltage is applied to one side of the detector so that current will pass through the photocell and a fixed resistor to ground. The voltage across the fixed resistor changes in relation to the light received by the photocell. This voltage is telemetered and indicates the apparent Earth flux when the Earth is within its field of view.

## D. Mariner Venus 1962 Design Evaluation Vehicle (DEV) Tests

The *Mariner* DEV was assembled from *Mariner 1* and 2 spare parts. Following its first system test on June 25, 1962, the *Mariner* DEV was used for special tests in support of the *Mariner 1* and 2 missions. Among these special tests was the verification of the *Mariner 2* midcourse maneuver commands on *Mariner* DEV prior to their transmission to *Mariner 2*, then on its way to Venus.

The following is a brief description of the DEV tests performed to date.

*Test 1: primary power voltage variation.* A spacecraft operational sequence was synthesized which allowed all spacecraft elements to be exercised. The power subsystem control circuit was adjusted to supply the required voltage levels. Each subsystem engineering group evaluated the performance degradation of their subsystem as the 2.4-kc primary power voltage was decreased to 42.5-v rms, then increased to 57.5-v rms.

The test data indicated that all subsystems could tolerate a wide variation in primary power voltage level if regulation was maintained at the changed level.

*Test 2: data conditioning system cyclic calibration noise.* The test objective was to determine the content

and level of noise needed to cause the science subsystem to go into the calibration mode, thus explaining the unscheduled science calibrations of the *Mariner 2*. A transient monitor was used to determine the presence and magnitude of transients.

The test did not reveal any areas significantly susceptible to noise, but it did eliminate a number of suspect areas. The *Mariner* DEV spacecraft was very insensitive to noise.

*Test 3: 2.4-kc frequency variation.* Each subsystem group evaluated the performance degradation of their subsystem as the 2.4-kc primary power frequency was decreased to 1920 cps, then increased to 2880 cps.

All subsystems operated normally when the 2.4-kc power frequency was varied 1%. This demonstrated that all subsystems will function properly with the 38.4-kc backup oscillator (frequency  $\pm 1\%$ ) planned for future spacecraft. With a 20% variation of the 2.4-kc signal, communications, central computer and sequencer, and command subsystems operated normally. At these wide frequency variations, the data encoder did not function. This response was in accordance with its performance specification.

*Test 4: noise susceptibility.* The noise existing between the various spacecraft grounds and the various operational support equipment grounds was mapped as the spacecraft was stepped through the modes of a simulated mission.

The noise mapped indicated that the spacecraft was relatively quiet. The most significant fact noted was that when certain loads were applied, there was a loss of data sync caused by a momentary change in frequency of the 2.4-kc primary power.

*Test 5: operation of 400-cps and 2.4-kc power amplifiers with booster regulator failure.* The effect of a 10% variation of the DC input to the 400-cps and 2.4-kc power amplifiers was determined using various system loads.

The data indicated that the 400-cps and 2.4-cps power amplifiers operated satisfactorily (as was expected) on input voltages of 52 v  $\pm 10\%$ . Since the specified input voltage tolerance is 1%, the power amplifiers would perform satisfactorily if a booster regulator failed.

*Test 6: spacecraft power factor determination.* The individual and the combined power factors of various loads

on the 400-cps and 2.4-kc power supplies were measured by several methods and the effect on waveforms recorded.

As required by system specifications, the power factors were consistently greater than 0.95.

*Test 7: data encoder and RF ground investigation.* The noise on the electrical grounds between the data encoder and RF equipment was measured. An attempt was made to isolate these grounds and substitute other grounding techniques.

One ground loop was discovered and corrected. As a result of this test, a complete theoretical study of grounds and grounding techniques was initiated.

*Test 8: Mariner DEV reflectance.* This test was made to determine the amount of heating which could be attributed to reflections between portions of the spacecraft.

Preliminary data reduction indicated that about 1% of a solar constant of reflected light was incident on the vertical hex faces and the surfaces of the Earth sensor. These results represent the first separation of the reflection effect from other modes of heat input. The test indicated the maximum effect of reflectance on spacecraft temperature will not exceed 10%.

*Tests 9 and 12: science case harness (Case I) evaluation, and data conditioning system ground investigation.* These tests were designed to determine whether the additional weight and bulk of shielded wires used in the *Mariner 2* science case harness was justified by a significant reduction in ambient noise levels or crosstalk.

Representative ambient noise levels were measured using the present fully shielded case harness, then using a harness in which only the AC power leads were shielded. With the unshielded case harness installed, the performance of the system and subsystem was observed in the normal operating modes. These results were compared with the results of previous tests using the shielded harness.

When the unshielded harness was used the subsystem functioned without observable performance degradation. In addition, the noise amplitudes noted were generally equal to or lower than those observed when the shielded case harness was used.

It was concluded that the *Mariner 2* science subsystem would have performed equally well without the extra weight and complexity of shields on most of the case

harness signal wires. The same conclusion could not be drawn regarding other subsystems without further testing.

*Tests 10 and 11: event-channel noise characteristics, and limiting of the 2.4-kc clock.* The 2.4-kc primary power input to the data encoder transformer-rectifier unit was monitored using the unassigned channels of the 10-channel transient monitor. As the spacecraft was operated through a simulated operational sequence, the amplitude of the transients as they appeared on the 2.4-kc input to the data encoder transformer-rectifier was measured.

The following conditions caused a momentary interruption of the 2.4-kc signal, resulting in a brief loss of data sync: (1) attitude control power *on*, (2) gyros *on* and *off*, (3) science *on* and *off*, (4) science calibrate *on* and *off*, and (5) Earth sensor *on*.

The 2.4-kc power to the data encoder was unaffected for all other conditions.

*Test 13: calibration of temperature transducers.* A decade box was substituted for each temperature transducer at the connector and the telemetry indication compared with the decade box resistance. A 10-ft unshielded wire was connected to the lower thermal shield transducer connector, then routed close to the spacecraft ring harness to determine the effect of spacecraft noise induced through this long unshielded wire.

When compared with the "black box" calibration method used previously, the decade substitution method proved superior in that long leads from the spacecraft to the operational support equipment were eliminated and the data encoder did not have to be removed from the spacecraft. Tests with the 10-ft unshielded wire indicated that a weight saving may be possible through the use of unshielded temperature transducer leads.

*Test 14: long-range Earth sensor reflection.* The objective of this test was to determine if the reflection of the sunlight from various spacecraft components would cause a degradation in the Earth intensity output. The possibility of a false reflected acquisition source was also investigated.

The test results showed that the reflected sunlight did not affect the light intensity output, nor did the components located on the antenna create any Earth sensor difficulties.

*Test 15: temperature control.* This test compared and correlated *Mariner 2* flight data, *Mariner* DEV test data, and temperature control model test data. The 25-ft space simulator was used to simulate *Mariner 2* Flight Days 240, 252, 303, and 305 (1, 13, 64, and 66 days after launch).

The simulated space conditions resulted in spacecraft temperatures about 10 to 22°F lower than the flight temperature information telemetered from *Mariner 2*. The temperature discrepancy was greater for higher simulated solar intensity values.

*Test 16: simulated midcourse interactions.* This test, which was performed at the Lockheed Research Center Space Simulation Facility, near Newhall, California, was designed to compare the actual autopilot performance and spacecraft dynamics in a simulated space environment with the results of analysis and analog computer simulation. Further, an attempt was made to determine the validity of the analytic approximations and identify those areas in which a more detailed simulation or complete change in concept was needed. Some of the approximations made in the theoretical analysis of autopilot performance were:

- (1) Backlash and friction were ignored; linearity was assumed.
- (2) Ideal jet vane characteristics were assumed.
- (3) Dynamic properties were based on a simple model comprised of rigid bodies coupled through springs and hinges.
- (4) Cross-coupling through resonant members was largely ignored.

The spacecraft was spring suspended on a 45-ft pendulum with three axes of freedom (Fig. 15). The spacecraft was balanced in each configuration so that the line of suspension went through the CG of the spacecraft and a near perfect balance was maintained. The spring suspension allowed 5-in. travel for the 50-lb thrust of the midcourse motor. This allowed enough free-flight time to examine the autopilot response through the first 100 to 500 msec of motor burn.

In each case, the effect of the analytic approximations was examined and individually evaluated. Modal analysis on the type of suspension system used in this test provided valuable information, and analysis and analog computer simulation results were substantially confirmed.

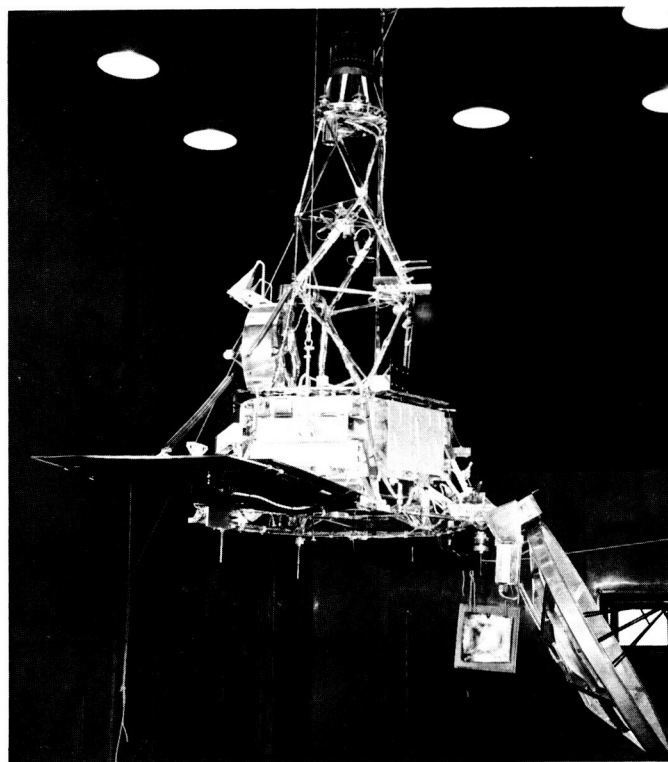


**Fig. 15. *Mariner* DEV in high altitude simulator during simulated midcourse interactions**

*Test 17: RF interference.* The objectives of this test were to make an RF signature of the *Mariner* DEV spacecraft, to irradiate the spacecraft with RF and locate possible RF interference, and then to compare the test results with the limits defined by JPL specification.

The test data indicated there was no RF radiated by the spacecraft system or any of its subsystems in excess of the limits required by specification. Also, the spacecraft system was found to be very insensitive to RF interference. Data from this test will enable future RF interference specifications to more closely represent spacecraft function and design.

*Test 18: radiometer scan.* The *Mariner* DEV radiometer was operated in slow scan for 4.2 hr in a test designed to find the cause for some apparently anomalous data received from *Mariner 2* during its Venus flyby. The test attempted to locate any sticking or fluctuation in the scan mechanism and determine the linearity of its scan.

The test results indicated that there is no strong evidence of binding or sticking of the scan mechanism; the fluctuations about the average could be statistical. The period of fluctuation (about 40 sec) did not correspond to any known periodic phenomenon on the spacecraft.

## IV. *Voyager* Project

The primary objective of the *Voyager* Project, a combination orbiter/lander mission, is the scientific exploration of Mars and Venus by means of spacecraft designed for use with *Saturn* boost vehicles. Secondary objectives are the scientific exploration of interplanetary space in the Mars-Venus region, and the determination of the feasibility of, the development of technology for, and the collection of scientific data necessary to successful manned flights to these planets.

*Voyager* flights are envisioned beginning in the 1967-69 period and continuing into the mid-1970's.

The *Voyager* Project is currently in the planning phase. The schedule is to submit to NASA management in September a *Voyager* Project Development Plan indicating the potential missions, the launch vehicle to be used, several development and flight schedules, estimated costs of the entire project, and a management plan. To generate the data required for this Project Development Plan, study efforts are now in process at the Marshall Space Flight Center (MSFC), at JPL, and in industry.

In the case of MSFC, a tentative decision was reached during this reporting period to use the MSFC-defined upper Stage S-VI on a *Saturn I-B* vehicle. Detailed con-

ceptual studies for Stage S-VI are currently being conducted at MSFC. The tentative payload capability of such a launch vehicle is currently estimated to be in the range of 6,000 to 7,000 lb.

At JPL the Advanced Planetary Spacecraft Study Committee has been performing mission analyses since May 1962. Results to date indicate that the optimum mission for the *Voyager* class of spacecraft is probably a combination orbiter/lander. It is, therefore, this concept on which mission studies are being concentrated.

To supplement the JPL studies, early in April NASA headquarters selected General Electric's Missile and Space Division, Valley Forge, Pennsylvania, and the Avco Research and Advanced Development Division, Wilmington, Massachusetts, to also perform mission studies for the *Voyager* spacecraft. These two companies were selected from an open competition to which a total of 13 companies responded with proposals. Most of the unsuccessful bidders have indicated a desire to continue at their own expense the same type of effort that General Electric and Avco are conducting. The results of these industry studies will be incorporated, as appropriate, into JPL's results in the preparation of the Project Development Plan.





# THE DEEP SPACE INSTRUMENTATION FACILITY

## V. Introduction

The DSIF is a precision tracking and data acquisition network which is designed to track, command, and receive data from deep space probes. It utilizes large antennas, low-noise phase-lock receiving systems, and high-power transmitters at stations positioned approximately 120 deg around the Earth. Its policy is to continuously conduct research and development of new components and systems and to engineer them into the DSIF so as to continually maintain a state-of-the-art capability.

The DSIF is comprised of three permanent deep space stations, one mobile station, and one launch station. The three permanent stations are located to provide continuous coverage of a deep space vehicle. Their locations are Goldstone (Pioneer and Echo), California; Woomera, Australia; and Johannesburg, South Africa. The Mobile Tracking Station (MTS) is presently located near the permanent station in South Africa and is used mainly for

early acquisition, and tracking and communications with spacecraft from injection into orbit to an altitude of about 10,000 mi. The Launch Station is used to provide real-time telemetry during the spacecraft prelaunch tests and to record spacecraft transmitted telemetry data from launch to the end of the visibility period.

The testing and development engineering of new equipment for the DSIF are performed at the Goldstone Space Communications Stations. In most cases new equipment is installed and tested at Goldstone before it is integrated into the system. An 85- and a 30-ft Az-El antenna are installed at the Goldstone Venus site for primary use in research and development.

Section VI of this Report, regarding the DSIF Program, is abstracted from SPS 37-21, Vol. III.



## VI. Communications Research, Development, and Facilities

### A. Engineering Development

#### *Laboratory testing of Flow Corporation drag spheres.*

A series of laboratory tests has been conducted on a 12-in. drag sphere manufactured by the Flow Corporation, Cambridge, Mass. The sphere used for the tests is considered representative of the drag spheres mounted on the wind towers at the Mars site (Fig. 1).

The wind measurement system set up on the site of the future 210-ft antenna, Mars site, makes use of the 12-in. diameter spheres to measure wind velocity in three

directions. Linearity, response, and hysteresis tests have been made on one of the spheres in order to determine the accuracy of the wind measurements.

*Digital instrumentation system.* The digital instrumentation system, which has been initially installed at Goldstone, makes use of two general purpose computers. The same basic computer structure (Fig. 2) is used in both. Each computer uses a parallel, random access, coincident current, magnetic core memory and serial arithmetic operation. Both computers have the same word size, instruction format, machine cycle time, and input-output capability; however, one unit has more instructions and

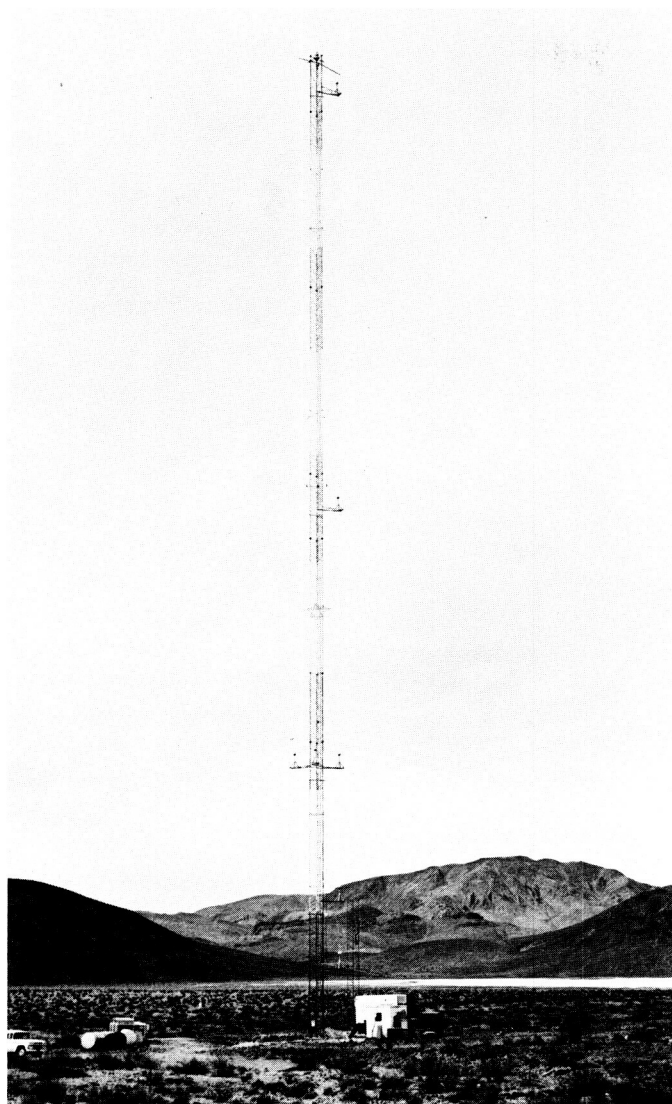


Fig. 1. Wind towers at Mars site

faster execution times. Each computer has an automatic power failsafe system.

*Installation of safety equipment at Woomera.* Staircases, platforms, and instrument cages have been installed at the Woomera Station to increase the safety of personnel working on the antenna and collimation tower. Over-all view of work performed is shown in Fig. 3.

*Mark I ranging subsystem.* The Mark I ranging subsystem is designed to furnish unambiguous range measurements to a range of  $8 \times 10^5$  km. In order to do this, the pseudo-random binary digital codes are generated in the receiver and transmitter coders and are made up of several components which are combined in different

forms to create various code lengths; they are also acquired or synchronized separately to decrease acquisition times. A 1-Mc, 31-stage, open-ended shift register is used as the timer and a Chinese number generator provides the numbers which must be added (or subtracted) to the cumulative range tally to obtain the doppler count.

## B. Research and Development

*Experimental low-noise systems.* Normal noise temperature calculations of a traveling wave maser assume a high gain per unit length. This is reasonable at bath temperatures of 1.5 to 2.5°K, but is not necessarily valid at a temperature of 4.2°K which is typical of cryogenic refrigerators. Measured data at 2300 Mc gives minimum and maximum noise temperatures of 4 and 9.3°K, respectively.

A mobile Dicke radiometer with a horn antenna was used to measure the average noise temperature of automotive ignition and fluorescent lamps. They were found to produce a flux density as much as  $-183$  and  $-187$  dbm/cps/m<sup>2</sup>, respectively, at 50 ft.

*Ground antennas.* The 30-ft antenna at the Goldstone Venus site has been fitted with a Cassegrain feed system which is a  $1/4$ -scale model of the feed that will be used on the 210-ft antenna. Using the Tiefert Mountain antenna range and a calibrated 6-ft antenna near the focal point of the 30-ft antenna, gain, beam width, and radiation patterns will be measured at about 16.5 Gc, which is 7 times normal frequency for the 210-ft antenna. A servo test program is continuing in an effort to determine the cause of discrepancies between the results of dynamic and transfer function tests.

As part of a program to determine the relationship between deformations of the surface of a paraboloidal antenna and RF performance, it is planned to physically distort the surface of the 30-ft antenna and to measure its change in performance. A computer program has been developed to calculate the change and a comparison has been plotted with actual measurements. Close agreement was noted.

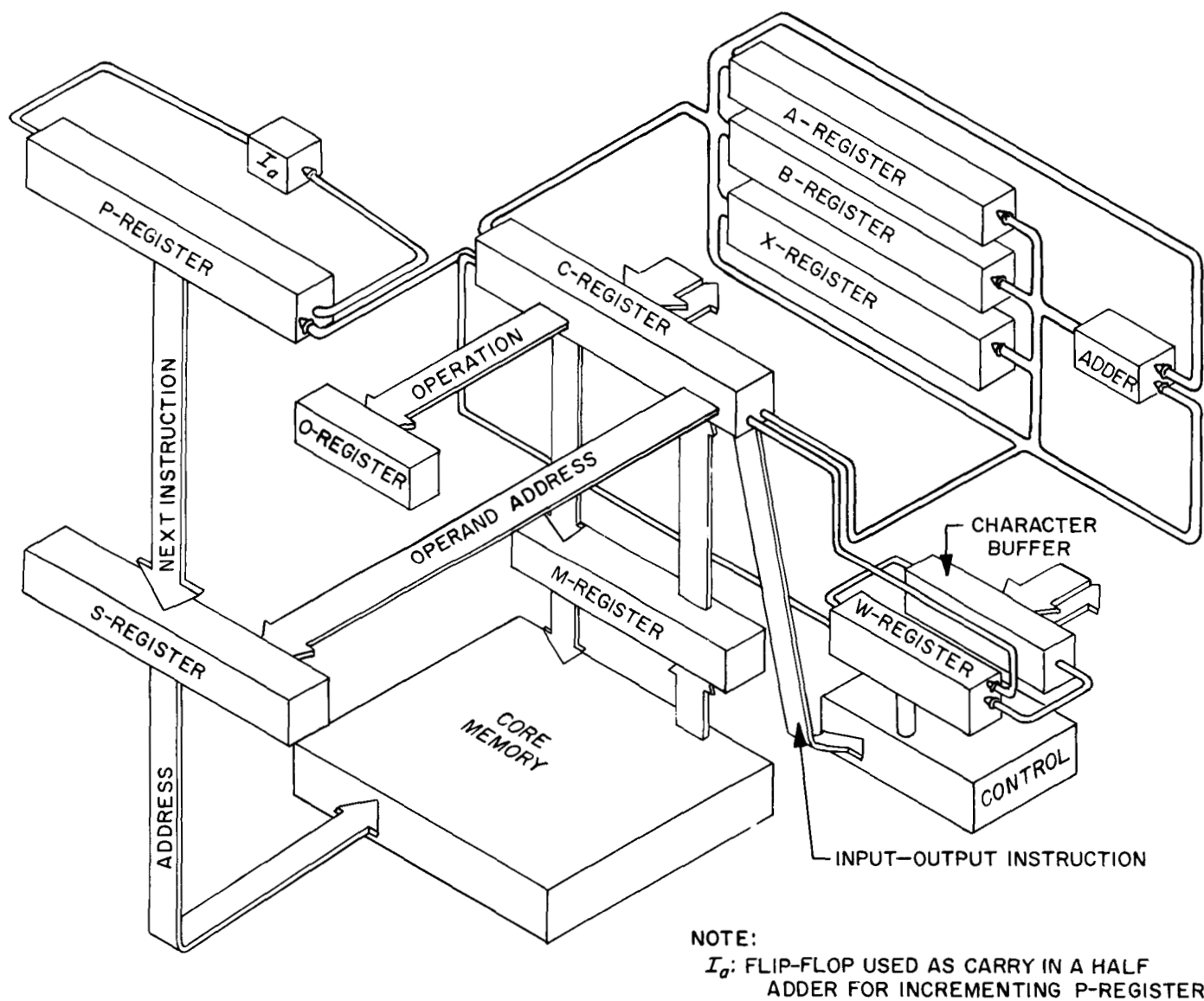


Fig. 2. Basic computer structure

An instrumentation van for testing antennas is nearly complete.

A metallic cylinder, or tunnel, was placed over the rim of a 6-ft antenna to provide isolation between it and the 85-ft antenna on which it was mounted. Using various "tunnel" lengths, antenna patterns and gain measurements were made. Calculations show that the antenna noise temperature can be reduced from 16.7 to 3.7°K and that the tunnel can be a useful and practical device for reducing antenna temperatures of small paraboloidal antennas.

An automatic acquisition device has been developed for use with phase-locked clean-up loops. It makes use of

a relay operated short on one of the resistors in the loop filter which widens its bandwidth until acquisition occurs, at which time an AND gate operates to remove the short and narrow the bandwidth when the reference frequency, VCO frequency, and a "no beat" condition all are present.

*Planetary radar.* Measurements made on the double cavity 2388-Mc maser at the Venus site show that there is an insignificant increase in noise temperature due to waveguide mismatch, and that there is an increase in gain and a decrease in noise temperature with an increase in ambient temperature. Reasons for this characteristic are unknown and are being investigated.

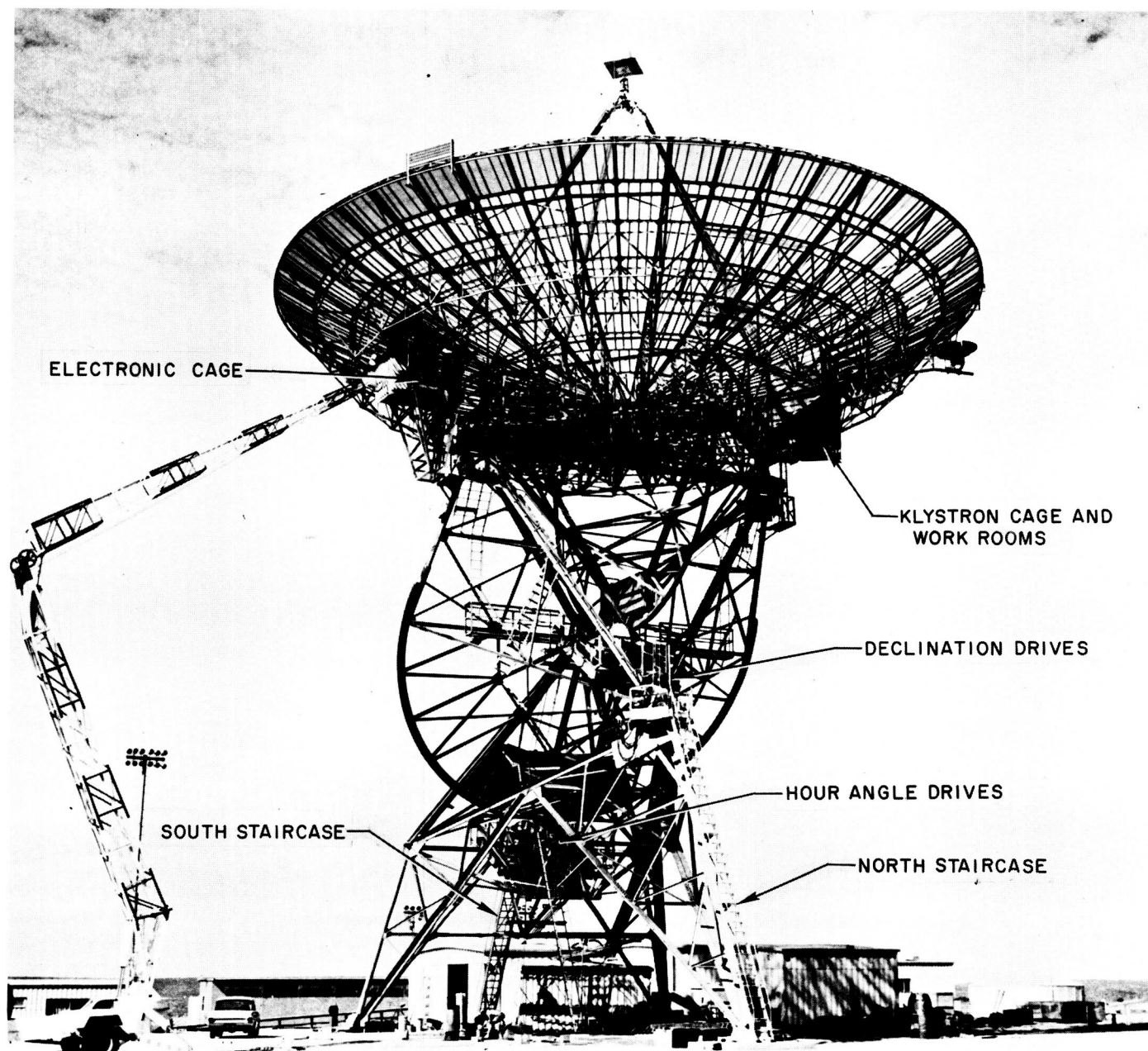


Fig. 3. Over-all view showing work performed

After investigating six proposals by different manufacturers, one was found which appears capable of building a satisfactory water rotary joint for use on large antennas. It will use a hard carbon face. Testing of the completed product will be done at JPL.

The Mod IV ranging equipment is essentially a digital phase tracking loop which provides a continuous real-time measurement of target range. In addition, it provides ephemeris programmed signals for use in spectrum,

radiometer, and multiple range gate analysis of the radar echoes and an ephemeris-controlled keying signal to control the alternate connection of transmitter and receiver to a single antenna.

Actual operations of the 100-kw transmitter revealed several deficiencies which have been corrected and reduced since the last radar experiment. The klystron amplifier, RF water load, and transmitter control cabinets were returned to the manufacturer for repair. The "crow-

bar," or high-voltage protective device, was modified to provide a large gap when the generator field was activated; better rectifier tubes were obtained and an unwanted resonance in the input to the power supply filter was essentially eliminated by adding a 0.0625- $\mu$ fd capacitor in parallel with the high-voltage cable.

The Mod IV planetary radar receiver is presently undergoing extensive evaluation tests prior to being installed at the Venus site for use in planetary radar experiments. The receiver has five separate channels: synchronous, AM spectrum, CW spectrum, ranging, and noise and operates with reference frequencies obtained from a synthesizer which receives coherent 1-Mc and 10-kc signals from an atomic frequency standard oscillator. Cooling is accomplished with liquid cooled heat sinks. Noise figure, bandwidths, mixer conversion efficiency and RF carrier tracking loop threshold, limiter suppression factor, closed-loop frequency response, bandwidth variation with signal strength, loop phase error with frequency offset, and internal coherent interference measurements have all been made.

*Ranging system development.* The Mod III ranging equipment (Fig. 4) is a development from the Mod II equipment which has been described previously. It is somewhat different in physical construction, has additional peripheral devices and a greater input-output

capacity. Although primarily developed for real-time automatic range acquisition and tracking at interplanetary distances, small additional features have been added so that it is essentially a general purpose stored program computer capable of on-line data handling and processing, automatic station check-out, and sequential and simultaneous control of other equipment. Input capacity is 128 word channels (25-bit, 1-Mc binary code-sequence words) and output capacity is 32 channels with 128 channels of on-off signals (64 internal and 64 external). Normal input is from a paper tape reader and normal outputs are a paper tape punch and digital strip printer.

Because of the general nature and complexity of the Mod III ranging equipment a set of programming, operating and maintenance manuals, check and diagnostic routines, and subroutines is being prepared. Some have already been published.

Whenever the sidebands of a modulated carrier have as much or more power than the carrier, it is possible to lock a phase-locked receiver on to one of the sidebands rather than the carrier. Several methods have been proposed for automatically preventing this. One which looks very promising theoretically is now being tried experimentally. It makes use of the principle that, with 50% duty cycles on a monostatic radar, only odd numbered sidebands are present, and these will be symmetrical with

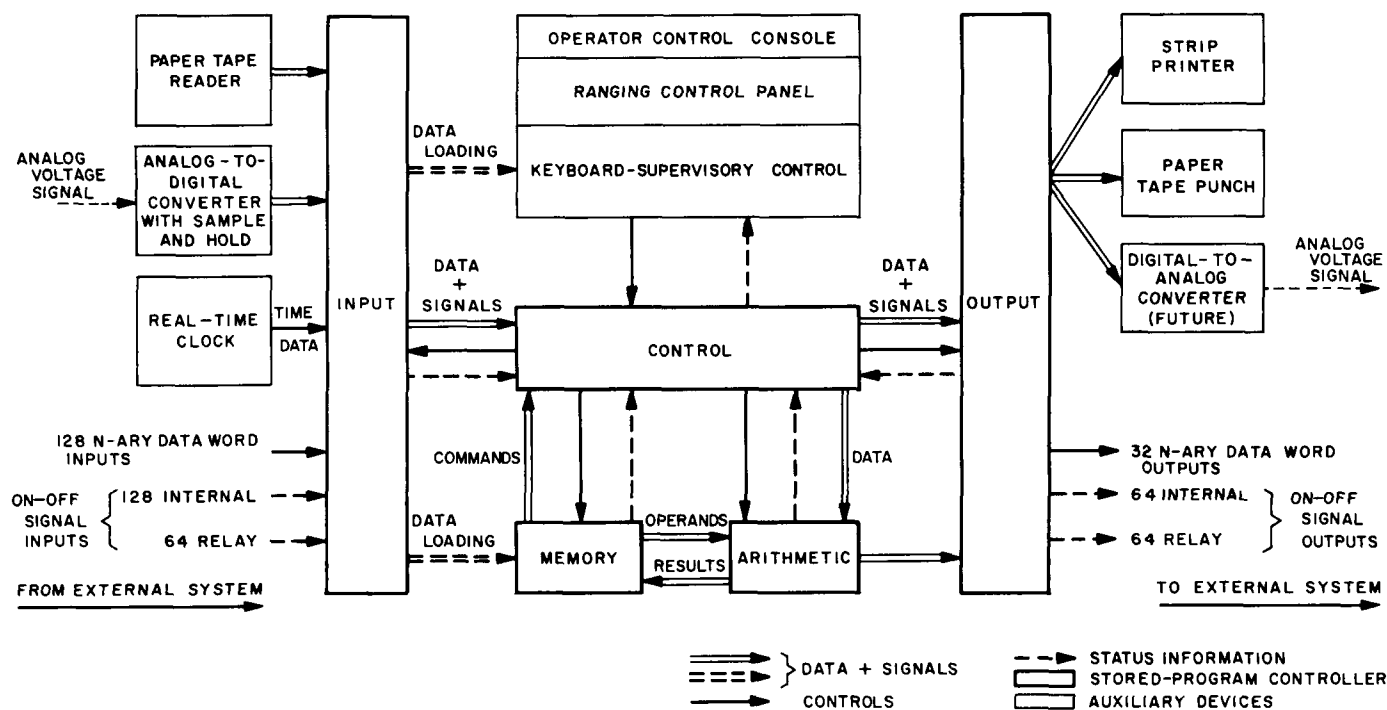


Fig. 4. Functional block diagram of Mod III ranging equipment

respect to the carrier. By measuring this symmetry and automatically cancelling all symmetrical voltages, a receiver phase-lock loop can be made to lock on the only voltage left which is the carrier. Lock indicators are provided.

The above principle is also being tried with telemetry modulation of a continuous carrier when strong signals are available. Another proposal being investigated utilizes a synchronous sideband detector where the local reference is available to measure a component of the dynamic phase error whose frequency is equal to the product of the fundamental modulation frequency and the order of the sideband to which the receiver is locked. It is hoped that this system will be useful for weak signals and fast acquisition on a monostatic radar.

## C. Facilities

*Tiefert Mountain antenna range.* This range is now complete with heliport, towers, buildings, power generators, and X-band equipment. S-band test equipment for use with the Echo site will be installed at a future date.

*Advanced Antenna System.* Contract negotiations with the Rohr Corporation for the construction of a 210-ft antenna at Goldstone have been completed, and the contract is in the process of being approved. Supporting studies are being conducted at JPL particularly through the use of the STAIR Computer Program, which has been modified to calculate the weight moment of inertia.

## OPERATIONAL AND TEST FACILITIES

### VII. The Space Flight Operations Facility

#### A. Introduction

A new facility is being developed at JPL to provide the spaceflight operational, technical and support functions required for the conduct of future unmanned lunar and planetary-interplanetary spacecraft missions. During operations, the facility and participating remote tracking and communications stations will function as a single information handling, analysis, interpretation, evaluation and command network, and will include extensive data processing and decision making capabilities. A summary presentation of the Space Flight Operations Facility (SFOF) physical configuration, functional capabilities and associated supporting activities was presented in SPS 37-20, Vol. VI, pp. 43-67. Bimonthly progress of the SFOF development will be reported in subsequent issues of the SPS, Vol. VI.

#### B. Scheduling

Scheduling activities within the SFOF utilize the PERT (Program Evaluation and Review Technique) system to depict the constraints and interdependencies between the major milestones or development activities comprising the SFOF.

The SFOF project is divided into 15 areas of cognizance: (1) SFOF Design Book, (2) SFOF Systems Operation Analysis Plan, (3) SFOF building, (4) digital data system hardware, (5) digital data system programming requirements, (6) telemetry process system, (7) telemetry data monitoring system, (8) voice communications system, (9) data communications system, (10) closed circuit TV system, (11) mission status display system, (12) user area display system, (13) spacecraft model sys-



tem, (14) command and control system, and (15) Space Flight Operations Complex integration. Cognizant personnel from each of these areas are reporting on a bi-weekly basis to relay information regarding the status of their particular schedule. Scheduling changes, reasons for these changes, and anticipated slippages of completion dates, of both the particular area in question and of the SFOF as a whole, are given.

The SFOF project (Stage I) is currently anticipating an October 1, 1963 building occupancy date with April 1, 1964 as an operational date.

## C. Facility Description

The basic building that will house the SFOF is initially, a three story structure consisting of a basement, first floor and second floor. This basic building will be available for occupancy in October 1963. A later revision to the building will be the addition of office space on the third floor. Concurrent with the addition of the third floor, will be the addition of a west wing to the basement, first floor, and second floor. This ultimate configuration will provide approximately 80,000 ft<sup>2</sup> of usable space.

### 1. Spacecraft Performance Analysis Area

The Spacecraft Performance Analysis Area (SPAA; Fig. 1) is one of the technical areas located in the Space Flight Operations Facility. The functions of the SPAA are to report, evaluate, and interpret the performance of spacecraft and the operation of the engineering experiments. In addition, the SPAA generates spacecraft commands affecting the performance of spacecraft.

The development of the SPAA is an evolutionary process. The initial configuration is relatively simple. Later configurations will become more sophisticated as experience is gained in the fields of display, and command and control. The development of equipments for this technical area, as well as the other technical areas, is strongly dependent on the requirements of the flight projects.

The SPAA will be staffed by the Spacecraft Data Analysis Team (SDAT). In addition, there will be a SPAA representative located in the Operations Area of the SFOF. Communications with the other technical areas will be made through the SPAA technical director's console. This console is also used to remotely enter spacecraft performance on the mission status board in the Operations Area.

*a. Data processing and display system.* The SPAA receives raw data via teletype printers from the com-

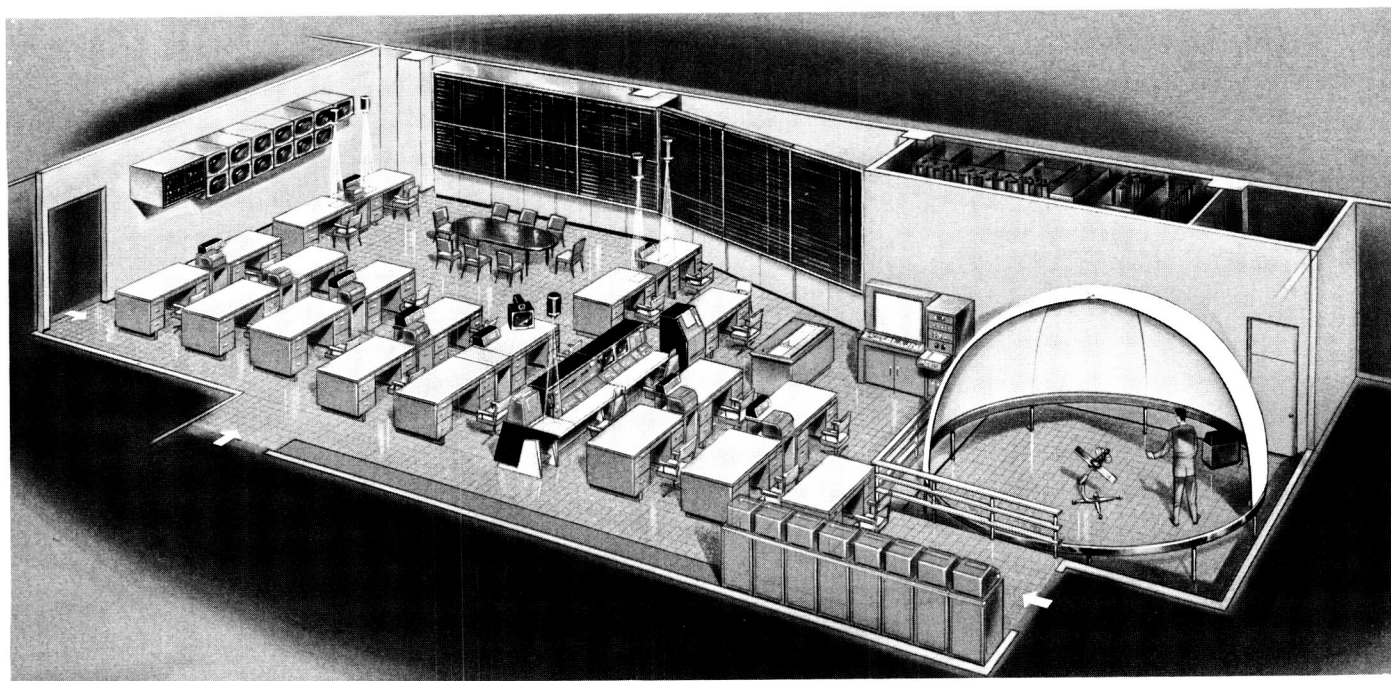


Fig. 1. Artist conception of the SPAA



munications terminus and processed data from the IBM 7094-7040 computer complex via plotters and printers. Access to the computer programming system can be achieved through a remote input/output console located in the SPAA. This console can alter the programs in the computing complex and monitor the status of programs.

The displays in the SPAA consist of two basic types. The first is for SPAA internal use by the SDAT and consists of semi-automatic and manual displays. The second is the SPAA mission display which is capable of displaying information remotely and of being controlled from other areas.

*Display for internal use of the SPAA.* The function of this type is to display information of a highly specialized nature for the exclusive use of personnel within the SPAA.

#### *SPAA flight sequence display.*

The function of this display is to depict the spacecraft flight sequence. Shown on this display will be the event name, the nominal time of occurrence, the predicted time of occurrence, the actual time of occurrence, and a space for remarks pertaining to event.

The display is divided into six identical modules as shown in Fig. 2. Each module has five columns and 14 rows. The first and second rows are used for labeling the information to be displayed in each of the five col-

umns. The remaining 12 rows represent one spacecraft event. The 12 rows contain the following from left to right:

- (1) A title space to identify the information in each row. These titles are attached to the board by means of magnetic nameplates.
- (2) The next three columns each contain a group of six remotely controlled numeric display units for displaying the variable time information.
- (3) The fifth column consists of a metallic blackboard surface which will be used to display the source of the variable information.

All alpha/numeric information will be of a uniform height of 1.5 in.

Information contained in each module is subject to change in the following manner:

- (1) Permanent information, such as module title and mission identification which appear at the top of the module are engraved on the display.
- (2) Semi-permanent information, such as column heading, event titles, and row indications are changed by the use of magnetic nameplates which are attached to the face of the display.
- (3) Variable information, that is, numeric time values, are displayed by means of remotely controlled display units.

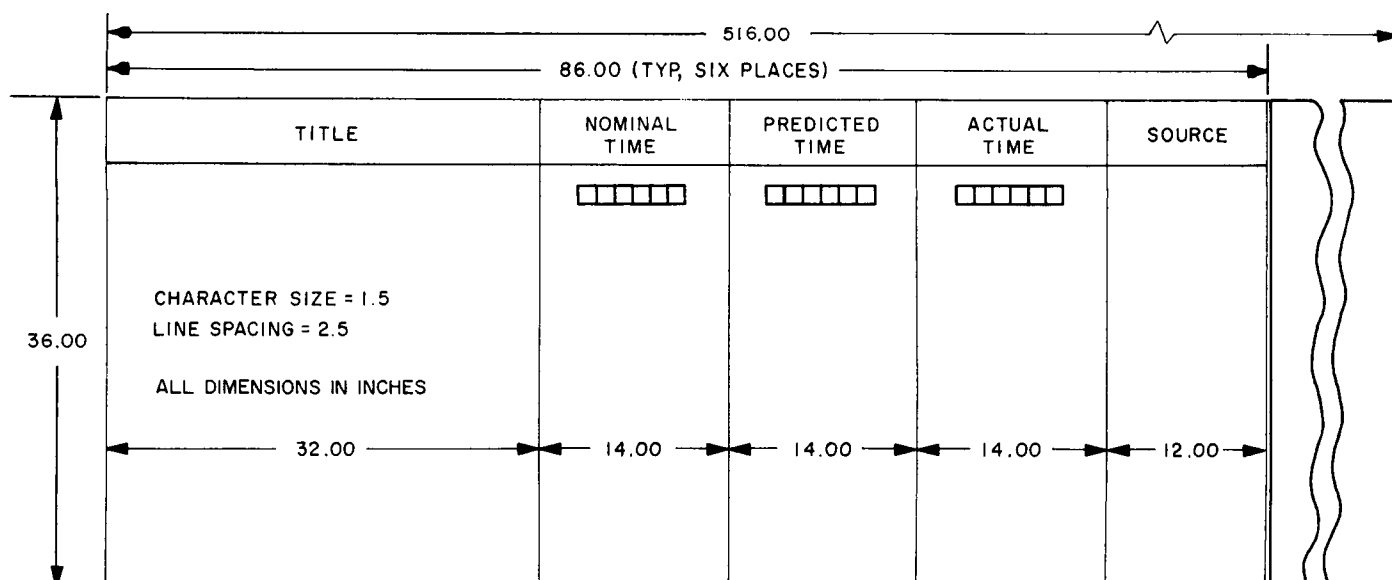


Fig. 2. SPAA flight sequence display module

- umn for station number, a column for the state of the data, and three light columns depicting data type (i.e., tracking, telemetry and administrative). The alpha/numeric information is affixed to the board by means of magnetic blocks. The lights are controlled from switches mounted on the front face of the display.

*Displays controlled from other areas* (Fig. 3). The function of the displays controlled from other areas and displayed in the SPAA is to provide information to the SPAA personnel about the other technical functions being performed in the SFOF. In general, this information presented on the SPAA mission display is required by the SPAA to perform its function of spacecraft performance analysis. Additionally, information of a more general nature pertaining to the over-all mission is also displayed in the SPAA. This information is primarily operational and relates to the status of the facilities supporting the mission. Closed circuit television is used exclusively to perform this function. Banks of 27-in. wall mounted television monitors are provided for the use of SPAA personnel. Information that is displayed on the television monitors is derived from hard-copy cameras; this information is prepared on sheets of paper and placed under the television camera. The formats are, therefore, very flexible and preparation time is minimized.

*Specialized displays: the spacecraft functional model system.* It is often necessary during the course of an operation to have a means of dynamically simulating the attitude of a spacecraft with respect to its celestial environment. An example of this requirement is illustrated

Figure 1: Example of a Mission Data Block. The diagram illustrates the structure of a mission data block, showing a sequence of TVM (Time Value Message) fields. The total length of the block is 180.75. The fields are organized into two rows, with a vertical dimension of 16.00 for the first row and 32.00 for the second row. The fields are: CRAFT COMMAND TVM, SPAA TVM, SPAA TVM, MISSION DIRECTION TVM, MISSION DIRECTION TVM, SIF TVM, SPAA TVM, SPAA TVM, SF OF STATUS TVM, and a T SEQUENCE section. The total length of the block is 180.00.

EA ALL DIMENSIONS IN INCHES

### Session display



by the value of a physical representation of the Earth sensor field of view during the Earth acquisition phase of a spacecraft maneuver.

To satisfy this requirement, the SFOF will provide, in the SPAA, an automated model of the spacecraft and its surroundings. The spacecraft functional model system will consist of three basic assemblies: the model, an automated gimbal assembly, and a hemisphere enclosing the model and gimbal assembly.

The initial model will be a reasonably detailed representation of a *Ranger* Block IV spacecraft, to approximately  $\frac{1}{2}$  scale. Provisions will be made to allow replacement with other model types as required by future programs. Each module and sensor will be readily identifiable and, in addition, the position of the high gain antenna will be manually adjustable. Projectors mounted unobtrusively on the model will provide light sources which accurately represent the fields of view of the Earth sensor and the TV system. A third projector will be provided to indicate the roll axis or the center of the Sun sensor field of view.

The model will be mounted on a three-axis, servo-controlled gimbal assembly that is actuated by a small coordinate transformation computer. The transformation equipment will provide the capability of accepting slew rates in a spacecraft-centered coordinate system and (responding with appropriate rates at the gimbal drives) of producing smooth rotations about the body centered axis of the model. Angular rates about the model axis will be adjustable in the range of 0 to 6 deg/sec.

A 17½-ft diameter translucent plastic hemisphere will house the model and gimbal assembly. Provisions will be made to depict the relative positions of various celestial bodies on the inner surface, and thus the dome will function as the simulated celestial environment for the model.

**Table 1. Summary of SPAA equipments**

Item	Quantity
<b>Data processing equipments</b>	
Remote input/output console	1
Administrative printer	1
High speed printer	1
30- × 30-in. plotter	1
11- × 17-in. plotter	1
Data printer	6
Analog oscillograph	1
<b>Communications and display equipments</b>	
SPAA directors console	1
Teletype page printers	8
Voice communications modules	7
Video interphone	1
SPAA mission display	1
SPAA communication status display	1
Spacecraft telemetry measurement display	1
SPAA flight sequence display	1
Spacecraft model system	1
Bulletin and chalk boards	4
Closed circuit television cameras	5

An accurate estimation of the spacecraft sensors fields of view during a maneuver can be made from observations of the light patterns projected from the model.

**b. Other equipments in the SPAA.** To perform spacecraft performance analysis a multitude of equipment is required. It is necessary that certain real-time control of the Data Processing System be accomplished from this area. Additionally, real-time and near-real-time data display is required. An extensive communications network is required for coordination between the mission directors and the technical areas. These capabilities were spelled out in detail in SPS 37-20, Vol. VI. A summary of the SPAA equipments is given in Table 1.

## VIII. Test and Support Equipment

### A. Environmental Test Laboratory

#### 1. 25-ft Space Simulator

*a. Status of the facility.* Work is continuing to upgrade the solar simulation system to produce a beam with an intensity variation of  $\pm 5\%$  over a 6-ft D ( $\pm 10\%$  over a 7-ft D; in the present system the variation is  $\pm 10\%$  over a 5-ft D). Virtual source glass surface mirrors have been ordered for the 6-ft D beam.

Work is also continuing to replace the aluminized-metal pseudohyperbolic and 33-in. mirrors with aluminized glass reflectors to improve the performance of the solar simulation system. Two of the mirrors in the pseudohyperbolic array have been replaced, with a resulting increase of 18% in the energy of the light reflected from the mirrors.

A rollaway monorail crane is being designed for handling flight spacecraft.

*b. Absorptivity test.* This test was to determine the absorptivity of sample surfaces (white, gold, black, and polished aluminum) of the *Ranger* Blocks III- and IV-type spacecraft in the environment produced by the 25-ft Space Simulator. The test environment was: vacuum,  $10^{-5}$  torr; cold wall temperature,  $-300^{\circ}\text{F}$ ; solar radiation intensity, 106 w/ft<sup>2</sup> with an 11-hr test time.

### B. Ground Support Equipment (GSE)

#### 1. Power Subsystem GSE, Mariner Mars 1964

*a. Power system test set.* The power system test set for the *Mariner Mars 1964* provides the necessary elements of power, monitoring and control to support the spacecraft power subsystem through test operations consisting of: initial power application, power subsystem evaluation, spacecraft system tests, environmental testing, and final integrated system tests conducted just prior to transport to the launch pad.

A functional block diagram of the power system test GSE is shown in Fig. 1. The design logically divides the equipment into two groups: (1) the monitoring and operator control area, and (2) the various power supplies, simulators, and associated logic and switching networks. System test sets, utilizing adapter racks, are provided for use in laboratory and flight acceptance testing. Additionally, the power system test provides simulation of interfaces which the flight equipment (when in the spacecraft) normally encounters with other spacecraft subsystems.

The test set is capable of automatic self-test before or during any operation in conjunction with the spacecraft or the power subsystem. This automatic sequence assures

that the monitor, recording, and power control functions of the GSE are operating within the required tolerances. No external equipment is necessary to complete the self-test.

***b. Launch control sets.*** The launch support sets contain all of the basic monitor and control features of the system test equipment but reflect the constraints and design considerations imposed by the launch operation and site. All launch equipment features and mechanizations are found in the system test sets.

The GSE for the central computer and sequencer (CC&S) flight equipment has the following capabilities:

- Capabilities (1) and (2) use identical equipment. Capability (1) is used in the laboratory and Capability (2) is used while the CC&S is installed in the spacecraft. GSE used in the blockhouse is identical and interchangeable

with panels found in systems GSE. This accomplishes three important things:

- (1) Operators using systems equipment are also familiar with blockhouse equipment.
- (2) Spare equipment is provided for the blockhouse by the systems equipment.
- (3) Launch complex operating modes and mechanizations are verified during system testing prior to actual launch operations.

### 3. Attitude Control Subsystem GSE

The attitude control GSE consists of the system test set (Fig. 2) and launch complex set.

*a. System test set.* The attitude control system test set is required to completely test and evaluate the attitude control system. It will perform this task by using the system test set in integrated spacecraft system tests, and subsystem tests in conjunction with the attitude control spacecraft system interfaces. All tests will be performed by using low risk, high reliability techniques developed

on previous programs and in the laboratory. These tests will be supplemented with a laboratory test set whenever necessary.

All components of the system test set will be self-tested from a test console. These self-test features will not interfere with the normal operation of the system test set. No self-test feature will react with flight equipment.

The system test set is comprised of one 6-ft console which will conform to JPL specifications. Twelve pressure-sensitive switches are used to monitor the attitude control cold gas valves. In conjunction with these are twenty-four gas check valves and a small compressed gas supply to facilitate self-testing. Four Sun sensor test assemblies, each containing four stimulus lamps, are used to test the acquisition and cruise Sun sensors. Two derived rate reset sensor test assemblies, each containing two stimulus lamps, are used to test the derived rate networks. There is one Sun-gate test assembly containing a collimated light source and one Earth-detector test assembly containing one stimulus lamp. Four analog position monitor-

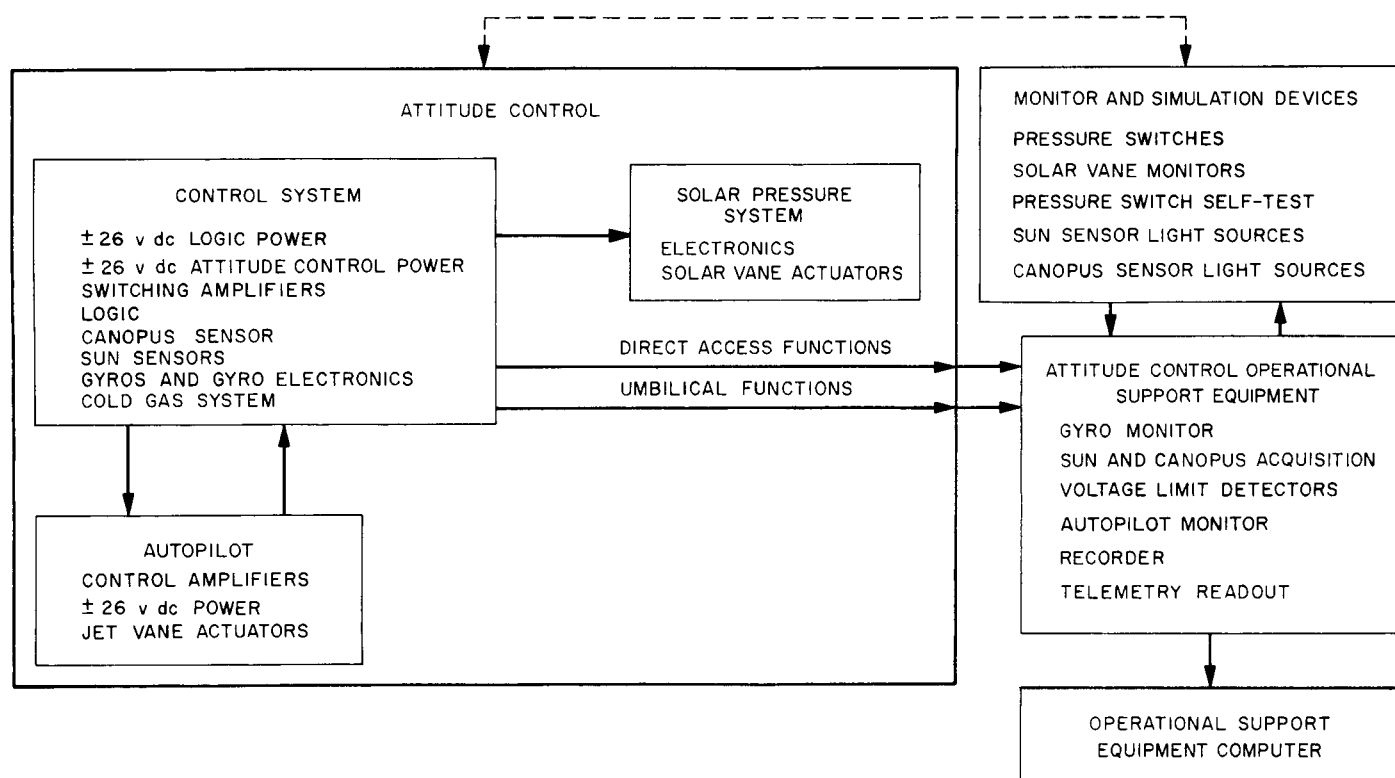


Fig. 2. Attitude control system test set

ing devices are used to monitor the solar vane movements. There is one Canopus and Sun shutter test assembly containing fifteen collimated, and one noncollimated, stimulus lamps which is used to test the Canopus sensor at all five cone angles, and at three set position offsets.

*b. Launch complex test set.* The attitude control launch complex test set is required to observe and measure critical subsystem functions. It will perform this task by using a portion of the system test set for maximum reliability and accuracy.

## SPACE SCIENCES

### IX. Space Instruments Development

#### A. Transfer Characteristics and Gray-Scale Reproduction for Space Camera Evaluation

The ability to distinguish between small variations in gray shades is one of the more important aspects of space photography (SPS 37-20, Vol. IV, pp. 151-155). Fidelity of reproduction in the gray shades is closely related to the camera system transfer characteristics. Included in an evaluation of the system transfer characteristics must be any of the instrumentation used for reproducing the observed data, e.g., oscilloscope presentations, photographic prints, or projected film, as these frequently have non-linear characteristics over the range of interest.

It is necessary to distinguish between static characteristics where data is accumulated point-by-point by measurement of discrete parameters and dynamic characteristics where the data is obtained by an active camera system and presented in the form of a scanned picture. In evaluating a slow-scan TV space photographic system for tone fidelity instrumentation problems arise due to the nature of the slow-scan process. Difficulties arise in particular with slow-scan display devices either with storage tubes or slow-scan oscilloscopes. Photographs that

play an essential part in slow-scan picture evaluation generally have an inadequate tonal range, which is coupled with difficulties in monitoring the developing and printing processes. The photographic processes are compounded with inaccuracies in the gray-scale values in standard test charts. This article discusses the means taken to evaluate the dynamic response of a slow-scan shuttered vidicon system with particular reference to fidelity of gray-shade reproduction.

Faithful reproduction of the gray scale is only possible if the exponent of the power law, which is a measure of the slope of the system transfer characteristics, approximates unity, i.e., when  $\gamma \approx 1$ . Camera system transfer characteristics are to a large extent controlled by the characteristics of the photo-sensor. The light transfer characteristics of the photo-sensor relate incident illumination to the electrical-signal output. The static light transfer characteristics of a vidicon may be determined for any given value of dark current by varying the incident illumination on the photoconductor and measuring the corresponding electrical output current. To ensure meaningful data this is accomplished with a modulated light signal, i.e., by exposure to an illuminated test pattern. The incident illumination on the photoconductor target is varied for static data by adjustment of the camera lens aperture.



If  $I_o$  is the corresponding output current and  $I_d$  the dark current of the vidicon, then the effective signal current that must be used for determining the transfer characteristic is  $I_s = I_o - I_d$ . The resultant curve plotted on log-log coordinates should be linear and noise free over the expected range of illumination for precise tonal rendition.

The dynamic performance of the camera for accurate gray-shade reproduction may be determined by exposure to a calibrated illuminated gray scale of adequate tonal range. The overall contrast range of pictures reproduced by conventional photographic processes is of the order of 30 db, and a readily observable change in illumination is 3 db. Hence, a step pattern comprising 10 shades of gray covering a range of 27 db is a generally acceptable standard for determining dynamic picture tonal response. The RETMA chart, which includes a 10-step gray scale, is a commonly used test pattern for determining the picture quality of television systems. For camera tests the chart takes the form of a 10- $\times$  9-in. celluloid film that may be evenly illuminated from a suitable light source.

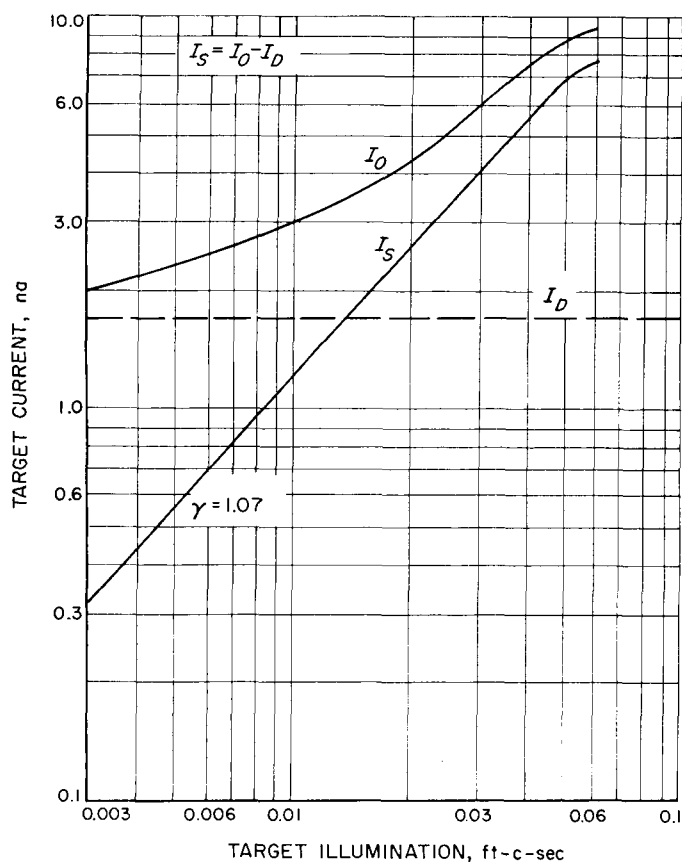


Fig. 1. Static transfer characteristics of GEC slow-scan vidicon

Both the static and dynamic characteristics of a vidicon have been measured for a slow-scan shuttered TV camera system. The static transfer characteristics for a GEC-type 1351B-1 vidicon inserted in the system are shown in Fig. 1. The output current  $I_o$  was measured in terms of a voltage at the output terminals of the preamplifier.  $I_o$  was then plotted from the observed data and  $I_s$  plotted from the estimated difference between  $I_o$  and  $I_d$ . The curve for  $I_s$  is seen to be substantially linear with a  $\gamma = 1.07$  over a range from 0.003 to 0.045 ft-c-sec, a 24-db range of illumination. At illumination levels greater than 0.045 ft-c-sec high-light saturation is becoming evident. The overall static response of the system as measured at the video amplifier output terminals is given for comparison in Fig. 2 and also indicates an average  $\gamma = 1.07$ . This indicates that all intermediate elements have a substantially linear response or compensate one another to produce a  $\gamma \approx 1$ .

Before measuring the dynamic response, the relative intensity in the gray-shade wedge of the RETMA chart was calibrated optically. This is required because of the known difficulty of reproducing an accurate wide range of density in photographic film. Microdensitometer measurements indicating relative illumination of the steps for

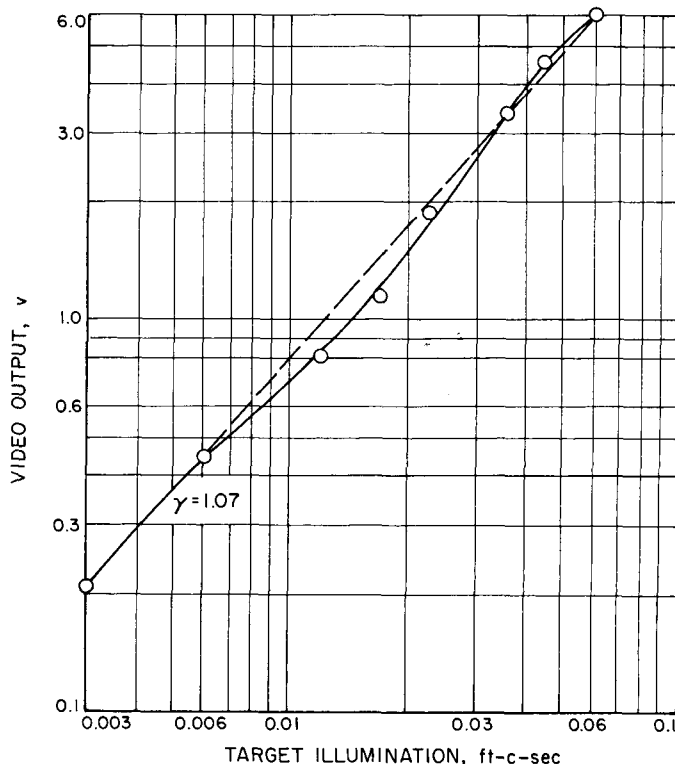


Fig. 2. Overall system static transfer characteristics

the particular RETMA chart used are shown in Fig 3. The overall range of the 10 steps on this chart is seen to be 22.5 db with an average of 2.5 db/step instead of the expected 3 db/step and variations of from 1.6 db to 4.2 db in step amplitude. A direct Polaroid print of this gray-scale wedge is shown in Fig. 4. The corresponding vidicon output signal as the gray-shade wedge is scanned, following a shuttered exposure to the chart, is indicated

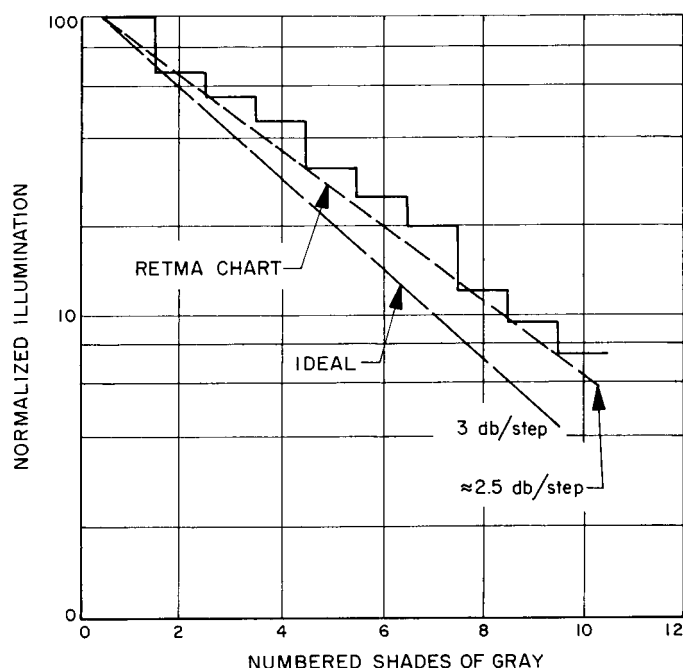


Fig. 3. Microdensitometer readings for RETMA chart gray scale

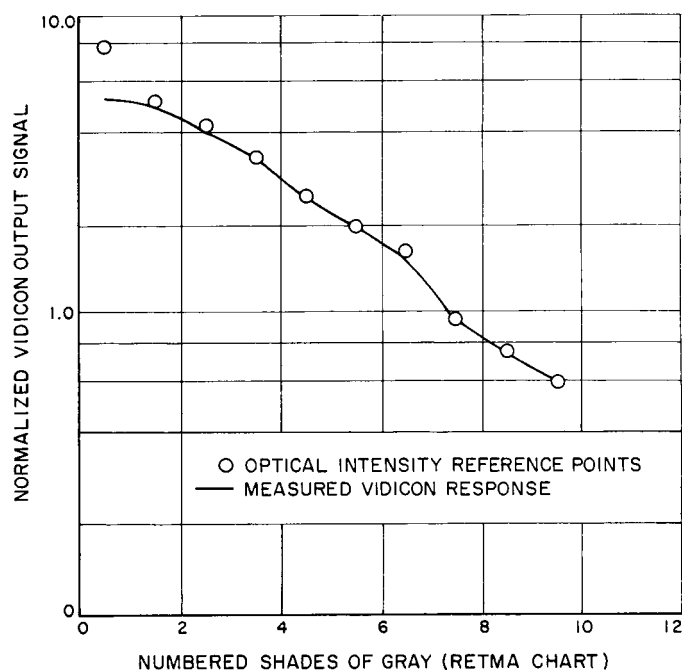


Fig. 5. Gray-shade reproduction with slow-scan vidicon

in Fig. 5. Signal amplitude was measured at the output terminals of the preamplifier using an A-scope line presentation. The optically measured points normalized to the electrical reference have been inserted for comparison. The vidicon output signal is seen to correspond quite closely to the light-intensity variations with the exception of the first step which has a lower output signal due to a combination of saturation and shading. The close agreement, otherwise, indicates the validity of the static measurement of the vidicon transfer characteristic illustrated in Fig. 1.

Amplifier noise tends to illuminate the darker parts of the picture, thus lowering contrast. An acceptable noise level for a planetary picture has been established at 30 db signal-to-noise ratio (S/N) when measured at maximum contrast with a test chart. Under these conditions the S/N is then defined by the ratio of the peak video signal to the rms noise. The S/N at varying illumination levels may be determined by changing the exposure and adjusting the video gain for maximum output at each illumination level. S/N data of this type is presented in Fig. 6 for the particular slow-scan vidicon system under consideration where the base bandwidth = 6.95 kc. The solid curve shown was taken for an optimally adjusted value of vidicon beam current which provides linear operation up to 0.056 ft-c-sec. At this beam current a 30-db S/N is achieved when the target illumination is 0.01 ft-c-sec. S/N data is most meaningful

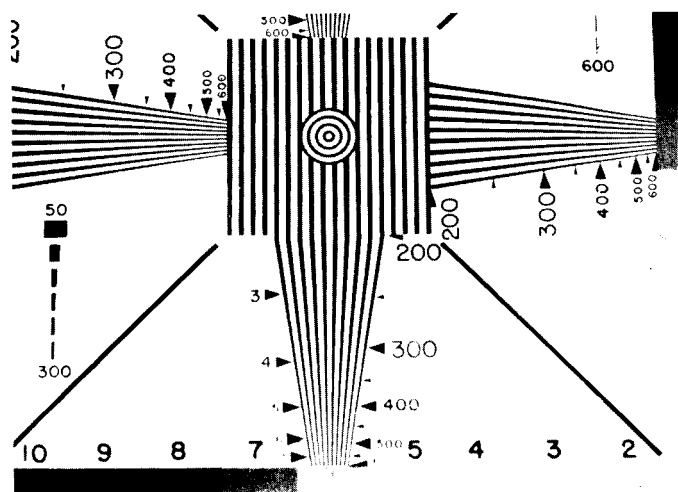


Fig. 4. Polaroid print of RETMA chart gray-scale wedge

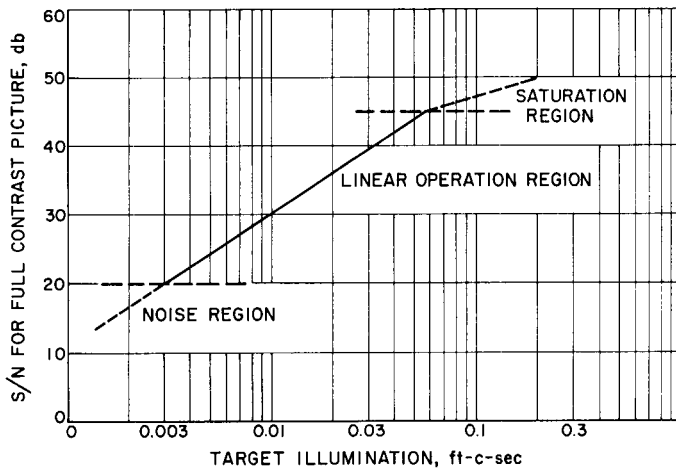


Fig. 6. S/N for slow-scan vidicon

in the linear region. Operation in the saturation region requires readjustment of the beam current with some degradation of picture quality over the operating region. Data taken in the noise region is of steadily decreasing value as the S/N drops below 20 db.

In a chopped-beam system where the vidicon output current is in the form of a modulated RF signal, the transfer characteristics of the detector become of interest. The measured transfer characteristics for a linear detector in terms of gray shades are as shown in Fig. 7 where each shade is 3 db and the overall range is 27 db. Non-linearity of the detector is evident at the lower input levels. For the RF level chosen  $\gamma > 1$ . Different input levels may be expected to produce corresponding variations in  $\gamma$ . This is illustrated in Fig. 8 where transfer characteristics were measured on the vidicon camera system for two levels of detector operation.

It should be noted that the chopped-beam system using a modulated-carrier video signal followed by a detector has the effect of reducing noise in the darker portions of the picture. The noise reduction may be explained as follows:

For linear rectifier followed by a band-pass filter the noise produced at the output terminals of the filter will decrease as the carrier is decreased (Ref. 1). If  $W_n$  = noise power,  $W_c$  = carrier power, and  $W_s$  = the signal output from the detector, then for  $W_c \rightarrow 0$ , corresponding to a dark picture,

$$W_{s_1} = W_n \left( \frac{\alpha}{\pi} \right)^2 \cdot \left( \frac{4 - \pi}{2} \right)$$

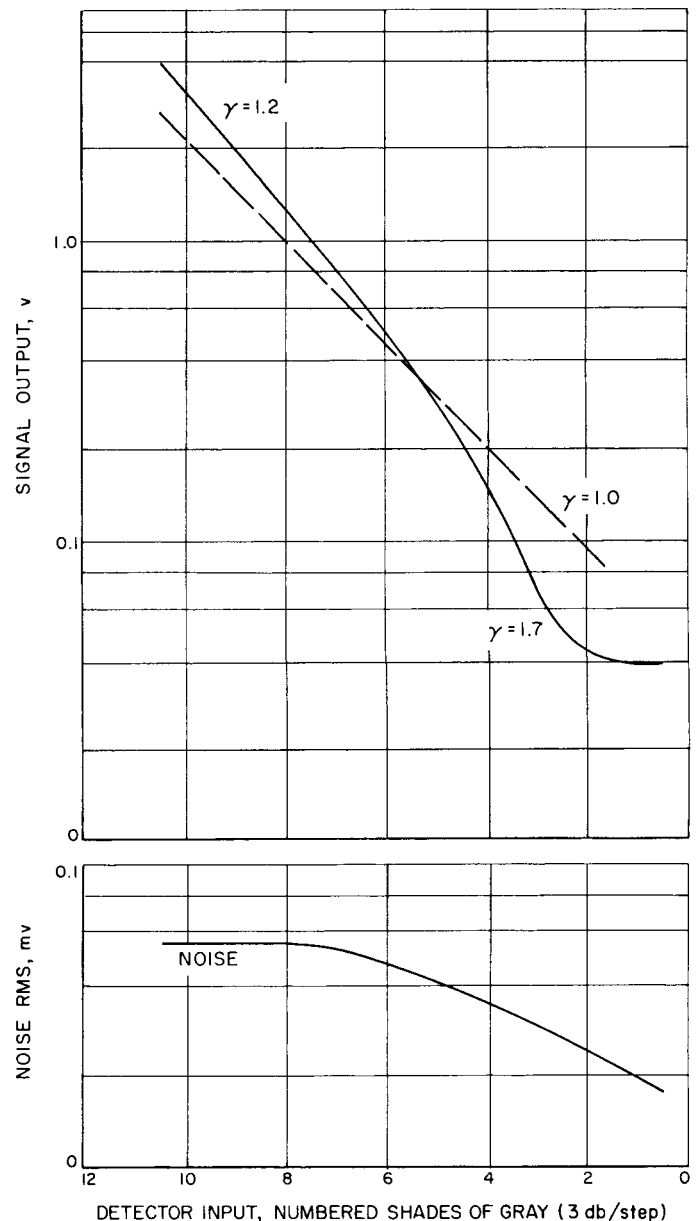


Fig. 7. Detector characteristics related to gray shades

where  $\alpha$  is a detector constant and terms relating to  $W_c$  are neglected. For  $W_c \gg W_n$ , corresponding to the high lights, the output signal becomes independent once again of  $W_c$  and

$$W_{s_2} = W_n \left( \frac{\alpha}{\pi} \right)^2$$

Hence, the ratio of the noise power for the bright and dark parts of the picture

$$\frac{W_{s_2}}{W_{s_1}} = \frac{2}{(4 - \pi)} = 2.33 = 3.7 \text{ db}$$

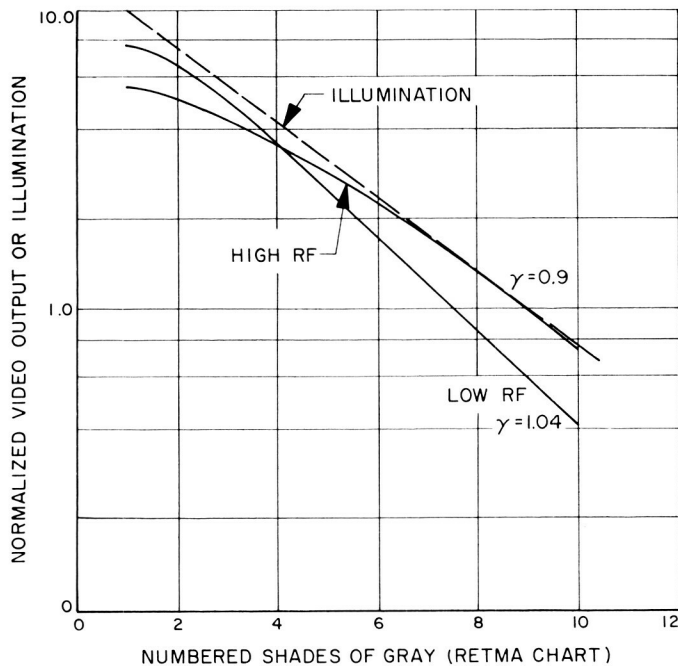


Fig. 8. Detector transfer characteristics for two RF levels

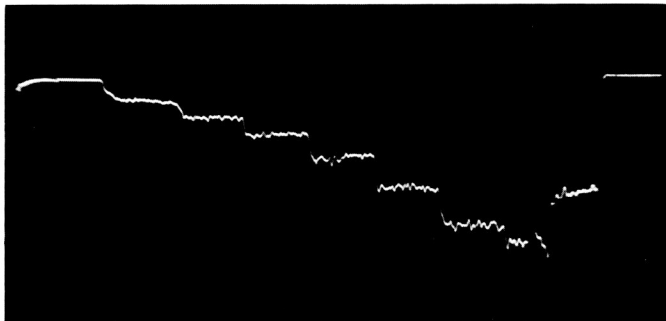


Fig. 9. Photograph of steps in output response demonstrating detector noise decrease

The addition of a low-pass filter increases this noise ratio still further as demonstrated in Fig. 7 where the difference between the gray-scale Step 10 and Step 1 is 8 db as measured at the filter output terminals. This further reduction in noise is because the maximum noise signal within the passband is generated by noise beating with the carrier, and as the carrier decreases with darker signals the noise also decreases. In addition, detector non-linearities, more relevant at low values of  $W_c$ , still further reduce the noise output. This reduction of noise during the scanning of a gray-scale wedge is illustrated in the A-scope presentation of Fig. 9.

To establish a more accurate gray scale than the wedge contained in the RETMA chart, a gray scale has been

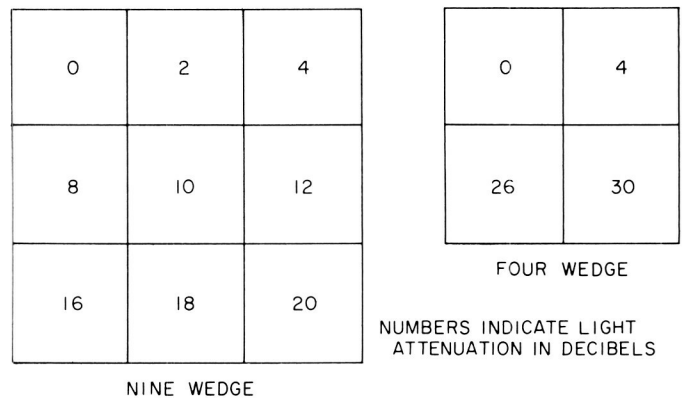


Fig. 10. Neutral-density filter optical wedges

assembled from neutral-density filters. The light attenuation of a given filter in db is related to the neutral-density filter number  $N$ : the attenuation db =  $20 N$ . Thus, a set of filters numbered from 0 to 1.0 in 0.1 graduations provides an 11-step gray-scale wedge of 2 db/step covering a 20-db illumination range. As the filter size readily available was  $2 \times 2$  in., and the illuminated picture test area was limited to  $6 \times 6$  in., only 9 of these filters could be utilized. However, by omitting 2 of the filters, a 20-db nine-step wedge could be assembled. In addition, an arrangement of filters was assembled to provide a four-step range of 30 db. Fig. 10 shows the arrangement of the filters with the light attenuation in db. Direct Polaroid exposures of these wedges were taken on 400 speed film and photo reproductions of the prints are shown in Fig. 11. Pictures were then taken with the TV camera system, displayed on a slow-scan oscilloscope and photographed with the same camera and film speed. Polaroid prints of the TV pictures so obtained were photographed and the prints reproduced as Fig. 12.

Inaccuracies in the photographic and printing processes in the reproduction of gray shades may be resolved for a camera system by measuring the amplitude response at the video output terminals with an A-scope. Such data is shown in Fig. 13, an A-scope presentation of isolated lines of the video signal as the camera scans the neutral-density-filter gray-scale wedge. Fig. 13a shows the response to the top three filters, Fig. 13b the response to the middle set, and Fig. 13c the response to the lower set. In addition, Fig. 14 shows the response to the lower filters of the 20-db (Fig. 14a) and 30-db (Fig. 14b) wedges expanded on the A oscilloscope to more clearly illustrate the differences in output level. Amplifier noise becomes more prominent with the increased sensitivity of the oscilloscope.

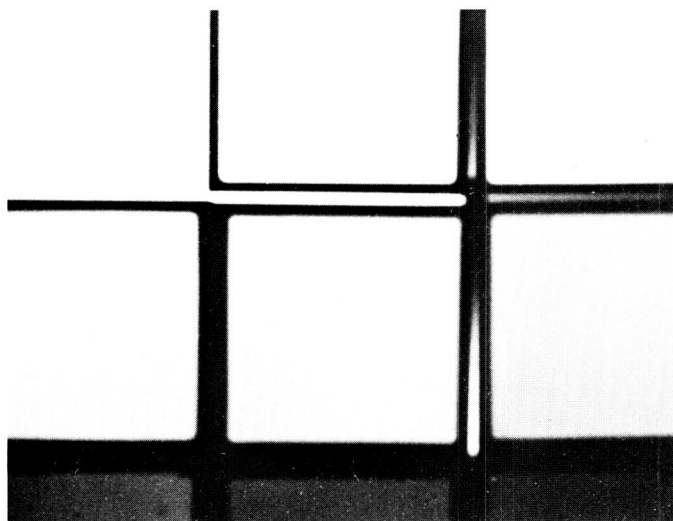


Fig. 11. Polaroid photographs of wedges

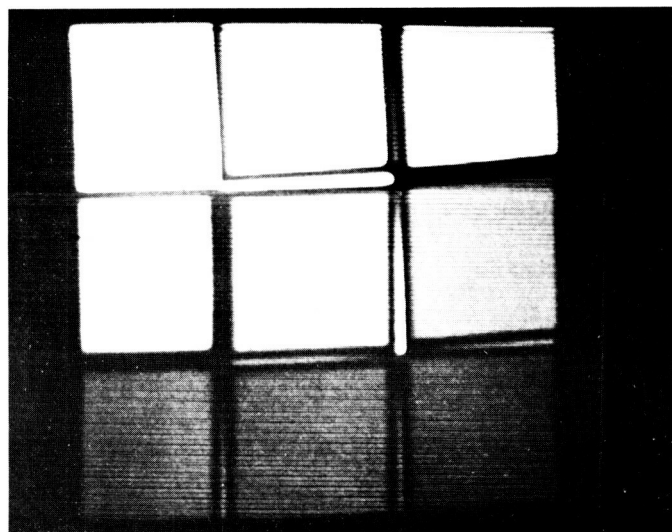
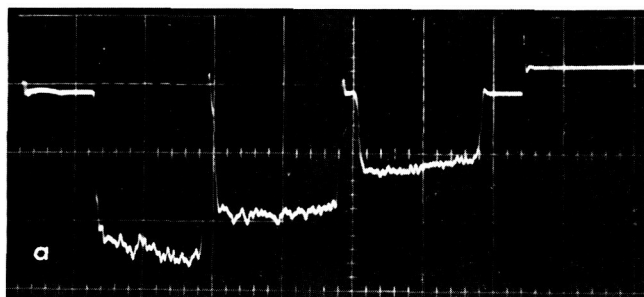


Fig. 12. TV pictures of wedges

**Conclusion.** Evaluation of the dynamic performance of a slow-scan TV camera system presents state-of-the-art problems ranging from inaccuracies in gray-scale test patterns to inadequacies in photographic picture reproducing techniques. In the camera system under consideration, the dynamic range was limited to 30 db by saturation at high illumination levels and noise at the lower levels. It appears that there is some reduction in noise in the darker portions of the picture with a chopped-beam system. The measured dynamic range represents eleven shades of gray at 3 db/step. The A-scope presen-

tations have shown that all of these steps can be clearly reproduced and demarcated. However, non-linearities in the Polaroid film print and in the slow-scan monitor oscilloscope limit the perceptible gray shades for dynamic picture reproduction to a value that is closer to 20 db. It is suggested that gray-scale wedges be built up from accurate neutral density filters and be assembled in a wedge pattern that fills the whole of the illuminated area. This will not only provide a more accurate gray scale but will reduce the effect of local photosensor inconsistencies that arise when the gray-shade wedge



covers only small strips of the total illuminated area as in the RETMA chart. As the Polaroid print still represents one of the best and most convenient means for communicating data for slow-scan systems, it is unlikely to be replaced in the near future. This implies some care by the observer in the evaluation of dynamic camera performance as related to gray-shade reproduction.

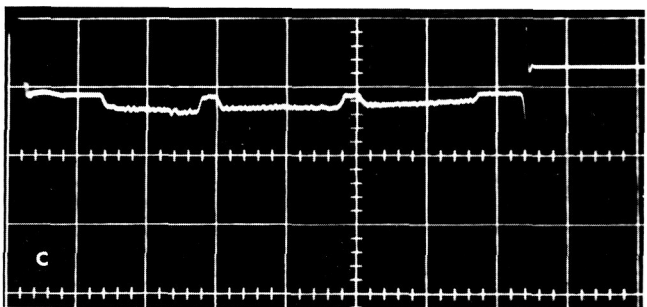
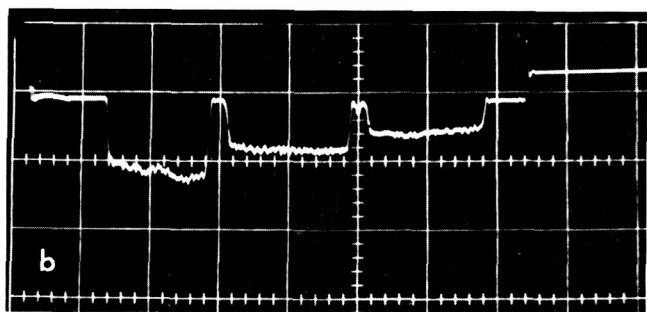


Fig. 13. A-scope presentation of nine-wedge response

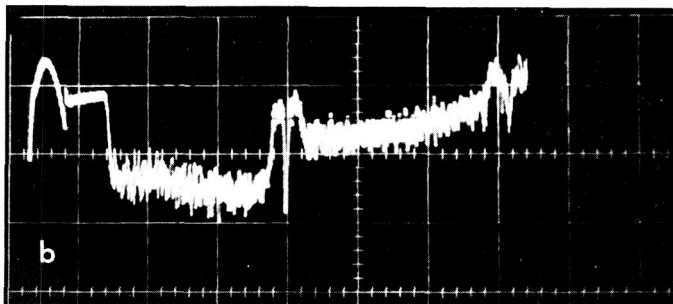
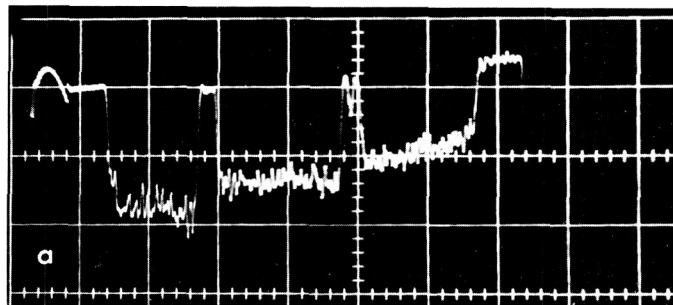


Fig. 14. Expanded A-scope presentations of lower wedges

## Reference

1. Goldman, S. *Frequency Analysis Modulation and Noise*, McGraw-Hill Book Co., Inc., New York, pp. 245-249, 1948.

## X. Space Instruments Systems

### A. Formulation of Electrical Network Problems for Computer Analysis

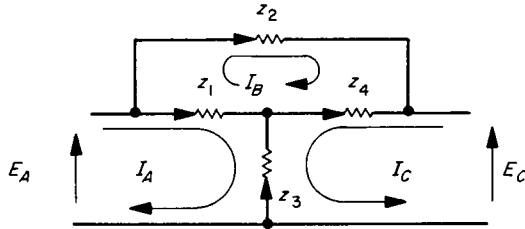
In attempting computer studies of networks, whether for the purpose of determining stability criteria or for an elaborate parameter study, an accurate mathematical representation is required. The reference here is to the accuracy with which the equations are compiled rather than to the adequacy of the mathematical model used. This is a difficult task even for circuits of moderate complexity. As complexity is increased, the desirability of having a complete solution may be insufficient stimulus to assure completion of the task. The purpose of this article is to present a means for generating the required matrix equations with a minimum of effort and, hopefully, with a minimum of errors.

Consider the following: (1) Each branch of the network is represented by the Laplace transform of its impedance. These impedances are then used as the elements of a diagonal matrix  $B$ . (2) The  $B$  matrix may now be transformed into the  $Z$  matrix for the network by means of a coincidence matrix  $C$ .

$$Z = C^t \cdot B \cdot C$$

The matrix  $C$  has rows corresponding to the branches of the network, and columns corresponding to the loops. The elements of  $C$  are either  $+1$ ,  $-1$ , or  $0$  as a function of the product of loop direction and an arbitrarily assigned branch direction.

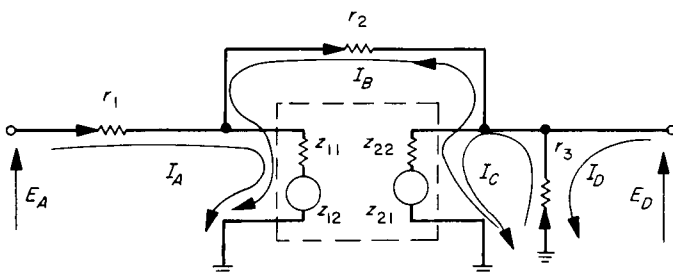
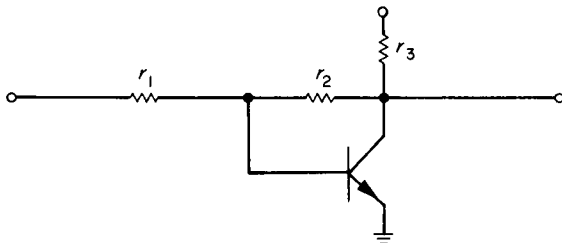
The transformation illustrated in Example 1 generates symmetrical matrices  $Z$  from diagonal matrices  $B$  and is not applicable to networks containing active devices.

**Example 1**

$$\begin{vmatrix} +1 & 0 & -1 & 0 \\ -1 & +1 & 0 & -1 \\ 0 & 0 & -1 & -1 \end{vmatrix} \cdot \begin{vmatrix} z_1 & 0 & 0 & 0 \\ 0 & z_2 & 0 & 0 \\ 0 & 0 & z_3 & 0 \\ 0 & 0 & 0 & z_4 \end{vmatrix} \cdot \begin{vmatrix} +1 & -1 & 0 \\ 0 & +1 & 0 \\ -1 & 0 & -1 \\ 0 & -1 & -1 \end{vmatrix}$$

$$Z = C' \cdot B \cdot C = \begin{vmatrix} z_1 + z_3 & -z_1 & z_3 \\ -z_1 & z_1 + z_2 + z_4 & z_4 \\ z_3 & z_4 & z_3 + z_4 \end{vmatrix}$$

It can be demonstrated (Example 2) that the non-symmetrical matrices required for active devices may be handled if the matrix representing the active device be included along the diagonal of  $B$  as a submatrix. Only the terminal impedances ( $z_{11}$ ,  $z_{22}$ ,  $z_{33}$  . . .) are used in forming  $C$ . The coupling terms are entered later in the appropriate row and column ( $z_{13}$  is placed in the row of  $z_{11}$  and the column of  $z_{33}$ ).

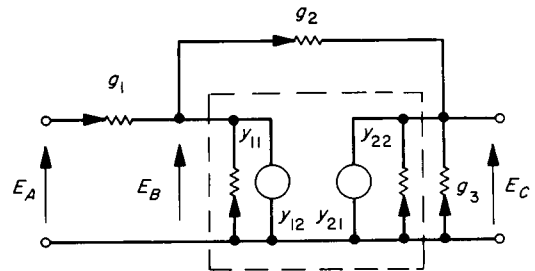
**Example 2**

TRANSISTOR IMPEDANCE MATRIX

$$\begin{vmatrix} 1 & 0 & 0 & 0 & -1 \\ 0 & -1 & 0 & 0 & -1 \\ 0 & 0 & -1 & 0 & 0 \\ 0 & 0 & -1 & -1 & 0 \end{vmatrix} \cdot \begin{vmatrix} r_1 & 0 & 0 & 0 & 0 \\ 0 & r_2 & 0 & 0 & 0 \\ 0 & 0 & r_3 & 0 & 0 \\ 0 & 0 & 0 & z_{11} & z_{12} \\ 0 & 0 & 0 & z_{21} & z_{22} \end{vmatrix} \cdot \begin{vmatrix} 1 & 0 & 0 & 0 \\ 0 & -1 & 0 & 0 \\ 0 & 0 & -1 & -1 \\ 0 & 0 & 0 & -1 \\ -1 & -1 & 0 & 0 \end{vmatrix}$$

$$Z = \begin{vmatrix} r_1 + z_{11} & z_{11} & -z_{12} & -z_{12} \\ z_{11} & r_2 + z_{11} & -z_{12} & -z_{12} \\ -z_{21} & -z_{21} & r_3 + z_{22} & r_3 + z_{22} \\ -z_{21} & -z_{21} & r_3 + z_{22} & r_3 + z_{22} \end{vmatrix}$$

The problem can be implemented on the node basis with equal ease (Example 3). In this case, an incidence matrix is generated by again assigning arbitrary directions to the branches and tabulating their incidence on the nodes of the network. Admittances of the branches replace the impedances.

**Example 3**

TRANSISTOR ADMITTANCE MATRIX

$$\begin{vmatrix} -1 & 0 & 0 & 0 & 0 \\ 1 & -1 & 0 & 1 & 0 \\ 0 & 1 & 1 & 0 & 1 \end{vmatrix} \cdot \begin{vmatrix} g_1 & 0 & 0 & 0 & 0 \\ 0 & g_2 & 0 & 0 & 0 \\ 0 & 0 & g_3 & 0 & 0 \\ 0 & 0 & 0 & y_{11} & y_{12} \\ 0 & 0 & 0 & y_{21} & y_{22} \end{vmatrix} \cdot \begin{vmatrix} -1 & 1 & 0 \\ 0 & -1 & 1 \\ 0 & 0 & 1 \\ 0 & 1 & 0 \\ 0 & 0 & 1 \end{vmatrix}$$

$$Y = \begin{vmatrix} g_1 & -g_1 & 0 \\ -g_1 & g_1 + g_2 + y_{11} & -g_2 + y_{12} \\ 0 & -g_2 + y_{21} & g_2 + g_3 + y_{22} \end{vmatrix}$$

Once the individual circuit matrices are determined, they may be combined and larger systems analyzed. This is accomplished as in Example 2. The coincidence matrix is written in terms of the self-impedances of each pair of terminals and the source and load resistances. In order that the polarities of the coupling terms be preserved, it is convenient to assign branch directions conforming with the normal matrix conventions.

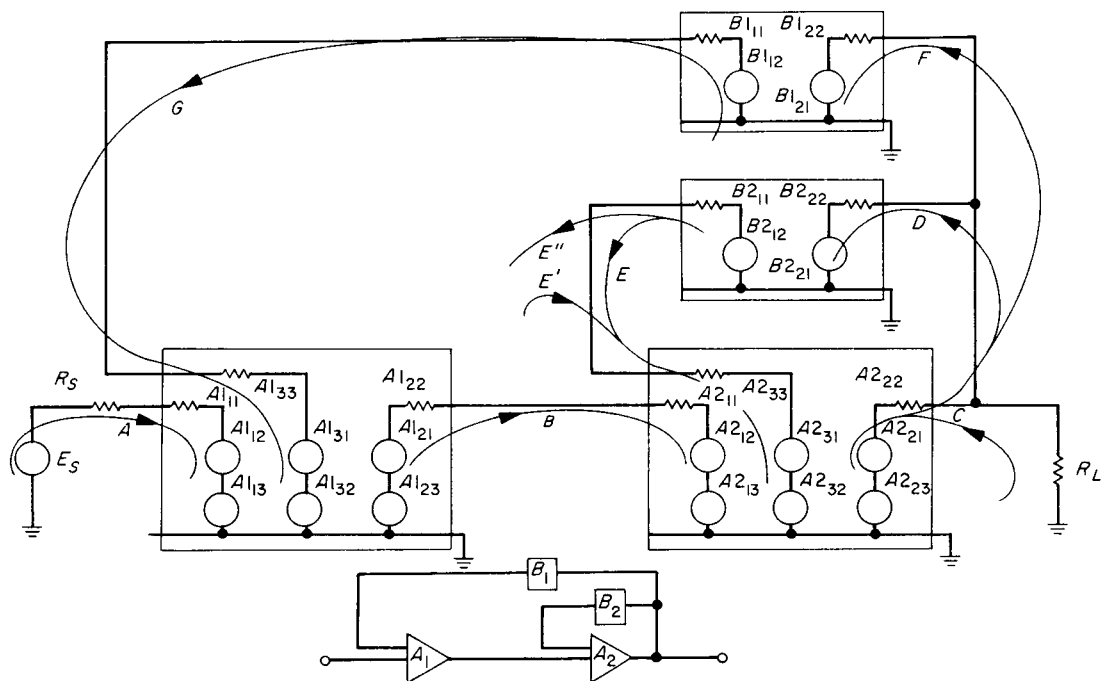
It is a simple matter to obtain any desired system function by proper arrangement of the coincidence matrix.  $C$  matrices, corresponding to three system functions, are illustrated in Example 4.



---

**Example 4**

---



$$\begin{array}{c}
 R_S \\
 A1_{11} \quad A1_{12} \quad A1_{13} \\
 A1_{21} \quad A1_{22} \quad A1_{23} \\
 A1_{31} \quad A1_{32} \quad A1_{33} \\
 B1_{11} \quad B1_{12} \\
 B1_{21} \quad B1_{22} \\
 A2_{11} \quad A2_{12} \quad A2_{13} \\
 A2_{21} \quad A2_{22} \quad A2_{23} \\
 A2_{31} \quad A2_{32} \quad A2_{33} \\
 B2_{11} \quad B2_{12} \\
 B2_{21} \quad B2_{22} \\
 R_L
 \end{array}$$

The system matrix without either feedback loop is obtained using:

$$C = \begin{pmatrix} 0 & 0 & 0 \\ 1 & 0 & 0 \\ 0 & -1 & 0 \\ 0 & 0 & 0 \\ 0 & 0 & 0 \\ 0 & 0 & 0 \\ 0 & 1 & 0 \\ 0 & 0 & 1 \\ 0 & 0 & 0 \\ 0 & 0 & 0 \\ 0 & 0 & 0 \\ 0 & 0 & 0 \end{pmatrix}$$

$$Z = C^t \cdot B \cdot C = \begin{vmatrix} A_{11} & -A_{12} & 0 \\ -A_{21} & A_{22} + A_{21} & A_{21} \\ 0 & A_{21} & A_{22} \end{vmatrix}$$

The system function with both feedback loops closed is obtained by augmenting  $C$  with the required additional loops:

$$C = \begin{pmatrix} 0 & 0 & 0 & 0 & 0 & 0 & 0 \\ 1 & 0 & 0 & 0 & 0 & 0 & 0 \\ 0 & -1 & 0 & 0 & 0 & 0 & 0 \\ 0 & 0 & 0 & 0 & 0 & 0 & 1 \\ 0 & 0 & 0 & 0 & 0 & 1 & 0 \\ 0 & 0 & 0 & 0 & 0 & 0 & -1 \\ 0 & 1 & 0 & 0 & 0 & 0 & 0 \\ 0 & 0 & 1 & -1 & 0 & -1 & 0 \\ 0 & 0 & 0 & 0 & 1 & 0 & 0 \\ 0 & 0 & 0 & 1 & 0 & 0 & 0 \\ 0 & 0 & 0 & 0 & -1 & 0 & 0 \\ 0 & 0 & 0 & 0 & 0 & 0 & 0 \end{pmatrix}$$

The stability of feedback Circuit E may be investigated by terminating the source and load terminals and making a "pliers type" entry into that loop. Loop E is thus split into E' and E'' and the source  $R_S$  and the load  $R_L$  are included. The corresponding coincidence matrix is:

$$C = \begin{bmatrix} A & B & C & D & E' & E'' & F & G \\ 1 & 0 & 0 & 0 & 0 & 0 & 0 & 0 \\ 1 & 0 & 0 & 0 & 0 & 0 & 0 & 0 \\ 0 & -1 & 0 & 0 & 0 & 0 & 0 & 0 \\ 0 & 0 & 0 & 0 & 0 & 0 & 0 & 1 \\ 0 & 0 & 0 & 0 & 0 & 0 & 1 & 0 \\ 0 & 0 & 0 & 0 & 0 & 0 & 0 & -1 \\ 0 & 1 & 0 & 0 & 0 & 0 & 0 & 0 \\ 0 & 0 & 1 & -1 & 0 & 0 & -1 & 0 \\ 0 & 0 & 0 & 0 & 0 & 1 & 0 & 0 \\ 0 & 0 & 0 & 1 & 0 & 0 & 0 & 0 \\ 0 & 0 & 0 & 0 & -1 & 0 & 0 & 0 \\ 0 & 0 & 1 & 0 & 0 & 0 & 0 & 0 \end{bmatrix}$$

E' is now considered as the input loop while E'' is considered as the output loop. The resulting impedance matrix is:

$$\begin{bmatrix} R_S + A_{11} & -A_{12} & 0 & 0 \\ -A_{12} & A_{12} + A_{21} & A_{22} & -A_{22} \\ 0 & A_{21} & A_{22} + R_L & -A_{22} \\ 0 & -A_{21} & A_{22} & A_{22} + B_{21} \\ 0 & 0 & 0 & -B_{21} \\ 0 & A_{21} & A_{22} & -A_{22} \\ 0 & -A_{21} & -A_{22} & A_{22} \\ A_{13} & -A_{12} & 0 & 0 \\ 0 & 0 & 0 & A_{13} \\ 0 & A_{23} & -A_{22} & -A_{13} \\ 0 & A_{23} & -A_{22} & 0 \\ -B_{22} & -A_{23} & A_{22} & 0 \\ B_{22} & 0 & 0 & 0 \\ 0 & -A_{23} & -A_{22} & 0 \\ 0 & -A_{23} & -A_{22} + B_{11} & -B_{12} \\ 0 & 0 & -B_{12} & A_{13} + B_{12} \end{bmatrix} = Z$$

The procedures presented allow for the setting up of matrix equations of complex circuits by means of a coincidence matrix and the matrix  $B$ , which is little more than a parts list. The matrix may then be used for solution by inversion, or for an eigenvalue routine. In the former case, frequency analysis can be obtained by incrementing the angular frequency and making repeated inversions. In the latter case, the form would be

$$\det [(C^t \cdot B_L \cdot C) \cdot p + (C^t \cdot B_R \cdot C) + (C^t \cdot B_S \cdot C) \cdot 1/p] = 0$$

where  $B_L$ ,  $B_R$ , and  $B_S$  are diagonal matrices consisting of only the branch inductances, resistances, and susceptances, respectively. It should be pointed out that the above transformation is not a "similarity" transformation since the rank of  $B$  is not that of  $Z$ . Hence, the eigenvalues of  $B$  are not those of  $Z$ .

A compact notation has been presented which allows for the manipulation of complex networks containing both impedances and nonsymmetrical matrices. It is believed that this method offers considerable advantage over hand compilation or other matrix combination schemes which depend upon transformation between matrix types as a function of the combination geometry. Hand compilation is quite tedious while the combination schemes are both complicated and of diminishing accuracy as the number of required matrix inversions is increased.

## B. Planetary Scan Subsystem for Mariner Mars 1964

### 1. Introduction

A continuing effort in the development of the planetary scan subsystem is described. A number of modifications have been made to accommodate new and revised requirements; otherwise, the subsystem is similar to that described in previous SPS. A block diagram of the subsystem is shown in Fig. 1.

When the subsystem is energized, a signal from a one-shot multivibrator circuit presets all logic circuits and the subsystem enters the planet searching mode of operation. The subsystem scans 180 deg in the process of searching for the planet. The scanning device provides the motion in one direction while the moving spacecraft provides motion approximately perpendicular to the scanning plane. A 400-cps motor is used for the scanning. Limit switch action is provided to reverse the direction of scan when the scanning of 180 deg is completed.

A planet sensor is utilized to detect the presence of the planet. The sensor, having a 50-deg circular field view, is sensitive to an image having a frequency range of 0.4 to 1.1  $\mu$ . When the planet comes into view, a signal from the planet-in-view logic switches the subsystem from planet searching to planet acquisition mode. The

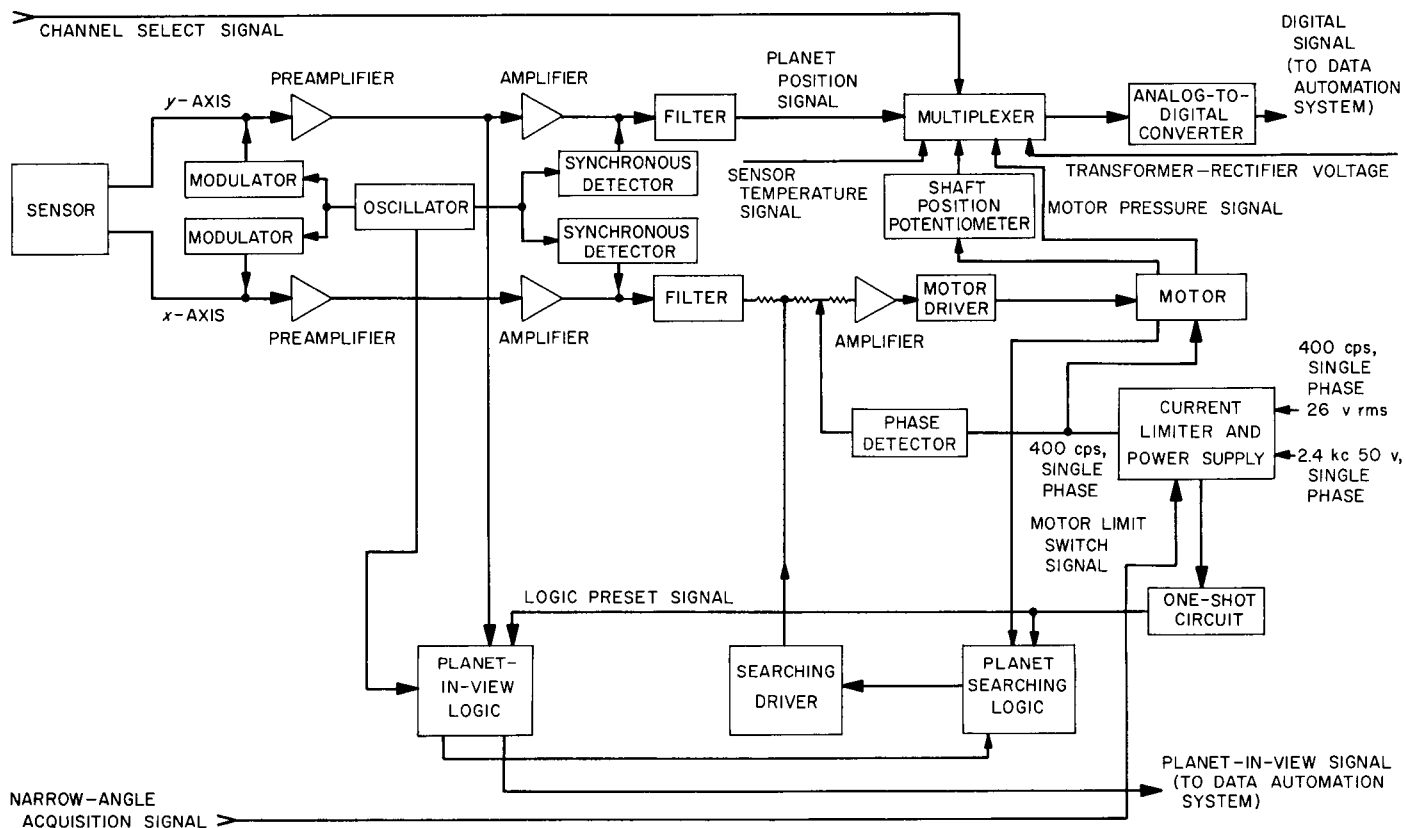


Fig. 1. Mariner Mars 1964 scan subsystem block diagram

subsystem tracks the planet at its first bisector through the use of the servo system.

Upon receiving a narrow angle acquisition signal indicating the planetary science instruments are in position, the scan and tracking motions of the subsystem will cease.

## 2. Fiber optic system

A fiber optic system is being developed as an integral part of the planet sensor assembly. The system consists of conventional optical elements coupled by a conical fiber element to form a compounded system capable of fast response over the wide angular field. The purpose of the fiber element is to reduce the size of the image, thus allowing the use of a conventional optic system with a larger aperture at a specified field of view. The characteristics of the compounded system are as follows:

- (1) Focal length: 10 mm.
- (2) Effective  $f$ -ratio:  $f/0.7$ .
- (3) Optical resolution: 20 line-pair per mm.
- (4) Frequency response: 0.5 to 1.1  $\mu$ .

(5) Field of view: 50 deg.

(6) Weight: 1 lb.

(7) Dimensions: 2 in. in diameter, 6 in. in length.

## 3. Sensor

The radiation tracking sensor is a semiconductor junction device which converts the  $x$ - $y$  coordinates of a light spot projected on its surface into a pair of voltages,  $V_x$  and  $V_y$ . A diagram of the sensor is shown in Fig. 2 with the polarities of the output voltages  $V_x$  and  $V_y$  as shown when the light spot is located in the indicated quadrant. When the light spot is located at the center,  $V_x$  and  $V_y$  are zero. Voltages from the sensor are self-generating and no bias voltage is required.

## 4. Electronics

A photomodulator device is used to modulate the DC  $x$ -axis output signal from the sensor. The photomodulator consists of a pair of small neon lamps and a matched pair of cadmium sulfide cells. An oscillator is used to drive the lamps at a frequency of 25 cps. The method of modu-

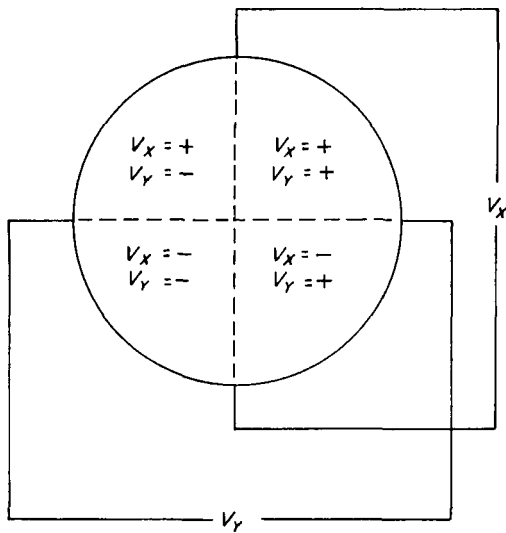


Fig. 2. Radiation tracking sensor

lation by photomodulator was chosen for its simplicity and reliable operation. It also produces extremely low offset voltages when operating over the required temperature range.

The modulated signal is amplified by a 4-stage AC pre-amplifier having a gain of 8000 and an input impedance of 3 megohms. The signal is again amplified by a 3-stage, zener-coupled, AC amplifier having a gain of 1000 and an output impedance of 300 ohms. The signal is then demodulated and filtered by a synchronous detector and a 3-stage R-C filter network. The DC signal from the filter network is phase detected using the 400-cps signal to the driving winding of motor as reference. The phase detected 400-cps signal is amplified and utilized to drive and control the direction of drive of the motor.

The  $y$ -axis output signal of the sensor is similarly processed and amplified. This signal, indicating the planet position, is then sent to the A-to-D converter via a multiplexer.

### 5. Logic and control circuitry

The logic and control circuits are as shown in Fig. 3. Searching and acquisition modes of operation are controlled by the flip-flop C (F-F C). When power to the subsystem is applied, a signal from the one-shot circuit presets all the F-Fs and the subsystem is in the planet

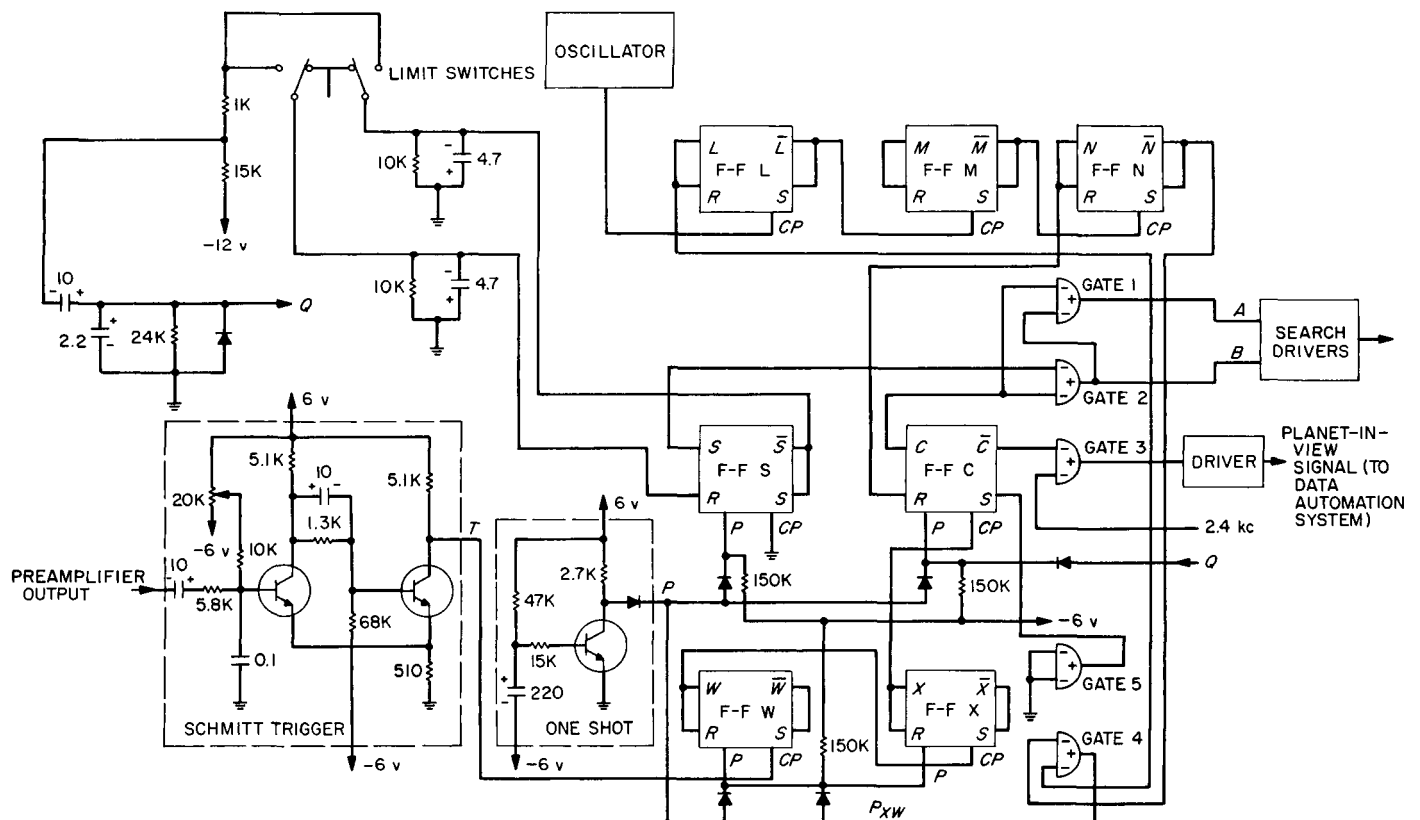


Fig. 3. Logic and control circuit

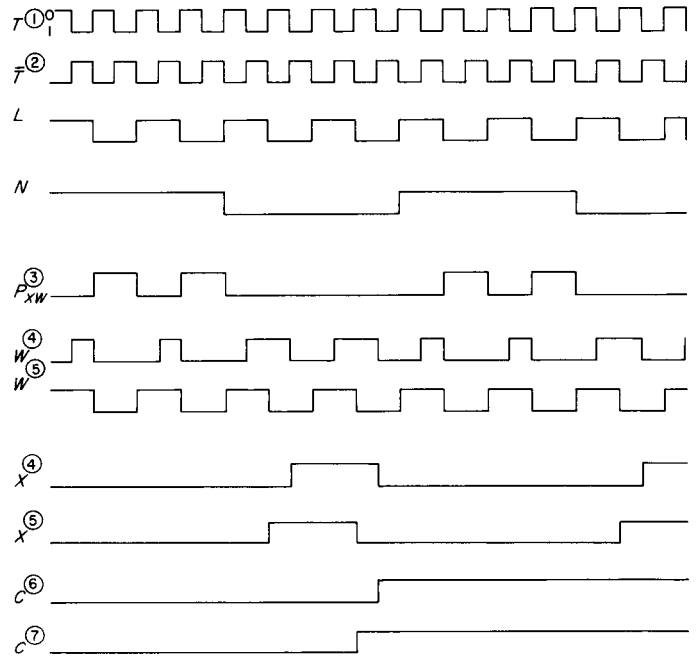
searching mode. The clockwise and counterclockwise motor drive signals are controlled by F-F S. The F-F S in turn is being set and reset by the limit switches through the wave-shaping circuits.

Logic equations for the searching mode operation are as follows:

$$\begin{aligned}
 \bar{B} &= CS \\
 B &= \bar{S} + \bar{C} \\
 A &= CB = C(\bar{S} + \bar{C}) \\
 &= \bar{C}\bar{S} \\
 \bar{A} &= S + \bar{C} \\
 \text{CW drive} &= AB \\
 &= C\bar{S}(\bar{S} + \bar{C}) \\
 &= C\bar{S} \\
 \text{CCW drive} &= \bar{A}\bar{B} \\
 &= (S + \bar{C})(CS) \\
 &= CS
 \end{aligned}$$

The planet-in-view logic consists of a Schmitt trigger, F-Fs W and X, and Gates 1, 2, 3, and 4. The Schmitt trigger is utilized to detect the voltage level of the modulated sensor signal from the preamplifier. Firing level of the Schmitt trigger is adjusted above the noise level. It is also so adjusted that the trigger will not fire when the spacecraft is at a distance from the planet beyond the acquisition capability of the subsystem.

A signal from the oscillator having the same frequency as the modulated sensor signal is frequency divided by eight through the use of F-Fs L, M, and N. This frequency-divided signal is utilized to control the sampling period. F-Fs W and X are used to count the number sensor signal pulses through the trigger during the sampling period. If eight or more pulses are gated during the sampling period, F-F C changes its state and the subsystem is now in the acquisition mode. If less than eight pulses are gated, F-Fs X and W are reset by the signal from Gate 4 during each sampling period. The counting operation resumes during next sampling period. Fig. 4 shows the wave form at the outputs of the various flip-flops and gates.



- ① SIGNAL  $T$  FROM SCHMITT TRIGGER WHEN SENSOR SIGNAL IS POSITIVE
- ② SIGNAL  $\bar{T}$  FROM SCHMITT TRIGGER WHEN SENSOR SIGNAL IS NEGATIVE
- ③ SIGNAL  $P_{XW}$  FROM GATE 4 USED TO RESET F-F X AND W
- $P_{XW} = N + \bar{L}$ ;  $\bar{P}_{XW} = L\bar{N}$
- ④ CORRESPOND TO  $T$ , CHANGE STATE WHEN  $P_{XW}$  IS 1 AND  $CP$  CHANGE FROM 0 TO 1
- ⑤ CORRESPOND TO  $\bar{T}$ , CHANGE STATE WHEN  $P_{XW}$  IS 1 AND  $CP$  CHANGE FROM 0 TO 1
- ⑥ CORRESPOND TO  $T$
- ⑦ CORRESPOND TO  $\bar{T}$

Fig. 4. Planet-in-view logic

$$\begin{aligned}
 \text{Acquisition mode} &= \bar{A}\bar{B} \\
 &= (S + \bar{C})(\bar{S} + \bar{C}) \\
 &= S\bar{C} + \bar{C}\bar{S} + \bar{C} \\
 &= \bar{C}(S + \bar{S} + 1) \\
 &= \bar{C}
 \end{aligned}$$

## 6. Power supply and power consumption

Preamplifiers and amplifiers are designed to operate on plus and minus 12 v, and logic and control circuits on plus and minus 6 v. The subsystem requires 3.0 w of 2.4 kc, single-phase and 3.0 w of 400 cps, single-phase of primary spacecraft power to operate.

## XI. Lunar and Planetary Studies

### A. Preliminary Results from Ranger 3 Gamma Ray Spectrometer

The *Ranger 3* gamma ray spectrometer was designed to measure gamma ray radiation emanating from the lunar surface and, by this means, to gain information on the surface composition (Refs. 1, 2). The spectrometer consists of a 2.75-in. cylindrical crystal of thallium-activated cesium iodide completely surrounded by a thin plastic scintillator, which permits the rejection of charged particles. The output of the detector is fed to a pulse height analyzer having 31 channels for discrete, incremental energy storage plus 1 channel for all signals with amplitude greater than that corresponding to channel 31. It was arranged that the instrument be operative for about 60 hr before lunar impact in order to make observations on the interplanetary gamma ray flux, as well as to obtain suitable background measurements for the lunar analysis. Although the spacecraft did not pass sufficiently near the Moon to allow its main function to be carried out, data for more than 40 hr of operation were transmitted back to Earth. A preliminary analysis of the data has been completed (Ref. 3).

Alternate spectra were taken with the analyzer covering the nominal ranges 0.1 to 3 Mev (low gain) and 20 to 600 kev (high gain). The gain ratio between the two modes was  $5.1 \pm 0.1$ , which was the value observed in final ground tests. The duration of each counting period was 459.5 sec, and a total of approximately 300 spectra was obtained in both positions. Sources of Hg-203 (279 kev) and Co-57 (122 kev) were mounted on the crystal to allow calibration in the high-gain mode. Because of an unexpected temperature rise, which approached 70°C shortly before boom extension, the over-all instrument gain departed significantly from the expected values. In the stowed position the low-gain spectrum spanned approximately 0.1 to 2.6 Mev, but in the extended position, 0.1 to 2.1 Mev. Except for an unexplained transient during rapid cooling following boom extension, all obvious indications pointed to proper functioning of the spectrometer in space.

The gamma ray intensity in the stowed position was found to be less than 2 times that in the extended position after correcting for a radioactive source that was discovered to have been on the spacecraft. Since the reduction in solid angle was about a factor of 20, it appears that the bulk of counts which comprise the outboard spectra are

not due to secondary radiation from the spacecraft. A low-gain corrected spectrum, representing an average of 87 spectra, is shown in Fig. 1 for the extended position. The total count rate between 0.5 and 2.1 Mev was  $0.27 \pm 0.01$  counts/cm<sup>2</sup>-sec, and above 2.1 Mev,  $0.67 \pm 0.02$  counts/cm<sup>2</sup>-sec (detector area = 58 cm<sup>2</sup>). The second value is not corrected for self-rejection by the phoswitch circuit.

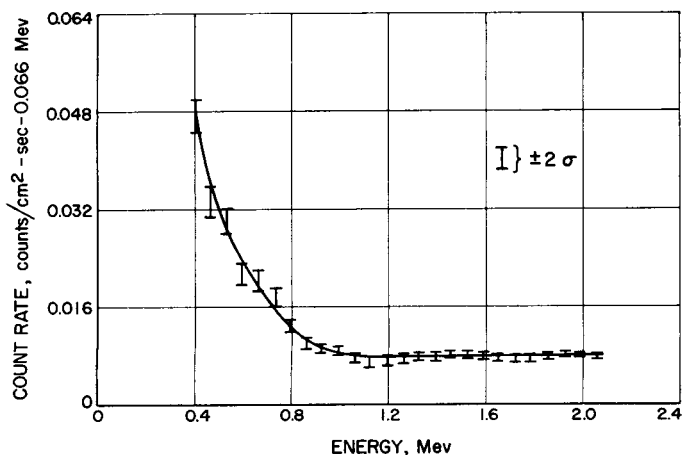


Fig. 1. Average low-gain spectrum obtained in cislunar space by the Ranger 3 gamma ray spectrometer with the detector 6 ft from the spacecraft

The observed count rates, assuming normal reject circuit operation, are surprisingly high both above and below 2 Mev. They are significantly greater than those reported by Vernov, et al., on *Lunik 2* (Ref. 4). The *Lunik 2* values were obtained using a 1.5- × 1.6-in sodium iodide crystal with a single threshold discriminator set at 0.45 Mev.

The data show very little variation with time and no indication of response to solar flares. This is consistent with the reports of low solar activity on these dates.

Interesting limits can be set for the intensity of the lines expected to be most prominent in the astronomical spectrum. These are the annihilation line at 0.51 Mev and the neutron capture line of hydrogen at 2.23 Mev. Almost any form of nuclear activity on the surface of stars or in interstellar space capable of producing gamma radiation at all should produce one or both of the lines prominently. An estimate of the intensity of the 2.23-Mev line can be

made from data taken in the stowed position. Although the line falls above the energy limit of the spectrum when the boom is extended, the presence of the first escape peak and the Compton edge at 1.75 Mev have been used for a separate estimate. The line at 0.51 Mev has been examined in both the low-gain extended and the high-gain stowed positions.

The upper limits set by the data are 0.01<sub>5</sub> counts/cm<sup>2</sup>-sec for the 0.51-Mev line and 0.03 counts/cm<sup>2</sup>-sec for the 2.23-Mev line. The lack of significant peaks indicates that the contribution of monoenergetic gamma ray lines from the quiet Sun and the general galactic environment is small compared to the continuum. The continuum falls roughly as  $E^{-2.4}$  up to 1 Mev and is essentially flat thereafter. The shape below 1 Mev is suggestive of a thick target bremsstrahlung spectrum. The shape above 1 Mev is puzzling; the absence of spectral data above 2.6 Mev precludes a unique unfolding of the instrument response. Further study of the *Ranger 3* data, together with that returned by *Ranger 5*, is expected to yield additional information.

## B. Surveyor X-Ray Spectrometer

The X-ray spectrometer was designed to perform elemental analyses on powdered samples of lunar material. A beam of energetic electrons is directed upon the sample. Radiation from the excited sample is viewed by an assembly of separate crystals, each positioned at a Bragg angle  $\theta$ , which is equivalent to a particular wavelength and therefore to a particular element. For each crystal and its accompanying radiation detector, a stack of flat-blade collimators is placed either between the target and the crystal or between the crystal and the detector. The detectors are geiger and proportional counters, with the latter used for the lighter elements to improve the signal-to-background ratio.

A breadboard model, constructed by Philips Electronic Instruments, has been undergoing tests at JPL for over one year. The test program has included studies of component performance, behavior of the sample under the beam, alignment of the instrument, calibration, and analytical capabilities of the unit. During the past few months, emphasis has been placed on improving stability and reproducibility, understanding certain design considerations, and examining progressively complex powders.

## References

1. Van Dilla, M. A., Anderson, E. C., Metzger, A. E., and Schuck, R. L., "Lunar Composition by Scintillation Spectroscopy," *IRE Transactions on Nuclear Science*, NS-9, pp. 405-412, 1962.
2. *Scientific Experiments for Ranger 3, 4, 5*, Technical Report No. 32-199, (Revised), Jet Propulsion Laboratory, Pasadena, pp. 12-16, 1962.
3. Arnold, J. R., Metzger, A. E., Anderson, E. C., and Van Dilla, M. A., "Gamma Rays in Space, Ranger 3," *Journal of Geophysical Research*, Vol. 67, pp. 4878-4880, 1962.
4. Vernov, S. N., Chudskov, A. E., Vakulov, P. V., Logachev, Yu. I., and Nikolayev, A. G., "Radiation Measurements During the Flight of the Second Soviet Space Rocket," *Space Research*, H. Kallman Bijl (Ed.), Interscience Publishers, Inc., New York, pp. 845-851, 1960.